Preparation and characterization of cross-linked chitosan beads for phosphate adsorption in aqueous solution

A Thesis Submitted to the College of
Graduate Studies and Research
In Partial Fulfillment of the Requirements
For the Degree of Master of Science
In the Department of Chemistry
University of Saskatchewan
Saskatoon

By

Mohammad H. Mahaninia

PERMISSION TO USE

In presenting this thesis in partial fulfillment of the requirements for a Postgraduate degree from the University of Saskatchewan, I agree that the Libraries of this University may make it freely available for inspection. I further agree that permission for copying of this thesis in any manner, in whole or in part, for scholarly purposes may be granted by the professor or professors who supervised my thesis work or, in their absence, by the Head of the Department or the Dean of the College in which my thesis work was done. It is understood that any copying, publication, or use of this thesis or parts thereof for financial gain shall not be allowed without my written permission. It is also understood that due recognition shall be given to me and to the University of Saskatchewan in any scholarly use which may be made of any material in my thesis. Requests for permission to copy or to make other use of material in this thesis in whole or part should be addressed to:

Head of the Department of Chemistry
University of Saskatchewan
Saskatoon, SK (S7N 5C9)
Canada

Abstract

Chitosan beads were cross-linked with glutaraldehyde (GA) and epichlorohydrin (EP), respectively, at variable composition. The cross-linked chitosan beads were further modified and doped using calcium chloride. Several techniques were used to characterize the structural and chemical properties of chitosan bead materials. These materials possess unique structural and chemical properties such as hydrophile-lipophile characteristics with variable chemical functionalities that affect the adsorption properties. The general features of the adsorption and textural properties of the bead systems were studied using model dye compounds such as *p*-nitrophenolate (PNP) and phenolphthalein (PHP). The results from the uptake study of the model dyes was used to complement a systematic adsorption study of hydrogen phosphate ion (HPO_4^{2-}) species and *p*-nitrophenolate phosphate (PNPP) at pH 8.5 and 295 K. Several model equations were used to analyze the adsorption data, as follows: Langmuir, Sips, and Dubinin–Radushkevich (D-R) isotherms. The Sips model provided adsorption parameters for the chitosan bead systems: (*i*) the monolayer adsorption capacity (Q_m) for PNP ranged from 0.30 to 0.52 mmol g^{-1}, and (*ii*) the Q_m values for the bead systems with HPO_4^{2-} ranged from 0.22–0.53 mmol g^{-1}, (iii) the Q_m values for the bead systems with PNPP ranged from 0.18–1.07 mmol g^{-1}. The kinetic adsorption results for hydrogen phosphate ions (HPO_4^{2-}) onto chitosan beads was analyzed at variable temperature to obtain the respective thermodynamic adsorption parameters using the pseudo-first order (PFO) and pseudo-second order (PSO) order kinetic models. The experimental rate constants for the bead systems with HPO_4^{2-} ranged from 0.04–0.11 (min^{-1}) for the PFO model and 0.0021–0.0045$g.mg^{-1}.min^{-1}$ for the PSO model. A molecular level understanding of the adsorption mechanism for the uptake of phosphate onto chitosan beads was proposed from these experimental results. Bead materials in this research have shown favorable adsorption–desorption properties and represent a promising tunable adsorbent system for the effective removal of phosphate anion species in aqueous solution.

ACKNOWLEDGEMENTS

If it was not the support of my supervisor Dr. Lee D. Wilson, I have never reached to this point. Through his tireless guidance, I have reached to the harvest time. I am grateful for his mentorship, as I have learned much in becoming a researcher and wish him the best in his future research projects.

I am also grateful to Dr. Abdalla Karoyo, Dr. Mohamed H. Mohamed, and Mrs. Dehabadi for their assistance on running my samples for TGA and FT-IR and providing comments and advice. I would like to thank Keith Brown, Jason Maley, and Liu Guosheng for their comprehensive training on various instruments.

I appreciate my committee members who acted as advisors and spared time in their busy schedule to guide my research. I offer my special thanks to Dr. Steve Reid and Dr. Robert Scott. Also, thanks to Dr. Jafar Soltan for accepting to be my external examiner.

Lastly, I am thankful for the funding provided by University of Saskatchewan Department of Chemistry through the graduate teaching assistantship. To Government of Saskatchewan (Ministry of Agriculture) through the generous support through the Agriculture Development Fund.

TABLE OF CONTENTS

LIST OF TABLES

LIST OF FIGURES

LIST OF ABBREVIATIONS

CHN ..... Carbon, Nitrogen, and Hydrogen Elemental Analysis
DSC..... Differential scanning calorimetry
DTG ..... Differential Thermogravimmetry
EP…..... Epichlorohydrin
Eqn. ..... Equation
Fig. ..... Figure
FT-IR..... Fourier Transform Infrared
Fwhm ..... Full-width at half-maximum
GA.....Gluteraldehyde
H-bonding ..... Hydrogen bonding
IR..... Infrared Spectroscopy
IUPAC .....International Union of Pure and Applied Chemistry
mM ..... Millimolar
NMR ..... Nuclear Magnetic Resonance
OPs ..... Organophosphates
DDT…..... dichlorodiphenyltrichloroethane
PHP..... Phenolphthalein
PNP ..... *para*-nitrophenol
PNPP ..... *para*-nitrophenyl phosphate
ppm ..... parts per million (mg/L)
PXRD .....Powder X-ray Diffraction
Pzc ..... Point of zero charge
rpm ..... revolutions per minute
SEM .....Scanning Electron Microscopy
SSA ..... Specific Surface Area
SSNMR .....Solid State NMR
TGA ..... Thermogravimetry Analysis
UV-Vis ..... Ultraviolet-Visible

CHAPTER 1

1 INTRODUCTION

1.1 Phosphate

The accumulation of phosphate in aquatic environments is supported by the growth of extensive algae blooms, and consequently, eutrophication of lakes and rivers (*cf.* Fig. 1.1) due to excessive runoff events in regions with agricultural activity. The high phosphate level in water contributes to potential hazards to human health such as cardiovascular disease, chronic kidney disease.[1] Phosphate is an important nutrient used for synthesizing fertilizers, and for this reason, inorganic phosphate is one of the main contaminants in aquatic environments.

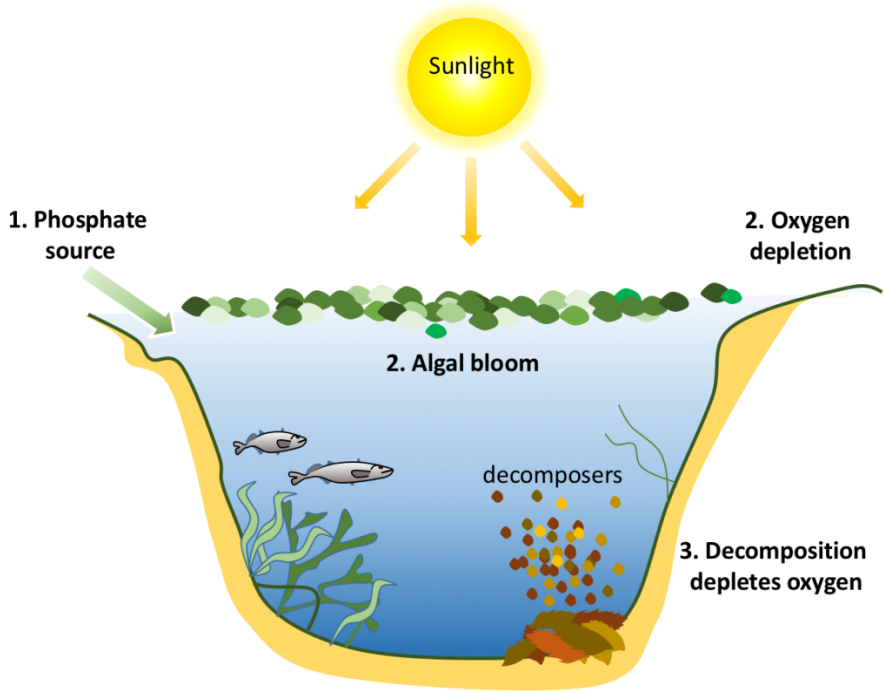

Figure 1.1 Effect of algae blooms growth on an aquatic environment.

The main application of phosphorus is for fertilizer production since phosphate is often a limiting nutrient for crops. Global demand for fertilizers has been increasing since the second half of the 20th century. The low solubility of natural phosphorus-containing minerals is a drawback such that the agricultural industry prefers to employ fertilizers that contain phosphate with variable composition. The major forms of these fertilizers are calcium dihydrogen phosphate ($Ca(H_2PO_4)_2$)

and calcium sulfate dihydrate ($CaSO_4 \cdot 2H_2O$) which can be produced by the reaction of sulfuric acid and calcium phosphate in water. In addition, minerals containing phosphorous like fluorapatite and hydroxyapatite are widely being used for the production of fertilizers.

Generally, organophosphate-based insecticides such as parathion are potential pesticide alternatives for dichlorodiphenyltrichloroethane (DDT). Organophosphate-based pesticides function by inactivating the enzyme acetylcholinesterase that is essential for nerve function in insects. One of the advantages of organophosphate-based insecticides is the relative ease with which they undergo degradation upon their release to the environment. Degradation of such chemicals can occur by hydrolysis on exposure to sunlight, air, and soil to produce phosphate. Although organophosphates degradation is somewhat fast, their acute toxicity poses health risks to people with exposure. Although the EPA banned most residential uses of organophosphates in 2001, such compounds are still in use by the agriculture industry (*e.g. quinalphos*). These compounds can be absorbed easily by the lungs or skin or by consuming contaminated foods.

1.1.1 Phosphate contamination in aquatic environments

Leakage of phosphate into waterways and lakes can lead to detrimental environmental effects. In recent years, there have been record algal blooms in several areas around the world. China produces more than 50% of the world's vegetables and involves the excessive use of fertilizers containing phosphate and this has resulted in extensive phosphate pollution of aquatic sources.

The occurrence of severe algal blooms in Lake Winnipeg and Lake Simcoe in eastern Canada was recently reported. Only during the 1970's, the growth of algal blooms in the Great Lakes prompted the legislation of serious regulations that restrict phosphate levels in laundry detergents.[2] The extent of eutrophication of Lake Winnipeg is considered problematic due to its large size and damage to the aquatic ecosystem and water quality.

Although the Government of Canada has announced regulatory standards for the use of phosphates in household detergents to offset the build-up of phosphate in Canadian lakes and waterways, the annual phosphate consumption has steadily increased from about 18,000 tons in the mid 1960's to almost 116,000 tons in 2000.[3]

Understanding the physical and chemical properties of the phosphate species can provide required information to devise a plan to control or eliminate its harmful effects.

1.1.2 Physical and chemical properties of orthophosphate (P_i)

In the field of inorganic chemistry, phosphate is defined as a salt of phosphoric acid while in organic chemistry, phosphate, or organophosphate, is regarded as an ester of phosphoric acid. Phosphate is a polyatomic ion that consists of one central phosphorus atom surrounded by four oxygen atoms with a tetrahedral geometry around phosphorous. The phosphate ion can carry a negative formal charge and has several protolytic equilibria. The phosphate anion (HPO_4^{3-}) is the conjugate base of the hydrogen phosphate ion, HPO_4^{2-}, which is the conjugate base of $H_2PO_4^-$, the dihydrogen phosphate ion is derived from phosphoric acid (H_3PO_4). The protolytic equilibria for the dissociation of H_3PO_4 to PO_4^{3-} is described by equations 1.1 – 1.3. In aqueous state, phosphate can exist in four variable species. In strongly basic conditions, the dominant phosphate species is PO_4^{3-}; whereas, the hydrogen phosphate ion (HPO_4^{2-}) is dominant in weakly basic conditions. In weakly acid conditions, the dihydrogen phosphate ion ($H_2PO_4^-$) is the most prevalent while phosphoric acid (H_3PO_4) is predominant in very acidic conditions.

$$H_3PO_4 \rightleftharpoons H^+ + H_2PO_4^- \qquad (1.1)$$

$$H_2PO_4^- \rightleftharpoons H^+ + HPO_4^{2-} \qquad (1.2)$$

$$HPO_4^{2-} \rightleftharpoons H^+ + PO_4^{3-} \qquad (1.3)$$

The corresponding dissociation constants for the above equilibria are described by eqns. 1.4 to 1.6:

$$K_{\alpha 1} = \frac{\left[H^+\right]\left[H_2PO_4^-\right]}{\left[H_3PO_4\right]} = 7.5\times10^{-3}\,(pK_{a1} = 2.12) \qquad (1.4)$$

$$K_{\alpha 2} = \frac{\left[H^+\right]\left[HPO_4^{2-}\right]}{\left[H_2PO_4^-\right]} = 6.2\times10^{-8}\,(pK_{a2} = 7.21) \qquad (1.5)$$

$$K_{\alpha 3} = \frac{\left[H^+\right]\left[PO_4^{3-}\right]}{\left[HPO_4^{2-}\right]} = 2.14\times10^{-13}\,(pK_{a3} = 12.67) \qquad (1.6)$$

The speciation diagram in Figure 1.2 was obtained using the pK_a values for the above equilibria which show three distinct pH regions that range between 0–4, 5–9 and 10–14, respectively. Using these pH regions, finding the dominant phosphate species at variable pH is phosphate.

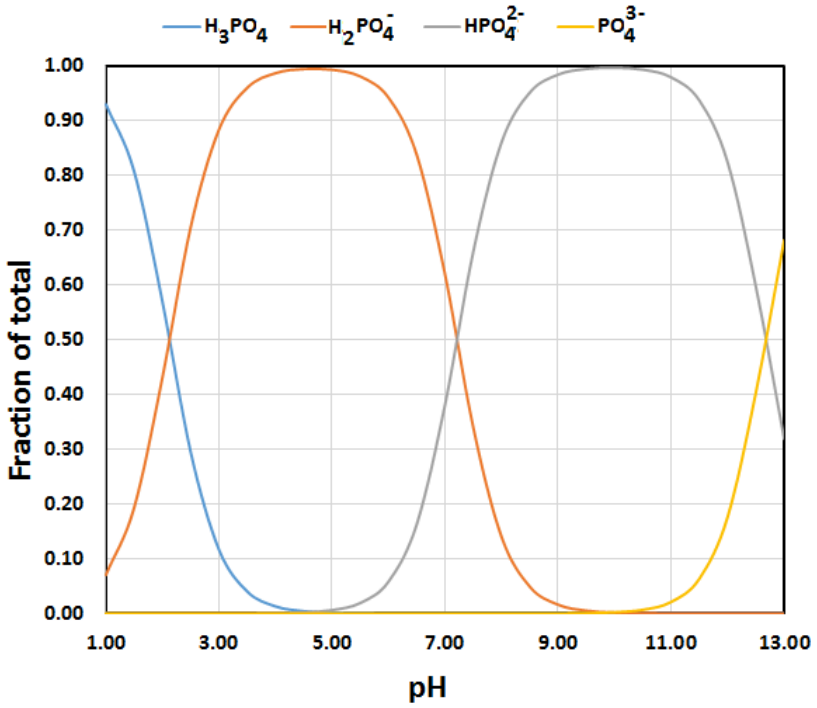

Figure 1.2 Speciation curve for phosphate in aqueous solution.

1.1.3 Physical and chemical properties of organophosphate (OP)

In the literature, the definition for organophosphates is sometimes not clearly stated which can cause confusion. Generally, compounds with a direct phosphorus-carbon (P-C) bond are considered as organophosphate and contain P-O bond as well. Organophosphates can adopt variable oxidation states, where it is common to classify the organophosphates as either phosphorus (V) or phosphorus (III).[4] As an organophosphate molecule, *p*-nitrophenyl phosphate (PNPP) may serve as a model molecule for inorganic forms of phosphate. PNPP is a chromogenic substrate that is measurable using a conventional spectrophotometric assay. PNPP has structural

similarity with common types of organophosphate compounds like Paraxon and Parathion (*cf.* Table 1.1). Paraxon and Parathion are two main compounds used in pesticides.

Table 1.1 Comparison between chemical structures of various organophosphates

Chemicals	Structures
p-Nitrophenyl Phosphate	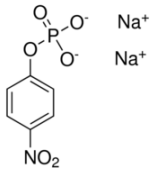
Paraxon	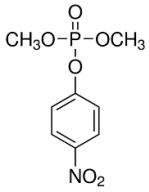
Parathion	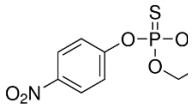

Firstly, PNPP was chosen as an organophosphate in this study because PNPP can serve as a surrogate species due to its similar structure to other types of organophosphates. Secondly, a comparison between adsorption properties of PNPP, phosphate ion, and PNP may provide a molecular level understanding of the mechanism of the adsorption process for adsorbents herein.

After studying the physical and chemical properties of variable phosphate species, consideration of effective methods for the characterization and quantification is of key importance.

1.1.4 Remediation of phosphate and organophosphate

Methods for the removal of phosphate include ion-exchange,[5] reverse osmosis,[6] electro-dialysis,[7] bioremediation,[8] and precipitation.[9] Several methods have been reported for organophosphate removal such as enzymatic biodegradation, [10] electrochemical, [11] catalytic oxidation, [12] atmospheric pressure plasma, [13] photolytic, [10] and hydrolysis. [14–16]

Adsorption-based processes are advantageous when compared with other techniques in terms of the infrastructure cost, modular design, simplified technological design, and operation. These techniques have been widely applied on both organic and inorganic phosphates. Recently, organophosphate removal and elimination using alternative adsorption techniques such as clay,[17] soil components,[17] and zeolites[18] have been reported.

The application of adsorption techniques for the effective removal of phosphates requires a better understanding of the molecular levels details, thermodynamics, and kinetic aspects of the process (e.g. mechanism, sorption optimization, etc.).

1.2 Physical adsorption

1.2.1 General overview

The term "sorption" is a combination of two phenomena: absorption and adsorption processes. In the case of adsorption, an adsorbate from the bulk phase is adsorbed by the external surface of the adsorbent, as shown in Figure 1.3. For porous materials, separation of the adsorption from the absorption process is not possible; therefore, applying the term "sorption" can account for the two processes.

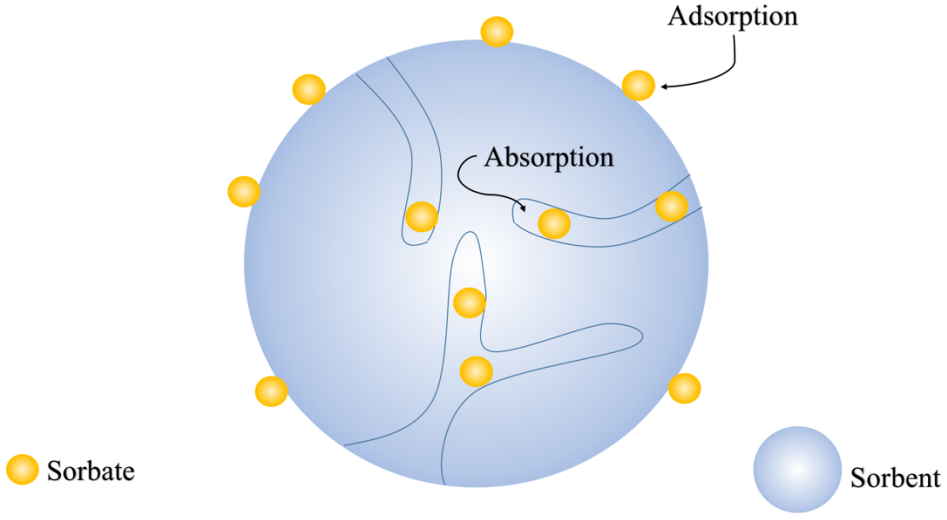

Figure 1.3 Comparative illustration of the absorption and adsorption processes.

While absorption phenomena occurs within the interior of the sorbent, adsorption is a surface-based phenomenon. Generally, the two main categories for sorption are physical and

chemical sorption defined by physisorption and chemisorption, respectively. Physisorption involves multiple intermolecular forces such as van der Waal's, hydrogen bonding, and dipole-dipole interaction, and play a key role for both adsorption and absorption phenomena. The interactions involving physisorption processes have desorption enthalpy values ranging from 20-40 kJ/mol, and are generally lower in magnitude than chemisorption energetics. Chemisorption involves chemical bond formation between the adsorbate and the surface with enthalpy values in the 100-400 kJ/mol range.[19]

In addition, physisorption is a reversible process, whereas; chemisorption is irreversible. Polarity of the interacting species plays an important role in physisorption since it can be driven by the relative polarity of the solvent in the surrounding according to the relative polarity of the adsorbate/adsorbent system. The polarity affects the intermolecular interactions of the solvent and the arrangement around the adsorbent and adsorbate by reducing or increasing the entropy of the process. Therefore, the hydrophile-lipophile balance of the adsorbate, adsorbent, and the solvent strongly influence the thermodynamic/kinetic properties of the adsorption process.

Adsorption isotherms enable an interpretation of the adsorption process of species from the gas phase and in solution. A description for the various isotherms are given in the next section.

1.2.2 Types of isotherms

Adsorption isotherms are classified by IUPAC into six general categories (*cf*. Fig. 1.4).[20] Surface area and pore diameter govern the type of adsorption isotherm. Pore sizes are generally categorized into three types according to their relative diameters:

1. Macropores: These have a diameter larger than 50 nm.

2. Mesopores: These pores are within the range of 2-50 nm. These pores are large enough to fit more than one gas molecule in the cross-sectional area. As well, capillary condensation can occur which gives rise to hysteresis loops often seen in adsorption and desorption curves.

3. Micropore: With pore diameters of 2 nm and lower, this system can capture only one gas molecule and can be seen in the type I isotherm.

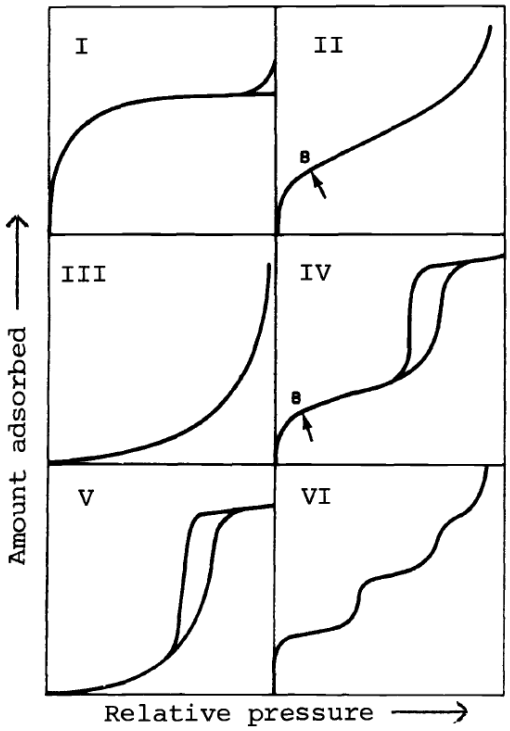

Figure 1.4 Types of physisorption isotherms. (Reprinted with permission from [20])

Type I Isotherm

This curve is a monotonically increasing curve that approaches a specific sorption capacity. Sorbents, which place into this type, are microporous materials where the cross-sectional area of the pores is too small to allow capture of more than one molecule into the pores.

Type II Isotherm

Isotherms following this profile usually show two trends in terms of pore size dimensions. This curve can be representative of large macropores with the large surface area that can produce multi-layer adsorption without any restrictions. Besides, this type of isotherm can be representative of nonporous materials where the only sorption sites are on the external surface.

Type III Isotherm

This isotherm corresponds to strong adsorbate-adsorbate interactions where the binding of the adsorbate to itself exceeds the interaction between the adsorbate and adsorbent.

Type IV Isotherm

Such isotherms type can be seen for multi-layer adsorption processes that are characteristic of mesoporous materials. The occurrence of capillary condensation may occur if a hysteresis loop is observed when the adsorbate is desorbed.

Type V Isotherm

Similar to the type III isotherm, the type V isotherm may correspond to the strong adsorbate-adsorbate interactions but the interactions between the adsorbates are generally weaker. This coupled with finite sorption sites enables an observable plateau, where the presence of hysteresis loops may suggest the desorption of agglomerated particles occur at once.

Type VI Isotherm

A step-wise multilayer adsorption profile can be seen in this isotherm, where one sorption site is filled firstly and another site is filled. A curve of this type suggests the energy required to adsorb at one site should be different from the energy required at the other site for the occurrence of preferential filling.

1.2.3 Hysteresis in solid-gas adsorption/desorption curves

IUPAC classification of hysteresis along with their definitions are listed below.[20] A regular nitrogen gas-adsorption isotherm is shown as a plot of Q_e against the relative pressure. By approaching the relative pressure to unity, pore condensation occurs. The obtained adsorption isotherm can reveal the shape of the pore before condensation. For instance, the adsorption isotherm for the H1 is more typical of cylindrical pores whereas H2 is observed for *ink-bottle* shaped pores. By condensation of nitrogen gas, the desorption process occurs in the solution state. Therefore, the isotherm for desorption differs from the adsorption isotherm. Studies of hysteresis loops have been considered for nitrogen porosimetry, where this technique can give useful information on the adsorption-desorption process (*cf.* Figure 1.5).

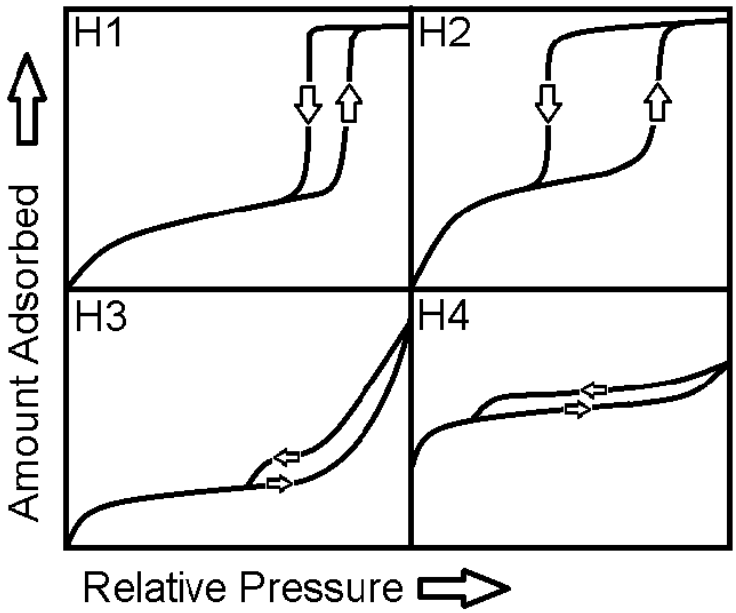

Figure 1.5 The four general hysteresis loops observed for nitrogen adsorption-desorption. (Reprinted with permission from [20])

Type H1 Isotherm

The adsorption isotherm follows Langmuir behavior where the gas adsorbs onto the sides of the pores to form a monolayer until all the pores are filled. This type of isotherm is associated with cylindrical pores as the filling of the pores can occur uniformly which allows for a steep asymptote when condensation occurs.

Type H2 Isotherm

Adsorption into the pores is similar to H1 where capillary condensation is attenuated due to the shape of the pore. The shape associated with this pore is an inkbottle shape, where there is a region inside the pore that is difficult to fill. This is represented by the elongated region before the asymptote. IUPAC notes that other effects involving the network of pores inside the material for the desorption isotherm is probably a significant factor but the shape of desorption curve cannot be fully explained.

Type H3 Isotherm

Beyond the monolayer coverage, interaction between adsorbates on the first layer and the n^{th} layer is relatively weak. One type of slit-shape that can promote this is a thin slit-like capillary.

Type H4 Isotherm

The high affinity adsorption isotherm for this category is a distinct indicator of microporosity as the small pore width ensures a strong adsorbent-adsorbate interaction. The desorption-isotherm is similar to H3 and the pore shape is likely slit-shaped.

The interpretation of the isotherm of adsorption is possible using various isotherm models, where some are described below.

1.2.4 Models of sorption isotherms

1.2.4.1 Langmuir isotherm model

Irving Langmuir proposed this type of isotherm model to explain kinetic results for the adsorption of hydrogen gas on a palladium surface.[21] In this isotherm model, several assumptions are made; firstly, the nature of the material should have a homogeneous surface (*cf.* Figure 1.6). Hence, the adsorption sites on the material have equal energy for adsorption and are equally probable for adsorption, regardless of distance between sites. Secondly, the sole formation of a monolayer is permissible for adsorbates. Finally, the adsorbate gas should behave as an ideal gas and interaction between the gases within the monolayer are negligible.

The Langmuir model can be expressed by Eqn (1.7).[21]

$$Q_e = Q_m \frac{K_L C_e}{1 + K_L C_e} \qquad (1.7)$$

Where Q_e is adsorption capacity at equilibrium, K_L is the Langmuir adsorption constant, C_e is the residual adsorbate concentration, and Q_m represents the monolayer adsorption capacity of the adsorbent.

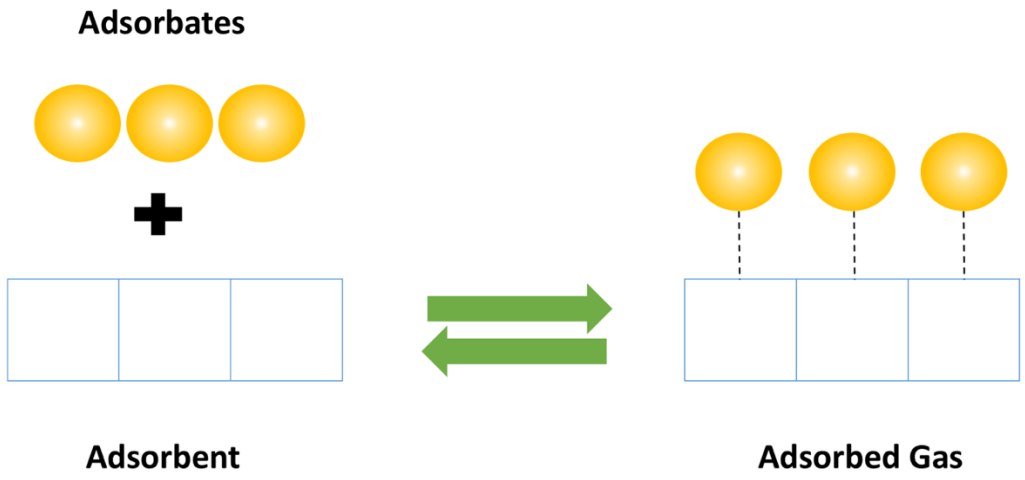

Figure 1.6 Langmuir model of physical adsorption of a gas onto a solid adsorbent at equilibrium.

1.2.4.2 Freundlich isotherm model

Herbert Freundlich derived his isotherm model after observation of this fact that not all trends in adsorption profiles form horizontal asymptotes like the predicted curves by the Langmuir isotherm model. Freundlich realized that the heat of adsorption for every sorption site is not uniform (*cf.* Figure 1.7).

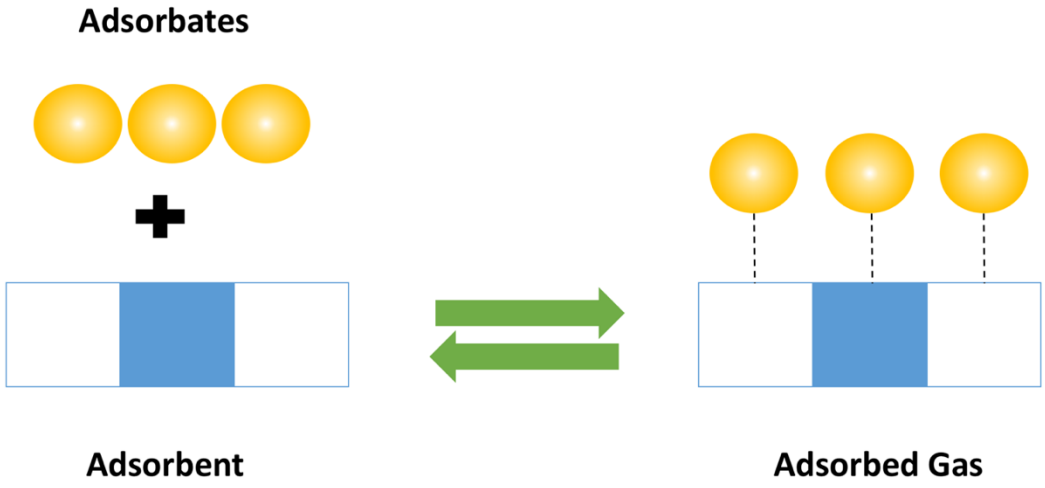

Figure 1.7 The Freundlich isotherm model of physical adsorption of gas at equilibrium. The blue and white squares of the adsorbent phase shows the non-uniformity of sorption sites.

The Freundlich model can be expressed by Eqn (1.8).[22]

$$Q_e = Q_m K_f C_e^{1/n} \qquad (1.8)$$

Where Q_e is adsorption capacity at equilibrium, K_f is the Freundlich adsorption constant, 1/n is an empirical constant, C_e is the residual adsorbate concentration after the adsorption process, and Q_m represents the monolayer adsorption capacity of the adsorbent.

1.2.4.3 Sips isotherm model

Langmuir and Freundlich isotherms are similar in one aspect where an assumption for the formation of monolayer adsorbates occurs. However, these models are differ since the Freundlich isotherm can indicate surface heterogeneity using the exponential parameter (n_s), while the Langmuir model assumes that monolayer surface coverage occurs solely. Thus, the Langmuir isotherm assumption of constant enthalpy of adsorption at the sorption sites is invalid in cases where the surface is not homogeneous. Therefore, the Sips isotherm model serves as a general model to enable determination of the sorption capacity at saturation (mg/g) as a function of the energy distribution of the sorption sites.

Expression of the Sips isotherm model is based on eqn. (1.9):[23]

$$Q_e = Q_m \frac{(K_s C_e)^{n_s}}{1 + (K_s C_e)^{n_s}} \qquad (1.9)$$

Where K_s is the adsorption constant, n_s represents the heterogeneity parameter of the sorbent surface, C_e is the residual adsorbate concentration, and Q_m represents the monolayer adsorption capacity of the sorbent (powder, bead, flake, etc.) material. Eqn (1.9) provides a measure of the heterogeneity of the adsorption process according to the value of n_s and this model accounts for Langmuir behavior when n_s~1. Freundlich behavior occurs when n_s deviates from unity since this model accounts for surface heterogeneities with a distribution of adsorption energy values. The Sips isotherm accounts for combined features of the Langmuir and Freundlich isotherms. The Sips model has the benefit of converging to the Freundlich isotherm at low pressures and approaches the monolayer capacity at high pressure similar to the Langmuir isotherm.

1.2.4.4 Dubinin-Radushkevich (D-R) isotherm model

The equilibrium uptake results were fit using the Dubinin-Radushkevich (D-R) isotherm model.[24] The nature of the sorption processes can be physical or chemical in nature according to the sorption energy parameter obtained from the D-R model. The magnitude of D-R model parameters enables determination of the type of adsorption process, which may be physical or chemical. The nonlinear form of the (D-R) isotherm equation can be expressed by eqn (1.10).[24]

$$Q_e = Q_m \exp(-\beta\varepsilon^2) \qquad (1.10)$$

Q_m is the adsorption capacity (mg/g) and β is the constant related to adsorption energy ($mol^2.kJ^{-2}$), ε is Polanyi potential which is equal to RT $ln(1 + 1/C_e)$, where R is gas constant, T is temperature (K), and C_e is the residual adsorbate concentration. The value of β is used to calculate the mean free energy E (kJ/mol) of the sorption process using eqn (1.11).[24]

$$E = \frac{1}{\sqrt{2\beta}} \qquad (1.11)$$

Indeed, there are differences between the adsorption process and isotherms in gas and solution media and recognizing such differences provides further insight on the thermodynamics and kinetics of the adsorption process.

1.3 Solution vs. gas-based adsorption

Sorption process in a solid adsorbent can occur while the adsorbate is a gas or a liquid. The difference between gas adsorption and solution-based adsorption processes are illustrated by Fig. 1.8:

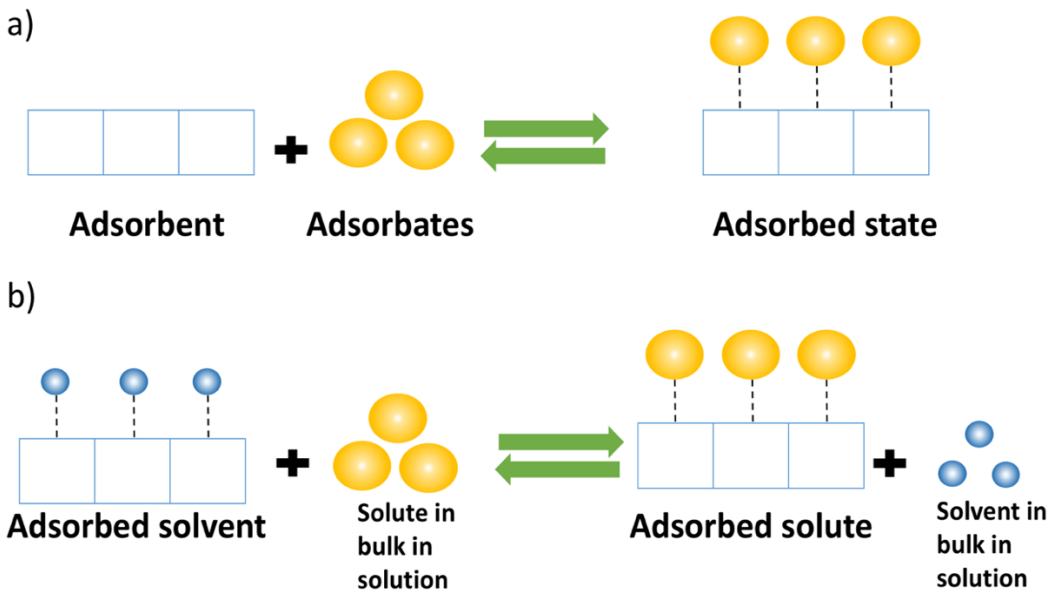

Figure 1.8 Adsorption processes using a solid substrate with an adsorbate in two phases: a) gas adsorption, and b) solution-based adsorption.

In gas adsorption processes, adsorption involves with noncovalent bonding to a vacant sorption site. Therefore, the sorption capacity for adsorbent is the amount of adsorbate adsorbed onto the adsorbent.

The assumption that there are vacant sorption sites on the adsorbent is invalid in the case of solution-based adsorption. This is because either a solvent or solute molecules occupy all sorption sites. For an entirely desorbed substrate, solvent molecules may occupy all sorption sites. Thus, the adsorption process in this case is the displacement of solvent molecules by the solute and all models for solution-based adsorption must consider the activities of the solute and solvent.[25]

Having knowledge about solution vs. gas-based adsorption processes provides a comparison for developing conditions for the uptake of adsorbates for various applications.

1.4 Applications of physical adsorption

Searching for the new techniques to overcome the issues involving environmental quality is the subject on ongoing research. Adsorption-based technology is one of the established techniques for addressing the removal of environmental contaminants both locally and globally.

Adsorption processes have been developed for recovering the water sources, removing nutrients from wastewater, recovery of carbon dioxide from stack gases.[26]

Physical adsorption could be employed for the above mentioned issues owing to its advantages when compared with other techniques in terms of the infrastructure cost, modular design, simplified technological design, and operation. Adsorption efficacy can be affected highly by the nature and type of the adsorbent. In recent years, studies on the use of low-cost adsorbents with suitable adsorption capacities have been increased. Diverse types of sorbent materials such as clays, zeolites, and activated carbon materials are commonly used industrial adsorbents for the adsorptive uptake of diverse contaminants in wastewater treatment applications.

The use of chitosan materials as an effective adsorbent has gained interest among researchers for many reasons which will be described in the following section.

1.5 Chitosan based materials

A large variety of adsorbent materials have been proposed and evaluated for their utility in the removal of different wastes from aqueous solution. However, searching for adsorbents with low-cost and high capacities are still under development to maximize the efficiency of removal process and minimize disposal issues. Much attention has been given to the various biopolymer and biomass sorbent materials that are available in sustainable quantities and relatively harmless in nature. Polysaccharides such as chitosan have been extensively studied as sorbents for the removal of wide ranging waterborne contaminants including organic and inorganic pollutants. The suitability of chitosan as a sorbent material can be justified by two main reasons: *i*) chitosan has low cost since it is a derivative of chitin which is the second most abundant polysaccharide in the world after cellulose; *ii*) chitosan has exceptional chelation behavior especially with heavy metal cation species).

The unique features of chitosan as an adsorbent comes from its structural and chemical properties. Therefore, developing an improved knowledge about these properties is essential for understanding the adsorptive behaviour of chitosan with variable adsorbates.

1.5.1 Origin and properties of chitosan

The discovery of chitosan dates back to 1859 by Rouget when he boiled the chitin in concentrated potassium hydroxide and the obtained product showed solubility behaviour in

acids.[27] Natural chitin is a precursor for preparing chitosan. Chitosan is a linear biopolymer composed of glucosamine and N-acetyl glucosamine that may be isolated by thermal–chemical deacetylation of chitin (Fig. 1.9). Research on biopolymers such as chitosan is going on since it is an abundant and renewable material. Chitosan can be modified to yield unique types of adsorbent materials with tunable physicochemical properties.

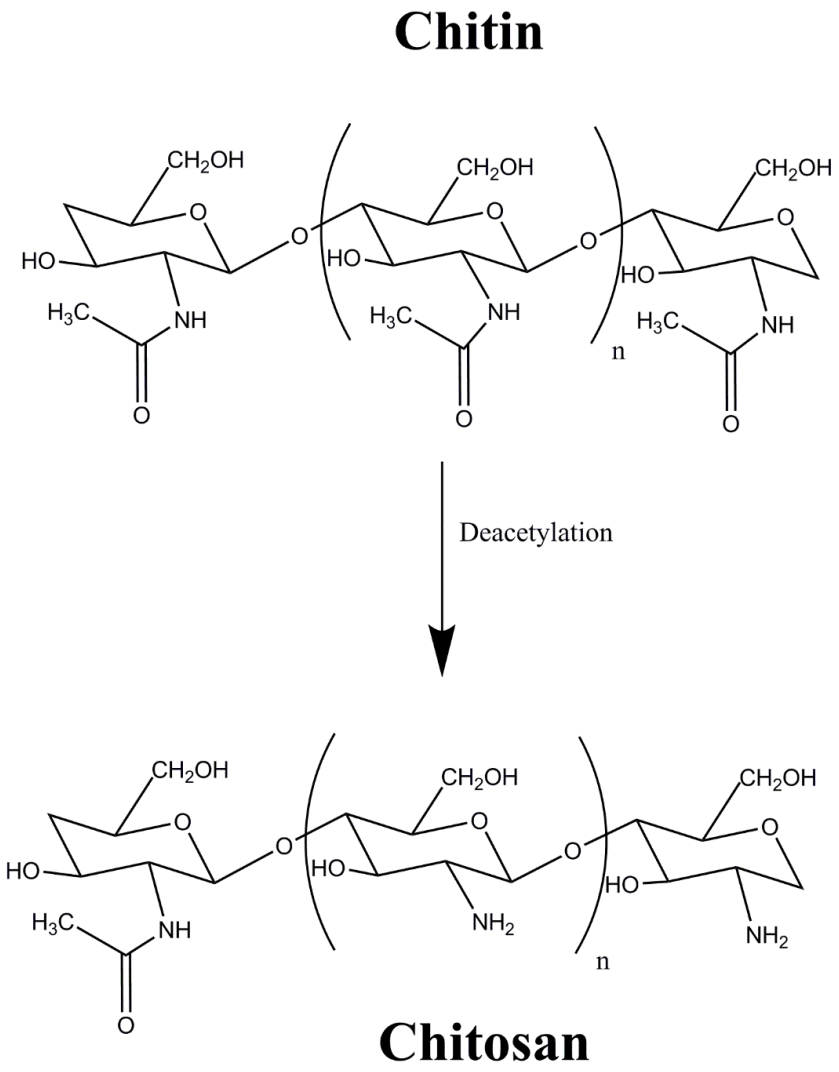

Figure 1.9 Partial deacetylation of chitin yields chitosan, where n denotes the degree of polymerization.

Chitosan is a stable polymer in air and it remains inert in the most solvents. Chitosan undergoes degradation in extreme conditions such as concentrated acids which depolymerize the chitosan.[28] The pK_a of the protonated amine groups in chitosan is in the pH region 5.5-6.5, depending on the degree of deacetylation. The average molecular weight of chitosan may range

from (1-5) x 10^5 g/mol, where the manufacturing process can lead to degradation of chitosan when harsh treatment conditions applied.[29]

Chitosan can undergo physical or chemical changes at different pH conditions. At pH values below 3, depolymerization occurs in chitosan via hydrolysis. Chitosan dissolves in acidic aqueous solutions and this unique behaviour distinguishes its properties from chitin. This behaviour relates to the protonation of the amine group of chitosan. At neutral and basic pH conditions chitosan can be precipitated out when pH > pK_a due to the decrease of the polarity relative to the condition when chitosan contains protonation ammonium forms.[30] Although chitosan is soluble at acidic pH conditions, hydrolysis and depolymerize can form monomer by lowering the pH below 3. This makes chitosan an attractive candidate for pharmaceutical industry as a disintegrant or carrier.[30]

The solubility of chitosan is also an important factor which may be affected by the polymer weight, the type and concentration of the acid used. The solubility of the chitosan in most non-aqueous solvents is very low unless a small amount of acid is present to alter the protonation state of the chitosan monomers. The solubility of chitosan depends on the molecular weight, degree of deacetylation, type of acid, and the strength of the acid. For instance, chitosan is soluble in a 2% acetic acid, and 10% citric acid solutions.[31]

The effect of acid addition to increase the solubility is understood by the protonation of amine groups. Chitosan has a pK_a near 6.2, so it is soluble at pH values near and below its pK_a where much of the amine groups are in their protonated form. At acidic pH values, an increase in the charge repulsion between amine groups increases the polymer volume as greater numbers of ammonium groups will be exposed to the solvent. The ion-dipole interaction relates to the formation of favourable interactions between ammonium groups and water. [31]

Several characteristic features for chitosan include the degree of deacetylation, the polymer molecular weight and the crystallinity.[32] These features have significant influence on the physicochemical properties of chitosan. The deacetylation degree of commercial chitosan products is variable with typical values of 75% to 80%. The deacetylation degree governs the fraction of free amine groups that will be available for interactions with variable ions, which can react at different pH condition with various ions through a chelation mechanism or electrostatic interaction. For instance, the amine groups can be easily protonated in acidic solution to create an

attraction to anionic compounds.[33] In fact, other than the number of free amine groups available for adsorbate uptake, accessibility of the free amine groups plays an important role. Without a doubt, not all the amine groups are available to interact with adsorbates but some of them are involved in hydrogen bonding.

Unfortunately, there are many drawbacks (e.g., poor chemical stability and low mechanical strength) for using pristine chitosan in the form of flakes and powders. Improved properties for chitosan typically require chemical and physical modification to improve its adsorptive capacity.

1.5.2 Chitosan and its modified forms: synthesis and applications

Chitosan is a heterogeneous, linear polysaccharide biopolymer with a high molecular weight. It is drived by deacetylation of chitin which is an extraction from some animal species specially from skeleton of sea living animals such as crayfish, lobsters, prawns, crabs and shrimps.[34] The most common form of final product of chitosan production process is chitosan flakes which posseses unique adsorption properties toward species such as metal cations and dyes.[35] The other form of chitosan is chitosan bead. Thorough the "*phase inversion*" reaction, dissolved chitosan can undergo phase separation due to coagulation in aqueous media to form the chitosan beads (*cf.* Fig. 1.10). The advantages of using chitosan beads over chitosan flakes are discussed in Chapter 1.6.1.

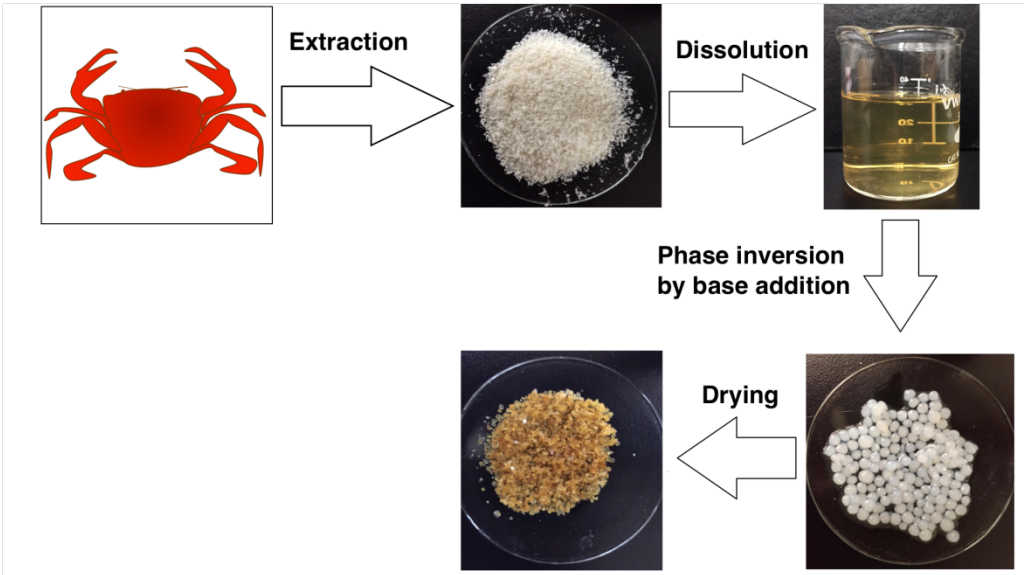

Figure 1.10 Chitosan isolation from crustacean sources and bead preparation steps.

The presence of abundant hydroxyl and amine groups on chitosan affords a semi-crystalline polymer. Both of these groups have the capacity to participate in hydrogen bonding which can enhance the crystallinity of the material. Cross-linkers such as glutaraldehyde (GA)[36] and epichlorohydrin (EP)[37] have been employed for the cross-linking of the chitosan powders and bead materials. Cross-linking of chitosan can increase the surface area of the material since the process leads to exposure of functional groups such as amine and hydroxyl groups. Firstly, sorption on chitosan can occur on the surface where the surface area of the particle governs and provides the number of active sorption sites. Secondly, sorption can also take place in the internal sites where intraparticle diffusion can play a role. Particle size controls the accessibility of these active sites for adsorption. By decreasing the particle size, the sites become more accessible and the equilibrium time for sorption process decreases.

1.6 Applications of chitosan and modified chitosan

1.6.1 Chitosan beads

The applications of chitosan powder are limited due to their high crystallinity, low hydrophilicity, low surface area, low porosity, resistance to mass transfer and low adsorption capacity [10].[38] Chitosan powder can not be employed practically in columns where the mobile phase is aqueous, due to its high crystallinty and hydrophobicity that increase its resistance to solvent flow, mass transfer rate, column clogging and high pressure drops which consequentlly result in greater operation costs. Two other factors, low surface area and low porosity also decrease the adsorption capacity and rate because access into the interior adsorption sites will be restricted.[39] In chitosan powders, all the adsorption sites (amino and hydroxyl groups) are not practically active or accessible for adsorbates.[40] Large adsorbate molecules cannot easily penetrate the porous network of the chitosan powder during the adsorption process. In addition, steric hindrance is increased along with increasing the saturation due to the packing of the chitosan particles. Also, measurment of adsorbates with spectroscopy techniques is difficult without separation of solid and solution phases (e.g., via filtration or centrifiugation) since chitosan particles can interfere. These disadvantages and restrictions of using chitosan powders imply that this form of material may not be suitable as an adsorbent. To overcome these obstacles, chitosan powder is subjected to physical and/or chemical modification by converting the powder into beads to increase porosity along with possible cross-linking to expand chitosan polymer chains, increase surface area, decrease

crystallinity and enhance the internal accessibility. All these improvements in chitosan properties will lead to enhancement of the adsorption capacity. -The following are selected examples from the litrature from different applications of chitosan beads toward phosphate removal from aqueous solution.

Sowmya and Meenakshi[41] synthesized chitosan-based resin with greater numbers of amino groups were introduced by grafted melamine with the aid of glutaraldehyde as cross-linker. This modified chitosan bead was employed for nitrate and phosphate uptake from aqueous solution and this adsorbent showed effective performance thorough ion exchange mechanism. Interestingly, this modified chitosan bead showed high performance even after the 10^{th} cycle of regeneration. These researchers also prepared cross-linked chitosan beads with quaternary ammonium groups with chloride counterions.[42] The modified chitosan beads with quaternary ammonium with chloride counter ion was found to be selectively effective toward nitrate and phosphate ions.[43] Likewise, the mechanism of adsorption was related to the ion exchange between chloride and the respective anions.

Elsewhere, Sowmya and Meenakshi[44] used cross-linked chitosan beads followed by protonation using hydrochloric acid or carboxylation using chloroacetic acid for the removal of nitrate and phosphate. All prepared sorbents showed higher sorption capacity at the acidic pH ranged between pH values 3-4. Physisorption processes such as electrostatic interaction between the anions and the positive functional groups occurred between modified chitosan beads and phosphate ions.

In another study, the cross-linked chitosan beads were doped with zirconium in order to enhance the adsorption of phosphate ions in aqueous solution.[45] The doped chitosan beads exhibited higher phosphate adsorption capacity than pristine materials. Electrostatic attraction was determined as the driving force for adsorption of phosphate on the modified chitosan beads alongside with chloride ion exchange.

Another research group also prepared chitosan beads modified with zirconium ions for the adsorption of phosphate ions.[43] Batch experiments were performed to study the effects of various conditions like contact time, the initial concentration of phosphate ions, temperature and pH on adsorption of phosphate ions. These studies showed that the adsorption mechanism involves both electrostatic attraction and ion exchange reactions between phosphate ions and the adsorbent.

Regeneration studies conducted on this adsorbent showed that it was effective as a reusable adsorbent for uptake of phosphate ions in aqueous solution.

1.7 Summary

In order to remove phosphate species whilst minimizing potential toxic by-products, an environmental friendly technique that employs physical processes is required. Adsorption as a promising and facile method is suitable for this purpose. Four key factors characteristic of a suitable adsorbent are as follows:

1. *Scale*: The adsorbent must originate from materials with favourable sorptive uptake which are available or can be processed at relatively large-scale.

2. *Cost*: The adsorbent preparation uses relatively inexpensive materials

3. *Reusability*: The adsorbent materials should be recyclable with minimal energy inputs.

4. *High Adsorption Capacity*: The uptake properties of the adsorbent are efficient for removal of phosphate species.

The first two items are met by using diverse range of materials like clay, activated carbon, cyclodextrins, and chitosan. The last factor, which is the increasing sorption capacity, will be the main subject of this thesis. One technique to achieve the high sorption capacity is to increase the surface area of the material. Generally, when the surface area increases, the number of sorption sites increased which result in increase in sorption capacity. This can include increasing both the exterior and internal surface area. Another method could be activating sites that are normally inaccessible by increasing the intraparticle diffusion. Both of these methods are achieved by tuning the materials through cross-linking and synthetic modification.

From a review of the different materials in the literature, chitosan bead materials are a potential choice because of their high surface area. The chitosan pK_a lies is a moderate pH range and functionalities like amine and hydroxyl groups can render active sites that favor the binding of phosphate species. By taking advantage of the importance of complementary hydrophile-lipophile interactions in adsorbent/adsorbate systems. The adsorption properties of different adsorbates on the adsorbent surface is understood by using variable linkers such as glutaraldehyde and epichlorohydrin to achieve the desired uptake properties of phosphate species. The hydrophobic nature of the sorbent can be altered by adjusting the level, content and type of cross-

linkers to yield a material with tunable hydrophile-lipophile character, in accordance with the law of matching water affinities (*vide infra*).

1.8 Research objectives

Long term objectives:

The long term objective of this MSc thesis is to prepare various cross-linked chitosan bead materials with improved adsorption properties toward orthophosphate and organophosphate species and to understand the molecular level details of the adsorption process.

Short term objectives:

In order to achieve the long term objective, several short term objectives need to be met. The short term objective of this master project are to synthesize, characterize, and study the adsorption properties of chitosan bead materials with variable levels of cross-linker. The bead materials vary according to the type and content of cross-linker (glutaraldehyde and epichlorohydrin) non-cross-linked chitosan beads. The chemical modification of chitosan enables the study of chitosan beads with variable textural properties and HLB character. A comparison of experimental parameters such as pH, concentration, temperature, and type of adsorbate (inorganic and organophosphate) provide information about the adsorption properties of such materials. The short- and long-term objectives are driven by several hypotheses, described below.

Hypotheses:

H1: Modified chitosan enhance the orthophosphate (P_i) sorption properties.

Chitosan in form of beads that are modified with cross-linkers such as glutaraldehyde (GA) and epichlorohydrin (EP) may show enhancement in sorption properties toward orthophosphate (P_i).

H2: Cross-linked chitosan beads possess enhanced sorption properties toward organo-phosphate.

An enhancement for organophosphate adsorption on the cross-linked chitosan beads can be expected due to previous results reported for the adsorption of an organoarsenical onto the chitosan polymers.[46]This study demonstrated that chitosan-based copolymers crosslinked with glutaraldehyde are versatile sorbents for the roxarsone uptake in aqueous solution. Cross-linked

chitosan-based polymers had greater sorption capacity. The favorable adsorptive properties reported by the Wilson group in this study suggested the potential of chitosan polymer sorbent materials for the efficient removal of organoarsenicals.

The modified chitosan beads have higher surface area and accessible functional groups (*e.g.,* OH and NH_2) which provide active binding sites for organophosphate. Besides, an organophosphate has phenol moiety which is organophilic in nature with a phosphate side chain that is hydrophilic. These moieties can adsorbed onto different sites of the chitosan beads with variable sorption affinity.

H3: Chitosan beads (cross-linked and non-cross-linked) doped with calcium ion possess enhanced sorption properties toward organophosphate.

Chitosan beads modified with metal cation species will show enhanced organophosphate adsorption.

H4: Molecular level studies of the adsorption process can provide insight on the molecular level aspects of adsorption and lead to improved adsorbent design.

Variable adsorption kinetic models (e.g., pseudo first order and pseudo second order kinetic models), and adsorption isotherms models (e.g., Langmuir, Sips, Dubinin-Radushkevich) can be employed to interpret the adsorption of phosphate species by chitosan beads. For instance, a previous study from by the Wilson research group indicated that kinetic studies showed an "apparent" negative value for E_a and $\Delta H^{\ddagger}$ for the adsorption of selenium due to a multi-step process. Individual steps involve contributions due to hydration multi-steps involving inner-sphere and out-sphere coordination of the adsorbate in the kinetic process.[47] The role of hydration effects on adsorption can be understood in greater detail by using various techniques such as Raman, DSC. In addition, pH studies reveal the role of chitosan functionalities on the sorption process. Accessibility of the surface functional groups can be evaluated using dye probe species (e.g., PNP, PHP) through determination of the functional group accessibility of the adsorption sites of the beads using spectroscopy.

1.9 Thesis outline

The following questions will be answered in this thesis: Does the type and mole ratio of cross-linkers have an effect on the bead sorption capacity? Chitosan beads cross-linked with two types of cross-linkers were synthesized and characterized at variable composition.

Does doping the beads with calcium affect the adsorptive properties of the beads? Cross-linked chitosan beads were impregnated with calcium and their adsorption properties were compared between doped vs. unmodified bead materials.

Can the mechanism and sorption capacity of phosphate species be understood through the adsorption of *p*-nitrophenol (PNP) and phenolphthalein (PHP)? The use of a surrogate dye probe such as PNP to evaluate the sorption capacity and relative surface area of the bead materials was studied. The analogous use of PHP in adsorption studies revealed the relative accessibility of OH groups on the adsorbent surface.

Finally, the question as to whether chitosan bead materials are capable of variable phosphate species removal was examined. The sorption properties of different phosphate species was studied at pH 8.5 to investigate the utility of the bead materials as adsorbents for the heterogeneous adsorption of phosphate species from aqueous solution.

Each chapter of this thesis will address part of each question proposed above. Following is a brief outline for each chapter:

Chapter 1 represents introduction of phosphate, chitosan bead and a literature review related to these subjects. Chapter 2 describes the instruments, experimental methods, synthesis procedures and experimental setups involved in the project. Chapter 3 describes the results and data analyses for the chitosan bead materials using theoretical and experimental results. Chapter 4 describes the results of water swelling and dye adsorption on bead materials in order to calculate important adsorption parameters such as surface area and porosity. Chapter 5 describes the adsorption and kinetic results for adsorption of phosphate. The study of isotherms under kinetic and thermodynamic conditions are described. A study of the effect of pH on the phosphate adsorption is outlined in chapter 5. Chapter 6 describes the conclusion and future work where some future studies are proposed to extend the results of this work. As well, field studies are proposed

which can be used for comparison of experimental results in order to demonstrate *proof-of-concept* and to further establish the utility of the chitosan bead materials for practical applications.

CHAPTER 2

2 MATERIALS AND METHODS

2.1 Introduction

For this chapter, methods and techniques (including analytical and instrumental) used in this project will be described. The materials and a synthesis protocol for synthesized chitosan beads also are included in this chapter.

2.2 Materials

Glutaraldehyde (GA), epichlorohydrin (EP), and low molecular weight chitosan (75–85% deacetylation, and a molecular weight range: 50,000–190,000 kDa) were obtained from Sigma–Aldrich Canada (Oakville, ON). All other materials (such as *p*-nitrophenol (PNP), *p*-nitrophenylphosphate (PNPP), KH_2PO_4, $CaCl_2$, acetone, acetic acid, sodium hydroxide, phenolphthalein (PHP), fluorescein, NaCl, KBr) also were purchased from Sigma–Aldrich Canada (Oakville, ON) used as received without further purification unless specified otherwise.

2.3 Synthesis

Figure 2.1 illustrates the steps involved in the procedure for making the cross-linked chitosan beads according to the phase-inversion method.[44] The methodology of bead preparation is described as follows. Chitosan (5 g) was dissolved in 2.0% glacial acetic acid solution (250 mL). The chitosan solution was dropped into a 0.5 M NaOH aqueous solution using a burette with an adjustable pipette tip of variable size (100–1000 mL) to enable the formation of spherical chitosan beads with a controlled size range. After imbibing the beads for a minimum of 16 h in aqueous NaOH (0.5M), the beads were washed with Millipore water to obtain a neutral pH in the filtrate washings.

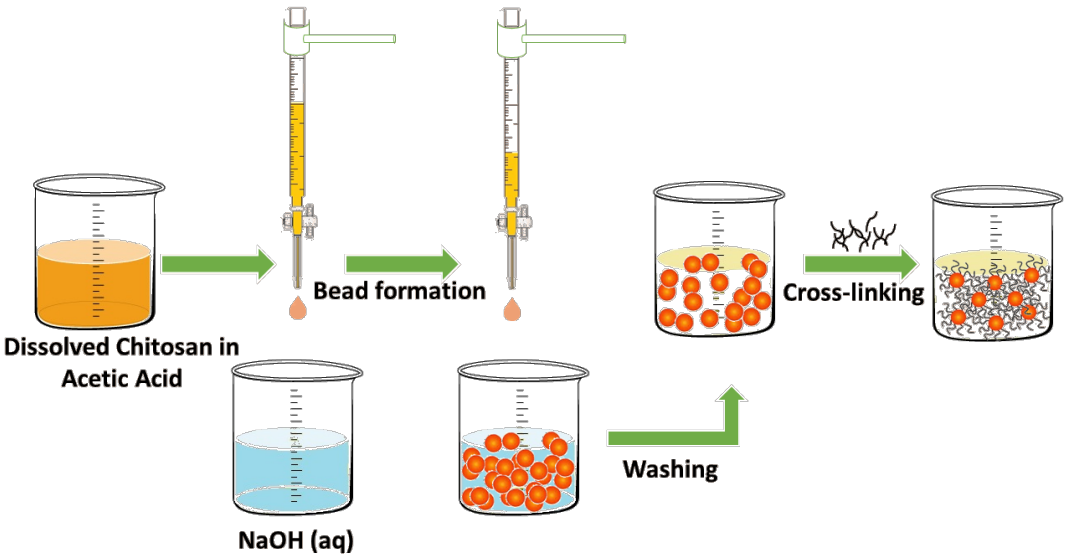

Figure 2.1 Schematic illustration of the preparation of cross-linked chitosan beads.

2.3.1 Cross-linked chitosan bead materials

Figure 2.2 schematically illustrates the formation of cross-linked chitosan beads with two types of cross-linker used in this study. An optimized cross-linked chitosan bead system was reported[44] using a stoichiometric excess (5 wt. %) of cross-linker. A cross-linker (GA and EP) of 2.5 wt. % corresponds to a 1:1 mole ratio (cross-linker: chitosan monomer) in Table 2.1. On the basis of complete cross-linking, the amount of cross-linker (2.5 wt. %) reached an optimal level of one cross-link between two monomer units of chitosan. The cross-linker content was studied at 2.5 and 5 wt. % to evaluate the composition effect.

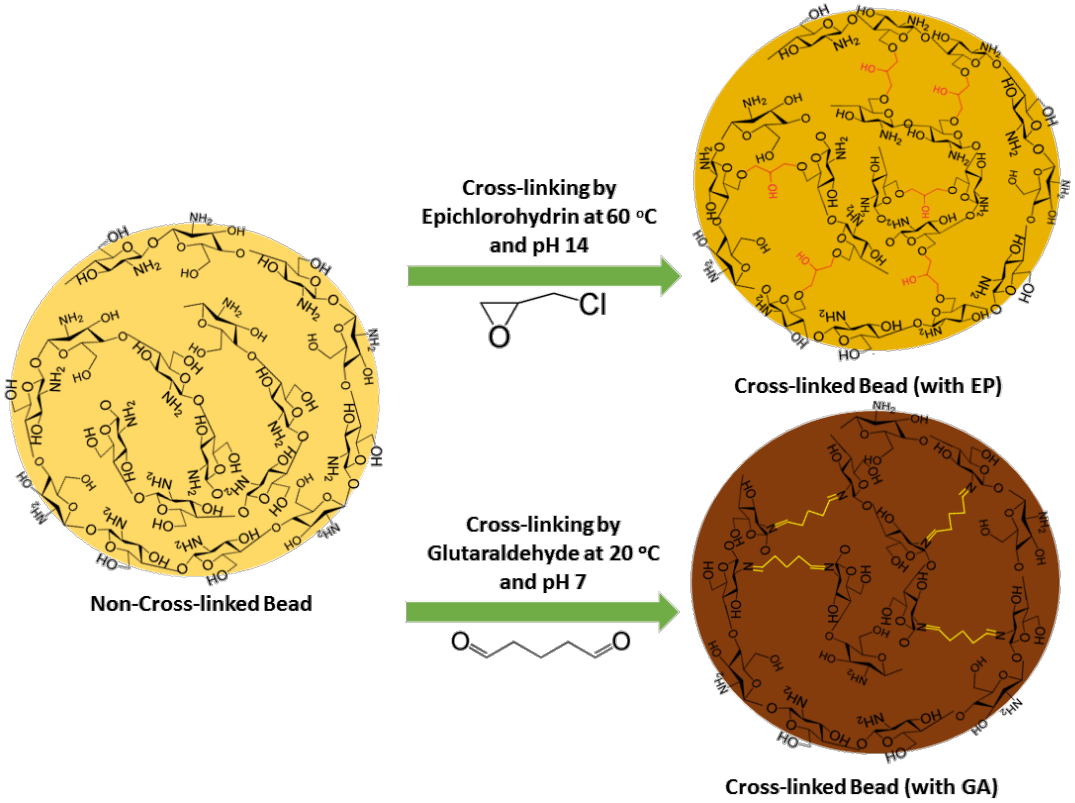

Figure 2.2 Schematic illustration of the cross-linking of chitosan beads with glutaraldehyde and epichlorohydrin cross-linkers.

2.3.2 Epichlorohydrin chitosan beads

The synthetic procedure is briefly summarized. The wet beads were cross-linked with 2.5 and 5.0 wt % EP. The cross-linking reaction occurred for 6 h at pH 14 with steady agitation. The cross-linked beads were immersed for 1 day and washed with 1 L of Millipore water to remove any unreacted cross-linker. The swelling characteristics of the beads in water were determined by weighing hydrated beads before and after drying at 60 °C to determine the hydrated and dry weight. The composition and sample ID of the bead systems are summarized in Table 2.1.

2.3.3 Glutaraldehyde chitosan beads

After preparation of the wet chitosan bead as describe above, the wet beads were cross-linked with 2.5 and 5.0 wt % GA. The cross-linking reaction occurred for 48 h for GA at pH 7 with steady agitation. The cross-linked beads were immersed for 1 day and washed with 1 L Millipore water to remove any unreacted cross-linker. The swelling characteristics of the beads in

water were determined by weighing hydrated beads before and after drying at 60 °C determine the hydrated and dry weight. The composition and sample ID of the bead systems are listed in Table 2.1.

2.3.4 Calcium doped chitosan beads

Figure 2.3 shows the materials design for doping the chitosan beads followed by cross-linking with two types of cross-linker units. Herein, the procedure for doping of cross-linked beads using calcium is briefly described. To ensure that adequate calcium is available to react with chitosan monomers, the number of chitosan units was calculated based on its weight, molar mass, and the degree of acetylation. The aqueous calcium solution was prepared by dissolving $CaCl_2$ in millipore water assuming that a 10-fold excess of calcium ions will be enough to guarantee a completed reaction between calcium and chitosan. Based on this assumption doping reaction is complete and the amount of calcium (0.1M) is adequate to reach an optimal level of doping. The composition and sample ID of the doped bead systems are listed in Table 2.1.

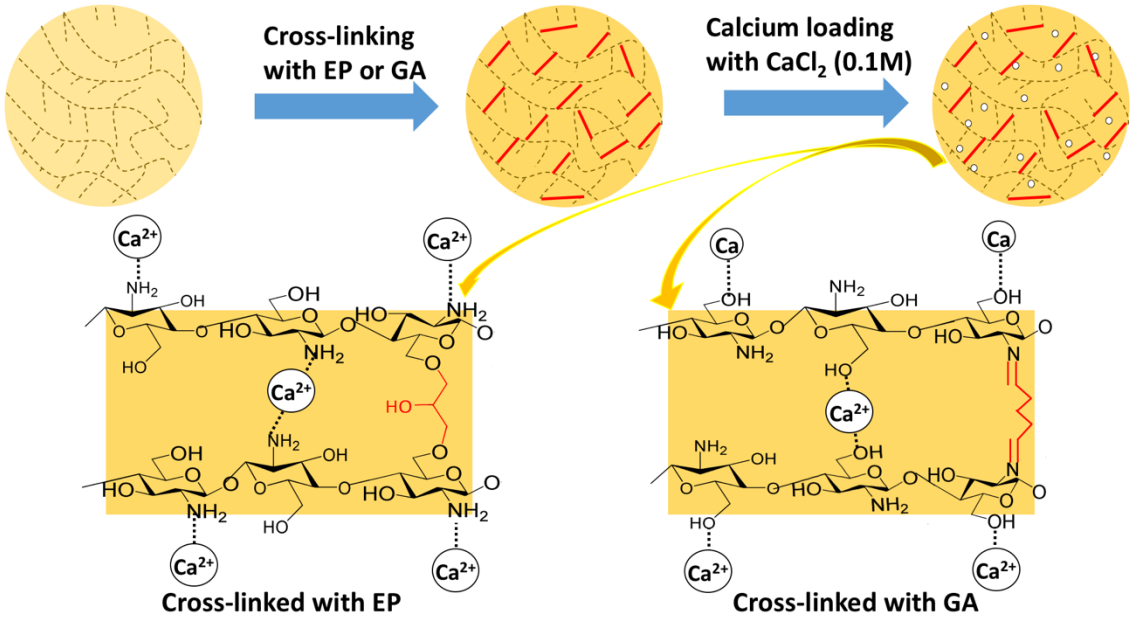

Figure 2.3 Illustration of cross-linking followed by calcium doping of chitosan beads using two different cross-linkers (Note: two proposed coordination models for structure of calcium doped chitosan including the bridge model (inside rectangular area) and the pendant model.

Table 2.1 Chitosan bead materials with variable composition and cross-linker (Glutaraldehyde (GA) and epichlorohydrin (EP).

Bead materials (Sample ID)	Chitosan mass(mg)	Cross-linker wt. %*	linker/Chitosan Mole ratio**	Calcium / Chitosan Mole ratio**
NCL	160 ±0.05	-	-	-
EP 2.5	160 ±0.05	2.5	1.7	-
GA 2.5	160 ±0.05	2.5	1.6	-
EP 5	160 ±0.05	5.0	3.4	-
GA 5	160 ±0.05	5.0	3.2	-
NCL-CA	160 ±0.05	-	-	10
EP2.5-CA	160 ±0.05	2.5	1.7	10
GA2.5-CA	160 ±0.05	2.5	1.6	10
EP5-CA	160 ±0.05	5.0	3.4	10
GA5-CA	160 ±0.05	5.0	3.2	10

*wt % is based on the cross-linker weight content in solution used for cross-linking.
** Given that the chitosan is fully deacetylated, and all chitosan monomers are available for cross-linking and the average chitosan molar mass is 120,000 g/mol, and amount of residual water content is negligible according to the TGA results.

2.4 Characterization

This section will describe the instrumental and analytical techniques for the structural characterization of prepared chitosan beads.

2.4.1 Characterization

2.4.1.1 FT-IR spectroscopy

FT-IR spectra were obtained with a Bio-RAD FTS-40 spectrophotometer, where 6 mg of sample was mixed with 60 mg of spectroscopic grade KBr with a mortar and pestle followed by drying at 60°C. The samples were analyzed as powders in reflectance mode where the Diffuse Reflectance Infrared Fourier Transform (DRIFT) spectra were obtained from multiple scans at 295

K. The spectral resolution was 4 cm^{-1} over the 400–4000 cm^{-1} region. DRIFT spectra were corrected relative to a background spectrum of KBr.

2.4.1.2 Raman spectroscopy

Raman spectra were obtained using a Renishaw system 2000 whose resolution (= λ/2) is 0.257 μm (laser spot size). Raman shifts were obtained at ambient temperatures by using an excitation wavelength at 785 nm laser with following operating conditions: spectral range (2000 ~ 500 cm^{-1}), power (20 mW with 50 % load), objective lens (20×), cosmic ray removal (On), detection time (10 seconds), and the number of accumulation scans (5 times).

2.4.1.3 Elemental analyzing

Carbon, Hydrogen and Nitrogen elemental content was obtained using a Perkin Elmer 2400 CHN Elemental Analyzer. The combustion oven temperature was above 925 °C while the reduction oven had a temperature over 640 °C. The instrument was purged using a mixture of pure oxygen and helium gas. The calibration standard was acetanilide. Both precision and accuracy of the results are within 3%.

2.4.1.4 UV–Vis spectrophotometry

A Varian Cary-100 Scan UV–Vis spectrophotometer was used to measure the absorbance spectra of PNP (λ_{max}=400 nm) and PNPP (λ_{max}=405 nm) directly in aqueous solution. Phosphate ion levels were indirectly estimated by colorimetric determination of a vanado–molybdo–phosphoric acid complex by measurement of the absorbance of the dye complex (λ_{max}=400 nm) at steady-state conditions.[48]

2.4.1.5 Thermal gravimetric analysis (TGA)

Weight loss profiles of the beads at various temperatures were measured using a thermogravimetric analyzer (TGA; Q50 TA Instruments). Samples were heated in open aluminum pans at 30 °C and allowed to equilibrate for 5 min prior to heating at 5°C /min up to 500°C.

2.4.1.6 Differential scanning calorimetry (DSC)

Differential scanning calorimetry (DSC) of the chitosan bead samples was acquired using a TA Q20 thermal analyzer over a temperature range of 25 to 400 °C. The scan rate was set to 10 °C /min, and dry nitrogen gas was used for regulating the sample temperature and sample

compartment purging. Samples were run in sealed aluminum pans where the tops of pans were punctured to release vapors produced during the temperature ramping cycle.

2.4.1.7 Solid state ^{13}C NMR spectroscopy (SSNMR)

Solid state ^{13}C NMR spectroscopy with a wide-bore (89 mm) 8.6 T Oxford superconducting magnet system equipped with a 4 mm CP-MAS (cross polarization with magic angle spinning) solids probe was employed for characterizing the samples. The acquisition and processing of spectra was carried out on a workstation console (Advance DRX360) running TopSpin 1.3 (Bruker Bio Spin Corp; Billerica, MA, USA) were used to control the parameters. Standard commercial pulse programs utilized were included in the TopSpin 1.3 software. Packing the samples were placed in 4 mm outer diameter zirconium oxide rotors capped with Teflon MAS rotor caps. Acquisition was carried out using MAS at a rotational speed of 5 kHz, 2-s recycle delay and 750 μs cross polarization time.

2.4.1.8 Scanning electron microscopy (SEM)

Scanning electron microscopy (SEM) was used for obtaining the surface images and studying the morphology of bead materials (SEM; Model JSM-6010, JEOL/EO). The bead samples were coated with gold and SEM images were collected under the following instrument conditions; accelerating voltage-10 kV, 9 mm working distance (WD), magnication-2000× and a sample spot size-50 at room temperature.

2.4.1.9 Confocal microscopy

A confocal microscope (BioRad MRC-1024) was employed for the investigation of the relative location of the adsorbate within the bead materials. The confocal microscope was equipped with a 15mWKrypton/Argon laser and FITC (excitation filter 470–490) filter sets. Individual beads were analyzed by horizontal scanning (section scanning). Chitosan beads were scanned before adsorption and the background of fluorescence was found to be negligible. Digital images were collected using personal computer and analyzed by the ZEISS LSM version 4.2 software.

2.4.1.10 Powder X-ray diffractometric analysis (PXRD)

Diffractometric analysis of bead materials was carried out using a PANalytical Empyrean Powder X-ray diffractometer. Monochromatic Co-Kα1 radiation was used while an applied voltage and current were set to 40 kV and 45 mA, respectively. Samples were mounted in a

horizontal configuration after crushing the beads to make the powder form. The PXRD patterns were measured in continuous mode over a 2θ range, where 2θ = 7–50° with a scan rate of 3.2° min^{-1}. The crystallinity index (Cr_I) was obtained by calculation from the height ratio between the intensity of the crystalline peak (I_{cr}) and amorphous peak (I_{AM}).

2.4.2 Swelling and wet porosity of chitosan beads

Swelling and wet porosity test for bead materials was conducted after the synthesis of the beads by calculating the weight lose corresponding to the solvent evaporation after drying process. Upon imbibing the chitosan beads in a suitable solvent, the diameter (D), the porosity (ε) of wet chitosan beads and swelling properties can be determined using Eq. (2.1), (2.2), and (2.3).[49]

$$D = \left[6 \frac{W_D/\rho_{CS} + \left((W_W - W_D)/\rho_W \right)}{\pi} \right]^{1/3} \quad (2.1)$$

$$\varepsilon = \frac{(W_W - W_D)/\rho_W}{W_D/\rho_{CS} + (W_W - W_D)/\rho_W} \times 100\% \quad (2.2)$$

$$\text{Swelling (\%)} = \frac{W_W - W_D}{W_D} \times 100 \quad (2.3)$$

W_W (g) is the weight of the hydrated bead material after removing non-absorbed water by tamping dry with filter paper; W_D (g) is the weight of the chitosan beads after drying; ρ_w is the density of water (1.0 g cm^{-3}); and ρ_{cs} is the anhydrous density of chitosan (0.87 g cm^{-3}). These measurements were obtained in duplicate. The density value above for chitosan represents the dry weight of chitosan in a hydrated volume of chitosan bead materials.

2.4.3 Surface coverage

The monolayer sorption capacity (Q_m) enables an estimate of the sorbent surface area (SA; m^2 g^{-1}) by Eq. (2.4) including the accessible surface volume (SV; m^3 g^{-1}) of the sorbent according to the quantity of dye adsorbed (V_{ads}) by Eq. (2.5).[50]

$$SA = \frac{A_m \times Q_m \times L}{N} \quad (2.4)$$

$$SV = \frac{Q_m \times L \times V_{PNP}}{N} \quad (2.5)$$

Q_m is the monolayer coverage of the sorbent defined by Eq. (1.4), A_m represents the cross-sectional molecular surface area occupied by PNP, where A_m for a *planar* orientation is 5.25×10^{-19} m^2 mol^{-1} and an *end-on* orientation is 2.5×10^{-19} m^2 mol^{-1}. L is Avogadro's number (mol^{-1}), N is the coverage factor which equals unity for PNP at these conditions, and V_{PNP} is the molecular volume of PNP (9.08×10^{-26} m^3).[50]

2.5 Sorption measurements

2.5.1 Dye sorption (*p*-nitrophenol, and phenolphthalein)

Fixed amounts (~10 mg) of the adsorbent (beads or chitosan powder) were mixed with 10 mL of *p*-nitrophenol (PNP) dissolved in 0.1M aqueous sodium carbonate–bicarbonate buffer using six-dram vials at variable concentration of PNP (5–10 mM). Samples were equilibrated at 293 K on a horizontal shaker table (SCILOGEX Model: SK-O330-Pro) for 24 h and 250 rpm. The initial concentration (C_o) was determined before and after adsorption (C_e) in triplicate at pH 8.5. The relative uptake of the adsorbate was determined by the difference between the initial blank (C_o) and residual PNP concentration (C_e) in solution after the adsorption process using eq. (1.4).

The surface accessibility of the hydroxyl groups of polysaccharides can be assessed using a dye adsorption method that employs phenolphthalein (PHP) as an adsorptive probe.[51] The variable decolourization of PHP occurs due to steric and electronic effects of polar functional groups such as hydroxyl functional groups on the adsorbent surface that form a complex with PHP. In this study, various chitosan bead systems were investigated at pH 10.5 and 20 °C with PHP solution (33 mM) at different dosage levels of beads.

2.5.2 Ortho-phosphate (P_i) adsorption

Fixed amounts (~10 mg) of each adsorbent (beads or chitosan powder) were mixed with 10 mL of solution that contain adsorbate (hydrogen phosphate ion; HPO_4^{-2}) in aqueous solution at pH 8.5. Samples were contained in 6 dram vials at variable concentration (30–200 ppm) of adsorbate and equilibrated at room temperature on a horizontal shaker table (SCILOGEX Model: SK-O330-Pro) for 24 h and 250 rpm. The initial concentration (C_o) was determined before and after adsorption (C_e) at 293 K at pH 8.5. The uptake of HPO_4^{-2} was measured in triplicate and the results were expressed as a difference between concentrations of the initial stock (blank) and residual adsorbate solution after the adsorption process, according to eq. (1.4). The error bars for the corresponding isotherm results denote the standard error determination.

2.5.3 Organophosphate adsorption

Fixed amounts (~10 mg) of the adsorbent in the form of beads were mixed with 10 mL of PNPP at variable concentration (5–70 mM). Samples were equilibrated on a horizontal shaker table (SCILOGEX Model: SK-O330-Pro) at 293 K for 24 h and 250 rpm. The concentration was determined in triplicate before adsorption (C_o) and after adsorption (C_e) in a sodium carbonate–bicarbonate (0.01 M) at pH 8.5. The relative uptake of the adsorbate was determined by difference between the initial blank (C_o) and residual PNPP concentration (C_e) in solution after the adsorption process using eq. (1.4). The error bars for the corresponding isotherm results denote the standard error determination.

2.5.4 Regeneration study

To study the adsorption–desorption profiles of an optimized chitosan bead system, a cycle of equilibrium adsorption–desorption experiments was performed. Desorption of phosphate was achieved by washing the bead adsorbed phosphate using a 50 mM NaCl solution. Since the adsorption of phosphate onto the chitosan beads is assumed to be primarily physical adsorption, saturation of the binding sites with monovalent salt at elevated levels resulted in desorption of the adsorbed phosphate by the chloride anion. The total and residual phosphate concentration was measured in triplicate by UV–vis spectroscopy, as described for the above isotherm studies above. The error bars for the corresponding isotherm results denote the standard error determination from triplicate uptake measurements.

2.5.5 Kinetic studies

Kinetic studies were conducted using "*one-pot*" setup at pH 8.5 and 20, 30, 40 °C.[52] The "one-pot" method differs from conventional batch methods since it enables the study of insoluble solid adsorbents in a single vessel without the requisite separation of the adsorbent (chitosan beads). The solution phase containing phosphate species was measured *in situ* by continuous sampling of fixed volumes at variable time intervals. The use of beads in the "*one-pot*" setup obviates the use of a semi-permeable barrier and offers some advantages over highly dispersed or colloidal solids due to the option of direct sampling and analysis (*in situ* or *ex situ*) to estimate the level of unbound adsorbate species.

Fixed amounts (~50 mg) of chitosan beads were mixed with 200 mL of solution containing adsorbate (HPO_4^{2-}) in aqueous solution at pH 8.5 in a home built glass vessel (*cf*. Figure 2.4) to allow study of ambient and variable temperature conditions. Sampling was done by sequential removal (2.5 ml) via over a time interval of 0-60 min using 50 mg/L phosphate solution.

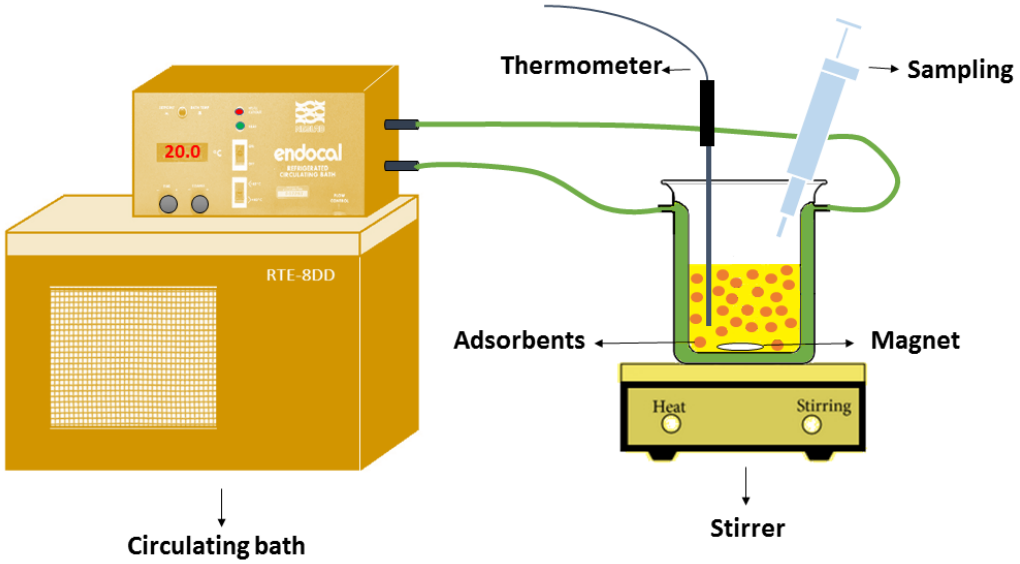

Figure 2.4 An illustration of the one-pot experimental setup for kinetic uptake studies of beads without barrier material with *in-situ* sampling of unbound adsorbate.

2.5.6 Kinetic equations and criteria of ''best-fit''

A non-linear form of the PFO model is given by eqn (2.6).[52]

$$Q_t = q_e(1 - e^{-k_1 t}) \qquad (2.6)$$

The time dependent uptake (Q_t) is the amount of phosphate adsorbed at time t (mg/g) where q_e is the adsorption capacity at equilibrium (mg/g), k_1 is the PFO rate constant (1/min), and t is the contact time (min).

The PFO rate constant (k_1) was determined from the best-fit results by non-linear least squares fitting using eqn (2.7). The adsorption kinetics may be described by the PSO model, where one expression of the non-linear form is given by eqn (2.7).[52]

$$Q_t = \frac{k_2 q_e^{\,2} t}{1 + k_2 q_e t} \qquad (2.7)$$

Q_t is the amount of adsorbed (mg/g) phosphate by the adsorbent at any time, k_2 is the PSO rate constant (g/mg.min), and q_e is the amount of phosphate adsorbed at equilibrium (mg/g).

The criteria of ‘‘best fit’’ between the kinetic models and the experimental results was determined by the best-fit (R^2) and the chi-square distribution (χ^2) by eqn (2.8) at the 95% level of confidence. The χ^2 minimization is a more sensitive best-fit criterion where χ^2 is the difference between the experimental ($Q_{e,i}$) and calculated ($Q_{c,i}$) uptake values, and N represents the number of experimental data points.

$$\chi 2 = \sum \sqrt{\frac{(Q_{e,i} - Q_{c,i})}{N}} \qquad (2.8)$$

2.6 pH studies

2.6.1 pH at point of zero charge (pzc) and potentiometry

The pH_{pzc} of the adsorbents were measured using the method reported by Noh and Schwarz[53] which relates to the measurement of the equilibrium pH after equilibration of suspensions of adsorbent in Millipore water containing NaCl (0.01 M) for 24 h under argon gas. The initial pH of the suspension was adjusted over a range of values (pH 2–12) using HCl (0.01 M) or NaOH (0.01 M). After measurement of the equilibrium pH, the limiting value was taken as the pH_{pzc}. A potentiometric titration method was used for the pK_a determination of chitosan. Chitosan powder (200 mg) was dissolved with stirring in 32 ml HCl (0.1 M) for 10 h, where the final pH of the solution was measured with a pH meter (Model Acumen 910) while the solution was titrated by NaOH (0.1 M) solution. As well, single point adsorption conducted for adsorption of hydrogen phosphate ion (HPO_4^{-2}) at different pH values to study the effect of pH on adsorption.

2.6.2 Phosphate and chitosan speciation curves

Based on the speciation curves for phosphate and chitosan a prediction was proposed for prediction of the interaction between adsorbents and adsorbates.

CHAPTER 3

3 RESULTS AND DISCUSSION: Synthesis and characterization of chitosan beads

One of the hypotheses for this project was outlined in Chapter 1; does modified chitosan enhance the phosphate sorption properties. In order to address this hypothesis, the cross-linked and calcium doped chitosan bead materials were synthesized. For this section, the cross-linking and calcium doping of chitosan bead materials will be discussed. In addition, instruments and methods used for characterization will be described in this section which may serve as a lead-up to the results and discussion in the following sections.

3.1 Synthesis

Photographic images of several types of synthetic chitosan bead systems; without cross-linking and two types of cross-linked beads (EP 2.5 and GA 2.5) are shown in Figure 3.1. The colour of the final products was a dark brown color for beads cross-linked with glutaraldehyde subtle variations that are seen according to the relative ratio of glutaraldehyde employed. Products with darker coloration were observed as the content of the glutaraldehyde increases; with all other reaction conditions held constant. The colour of the final products was almost transparent yellow color for beads cross-linked with epichlorohydrin. Products with darker color were observed as the content of the glutaraldehyde increases, where all other reaction conditions were held constant. EP2.5 appears to have the lightest colour and GA5 is the darkest coloured material.

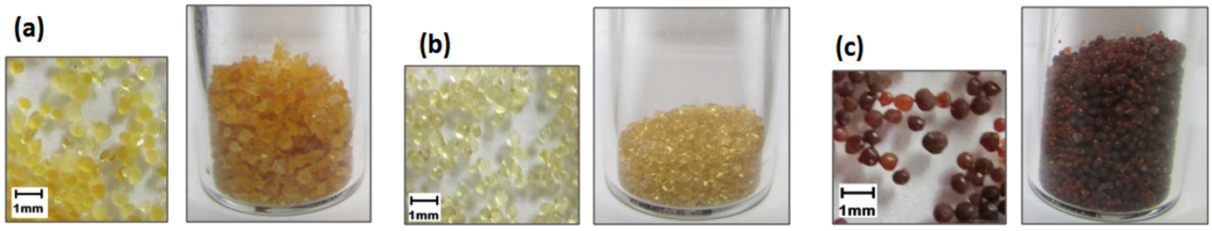

Figure 3.1 Photograph images of chitosan beads: (a) beads without cross-linking), (b) EP 2.5 beads, and (c) GA 2.5 beads.

3.1.1 Cross-linking

Cross-linked chitosan beads were prepared with variable weight content of GA and EP. The epoxide ring of EP can undergo nucleophilic substitution to form ether bonds via the deprotonated hydroxyl groups of chitosan (*cf.* Fig. 3.2).[40,54]

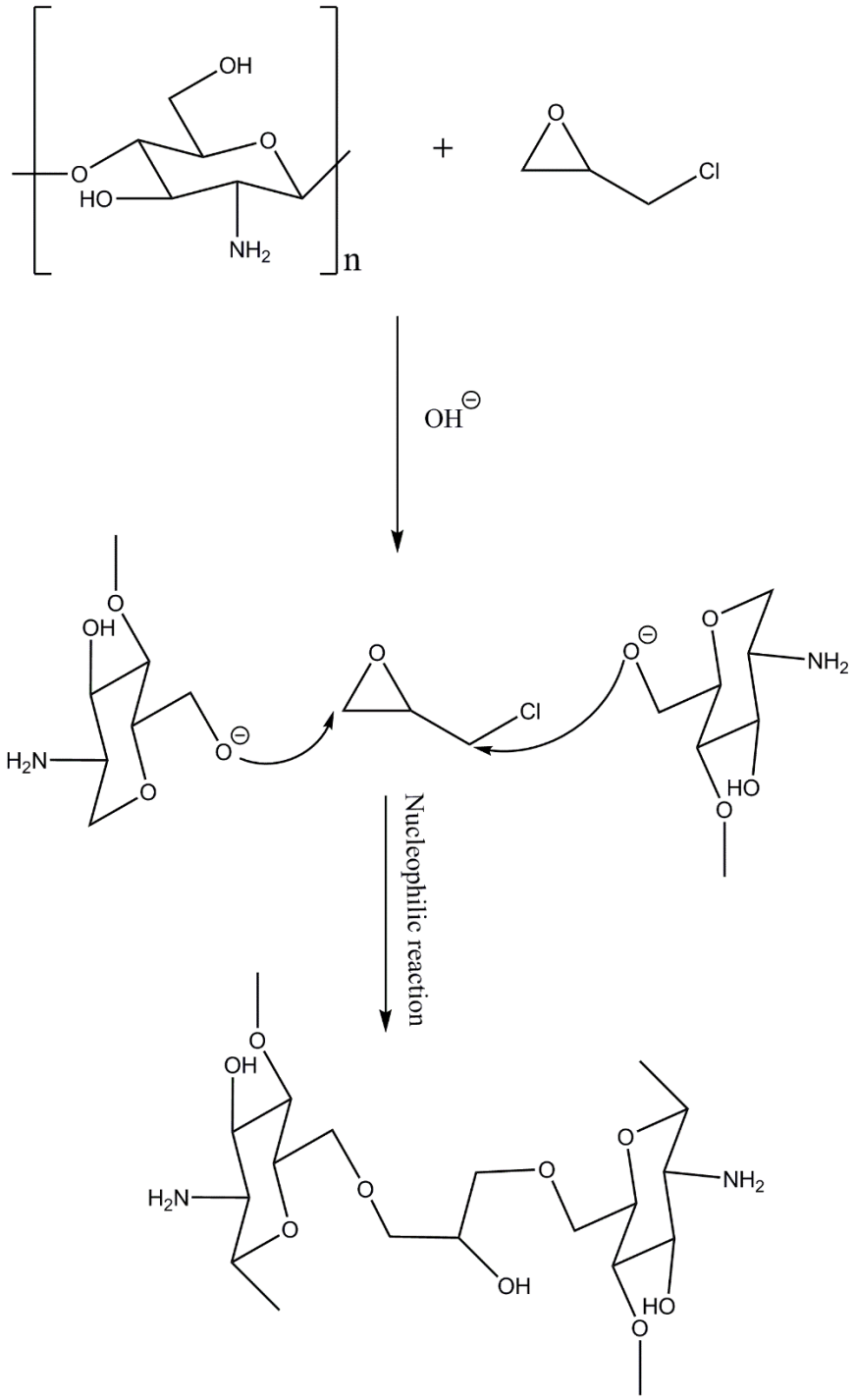

Figure 3.2 Cross-linking mechanism of chitosan and ECH under alkaline conditions.

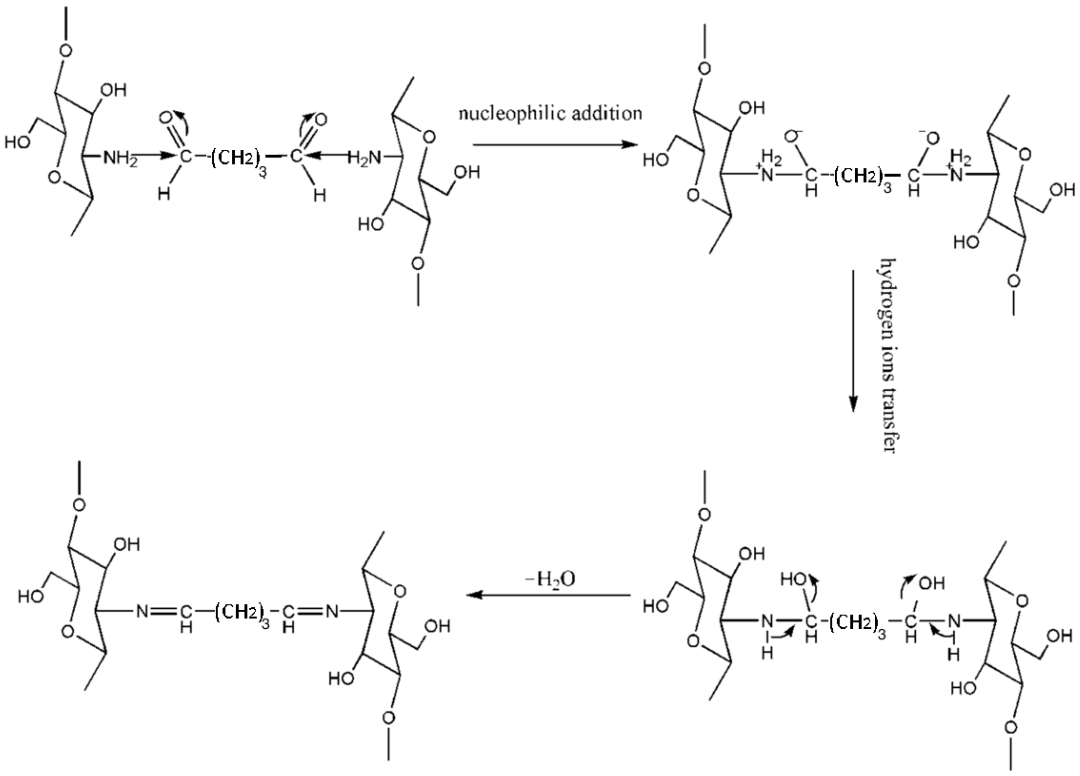

Figure 3.3 Mechanism for reaction of chitosan and glutaraldehyde (GA). The aldehyde groups of GA form imine bonds with the amine groups of chitosan at C-2 via the Schiff base reaction.[55]

3.1.2 Calcium doping

Calcium doping also known as coordinate [e.g., Ca(II)] crosslinking of chitosan. The effect of metal ion coordination will disrupt the H-bonding between adjacent polymer units, thereby creating favorable binding sites for adsorbates. The structure of the calcium-imbibed systems for different chitosan bead materials is poorly understood. However, the results infer the role of the bridge and pendant models of calcium-imbibed chitosan beads shown in Fig. 2.3.

3.1.3 Yield and characteristics of the cross-linked chitosan beads

The yield was calculated assuming that all the cross-linkers reacted with the monomer units of chitosan according to the mole content of the available amine groups according to the degree of deacetylation and availability of hydroxyl groups. To calculate the yield for materials cross-linked with the glutaraldehyde, it is assumed that all the glutaraldehyde was cross-linked with chitosan,

either through an aldol condensation or through an amine-catalyzed aldol addition. Both reactions resulted in the loss of two water molecules for every equivalent of glutaraldehyde cross-linked. Therefore, the molar mass of the product ($M_{Chi\text{-}GA}$) was calculated using Eqn 3.1.

$$M_{Chi\text{-}GA} = M_{Chi} + nM_{GA} - 2nM_{w} - M_{res} \qquad (3.1)$$

To calculate the yield percentage for materials cross-linked with the epichlorohydrin, it is assumed that all the cross-linkers were cross-linked with chitosan through ring opening of the epoxy group on EP. The complete reaction resulted in the loss of one HCl molecule for every molecule of EP that undergoes cross-linking. Therefore, the molar mass of the product ($M_{Chi\text{-}EP}$) was calculated using Eqn 3.2.

$$M_{Chi\text{-}EP} = M_{EP} + nM_{GA} - nM_{HCl} - M_{res} \qquad (3.2)$$

Herein, the molecular weight of chitosan (M_{Chi}) ranged between 50,000-190,000 g/mol where an average value of 120,000 g/mol was used. Unreacted glutaraldehyde (M_{Glu}) and epichlorohydrin (M_{EP}) had a molecular weight of 100.1012 and 92.52 g/mol, respectively. Since more than one type of cross-linker was added, the total molecular weight was multiplied by the number of cross-linkers molecules added (n) for a single chitosan. Lastly, residual solvents (M_{res}) remaining in the polymer can be determined using TGA which was considered negligible.

The product yield (%) of cross-linked bead materials is listed in Table 3.1. Accordingly, the cross-linking of two chitosan monomers occurs with one equivalent of GA and involves the loss of two water molecules (at pH 5–7), while the cross-linking of two chitosan monomers with EP involves the loss of HCl at alkaline pH.

Table 3.1 Product yield (%) of cross-linked bead materials congaing either Glutaraldehyde (GA) or epichlorohydrin (EP).

Bead materials (Sample ID)	Product Yield (%) *
NCL	-
EP 2.5	83.1
GA 2.5	63.3
EP 5	65.8
GA 5	40.5

* Given that the average molar mass is 120,000 $g.mol^{-1}$, and amount of residual water content is negligible according to the TGA results

3.2 Characterization

3.2.1 Material characterization

3.2.1.1 Elemental analysis

Elemental Analysis (EA) is a common technique used for determination of the relative amount of carbon, hydrogen and nitrogen (C, H and N) composition through combustion analysis. In the materials containing impurities such as unreacted starting materials, residual solvents and moisture, the results from this technique provide quantitative results with variable accuracy, depending on the chemical composition of the reactant species.[56] If the relative CHN content of chitosan and the cross-linkers vary considerably, the CHN results of the product may provide greater insight on the product composition. EA is useful when comparison between the theoretical composition with experimental values is possible. In order to calculate a theoretical estimate, the weight of the products from a polymerization reaction, an understanding of the reaction mechanism is necessary. Several reaction mechanisms have been proposed involving chitosan/GA and chitosan/EP (two-component) polymerization reactions. The theoretical CHN analysis was calculated based on the assumption that cross-linking reaction was complete.

Elemental analyses for the various systems are listed in Table 3.2. The CHN results do not provide unequivocal support the type of functional groups. The variable composition of the chitosan beads according to the different types of cross-linkers provides additional support of the cross-linking process. The results from the CHN analysis are unlike the TGA results since a facile qualitative measurement of cross-linker content is possible from the integrated line intensity of the

thermogram results (cf. vide infra). According to CHN results, the elemental C content (%) would increase as more GA and EP cross-links are formed. As well, there is no N contribution from the EP cross-linker; however, the N content decreases as the level of cross- linking with GA increases. This was shown where the percent by weight of C increases from 40.9% in Non-cross-linked chitosan bead (NCL) up to 51.4% and 43.3% for GA 2.5 and EP 5 bead systems, respectively. As stated before, a theoretical calculation for the elemental composition of the beads was carried out to provide further interpretation of the CHN microanalyses results. The theoretical estimates are in reasonable agreement based on residual water content (ca. 3–4%) when compared to the experimental values, where relatively minor variations are noted for the difference in CHN values; 3.26%, 0.0%, and 0.96%.

Table 3.2 Elemental CHN analysis of chitosan beads with and without cross-linking.

Sample ID	Experimental (%)				Theoretical (%) **				Difference %***			
NCL	**C**	**H**	**N**	**O***	**C**	**H**	**N**	**O***	**C**	**H**	**N**	**O**
EP 2.5	40.9	6.8	7.7	44.5	44.7	6.8	8.7	39.8	-3.8	0.0	-1.0	4.7
GA 2.5	41.9	6.7	5.5	45.9	47.1	6.9	7.6	38.4	-5.2	-0.2	-2.1	7.5
EP 5	51.4	6.6	4.2	37.8	47.5	6.2	3.2	43.0	3.9	0.4	1.0	-5.2
GA 5	43.3	6.5	5.5	44.7	46.6	6.9	7.8	38.8	-3.3	-0.4	-2.3	5.9
EP 2.5	50.6	6.9	3.9	38.6	46.7	6.5	10.6	36.2	3.9	0.4	-6.7	2.4

*Calculated by summing the percentages for C, H, and N and subtracting by 100%.
** A theoretical calculation for the elemental composition of the polymers can be calculated by assumptions: known average molar mass (120,000 $g.mol^{-1}$), percentage of deacetylation (80%), residual water of chitosan (negligible according to TGA data), and terminal monomers.
*** The differences were obtained by subtracting the experiential by theoretical results.

3.2.1.2 FT-IR Spectroscopy

The FTIR spectra of chitosan beads are given in Figures 3.4 and 3.5. The prominent band for each bead material occurs in the 3400–3500 cm^{-1} region corresponding to –OH and $–NH_2$

stretching. IR bands near 2900 cm^{-1} correspond to aliphatic C–H stretching, and the signature at 1635 cm^{-1} corresponds to $–NH_2$, while the band at 1380 cm^{-1} corresponds to –CH symmetric bending vibrations of –CHOH.[44,57] The IR band near 1100 cm^{-1} was attributed to C–O stretching of C–O–H groups. Since 20–25% of chitosan contains acetyl groups, the corresponding carbonyl signature above 1710 cm^{-1} may be assigned to pendant aldehyde groups where the GA is cross-linked at one end of the linker [*cf.* Figure 3.4; panels d and e]. The vibrational band at 1660 cm^{-1} indicates the carbonyl signature of an acetyl group. The signature at 1640 cm^{-1} overlaps with the imine group and provides support that cross-linking of chitosan occurs with GA. Figure 3.5 illustrates the FTIR spectra of calcium doped chitosan beads. The coordination of Ca^{2+} with chitosan according to the ‘‘bridge’’ model (*cf.* Fig 2.3) is supported by an enhancement of the C=O band at around 1150 cm^{-1}. N-H bending spectrum of amine group shows a spectral shift from 1591 to 1560 cm^{-1} in doped samples providing additional support for the formation of Ca^{2+} complexes. The bands above 3500 cm^{-1} is observable for calcium doped chitosan beads, but these characteristic peak for samples cross-linked followed by doping is not readily apparent which suggest that fewer amine groups are available on the surface of previously cross-linked materials with the organic cross-linker.

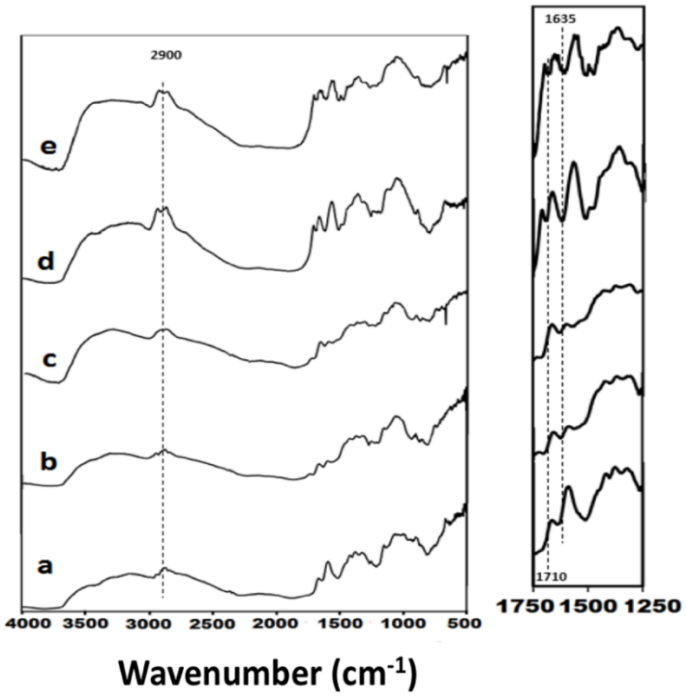

Figure 3.4 FT-IR spectra for different chitosan beads; where (a) NCL, (b) EP 2.5, (c) EP 5, (d) GA 2.5, and (e) GA 5. Note Note: The ordinate units are not normalized with respect to each spectrum.

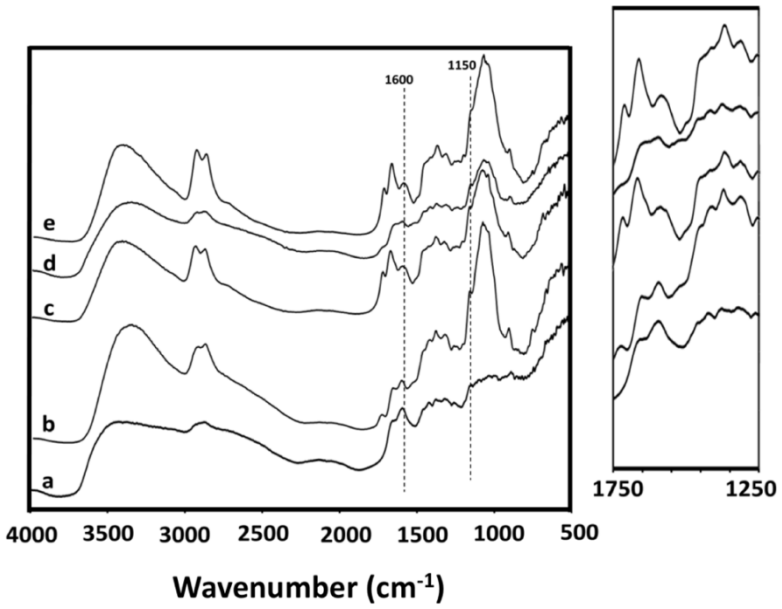

Figure 3.5 FT-IR spectra for different chitosan beads doped with calcium; where (a) NCL, (b) EP 2.5-CA, (c) GA 2.5-CA, (d) EP 5-CA, and (e) GA 5-CA. Note: The ordinate units are not normalized with respect to each spectrum.

3.2.1.3 Thermogravimetric analysis (TGA)

The level of cross-linking for chitosan beads was estimated by the decomposition profile of the cross-linked beads relative to the thermogram of the unmodified chitosan powder, as shown by the DTG results in Figure 3.6. A decomposition temperature between 200°C and 250°C occurs for cross-linked beads and at a higher temperature range (250°C and 350°C) for chitosan beads without added cross-linker. The thermal event at 425°C and 475°C correlate to the decomposition of linker units of GA and EP, respectively. The reliability of this approach depends on well-resolved thermal decomposition events for chitosan and the respective cross-linker units.

The result of thermal gravimetric analysis for doped samples are shown in Figure 3.7. The thermal event of doped samples appeared at lower temperature compare to nod-doped samples. This reduction in thermal stability relates to the effects of doping because it likely reduces the thermal stability due to changes in heat capacity. Change in the structure affects heat capacity by attenuation of the intermolecular hydrogen bonding between neighboring chitosan polymer units. The greater thermal stability of cross-linked chitosan corresponds to the presence of Ca^{2+} complexes, according to the observed activation energy and temperature effects of the degradation

process.[58] Beads doped with Ca^{2+} showed another thermal event between 200–300 ºC range (*cf.* Figure 3.7), indicating that calcium may be bound at multiple coordination sites of chitosan.[59] Thermal events in the 300–500 ºC range are attributed to the glutaraldehyde and epichlorohydrin cross-linking effects because of the greater thermal stability of such copolymers, as reported previously.[60]

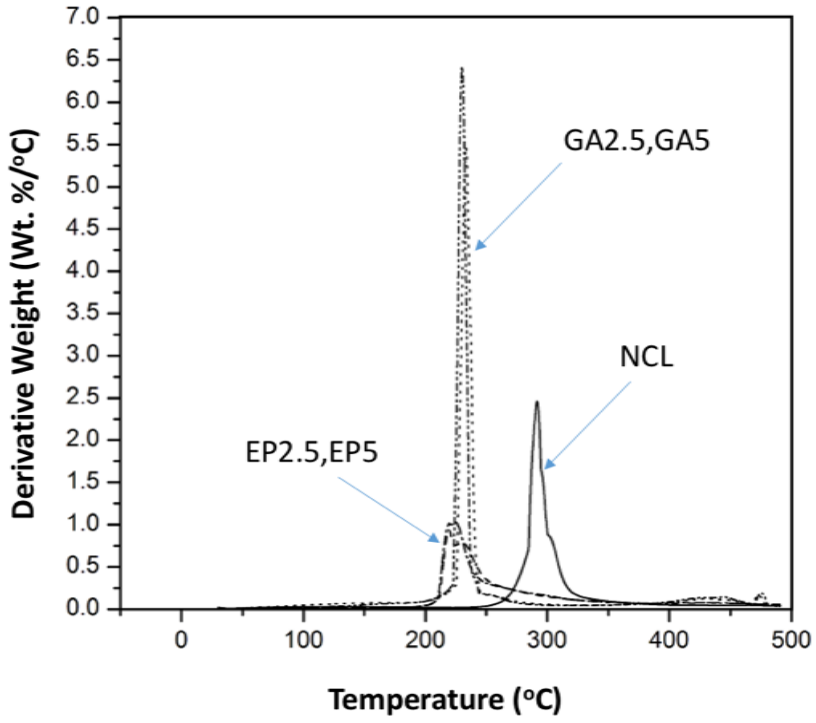

Figure 3.6 TGA results for different chitosan bead materials.

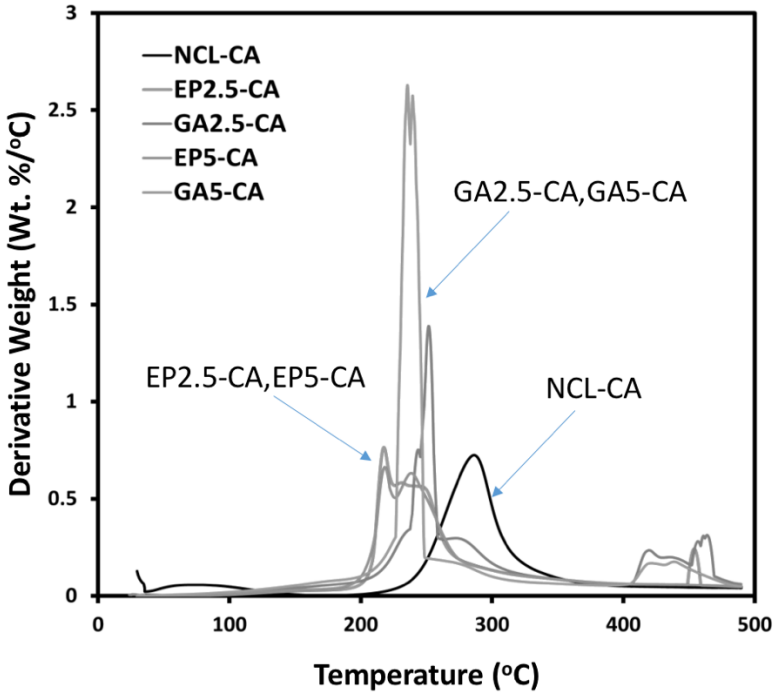

Figure 3.7 TGA results for different chitosan bead materials.

3.2.1.4 Scanning electron microscope (SEM)

SEM images for several bead materials are shown in Figure 3.8. The SEM results illustrate that the cross-linked chitosan beads [*cf*. Figure. 3.8 (c, d)] have a regular microporous structure compared with beads without cross-linking [cf. Figure 3.8(a)]. An image of the hemisphere structural view of cross-linked chitosan beads are shown in Figure 3.8 (d, f). The results reveal that the outer surface layer of beads is amorphous and cross-linked, while the core of the bead has a layered textural porosity similar to surface of NCL bead systems. It should be point out that the preferably outer surface of the chitosan bead undergoes cross-linking relative to the core side.

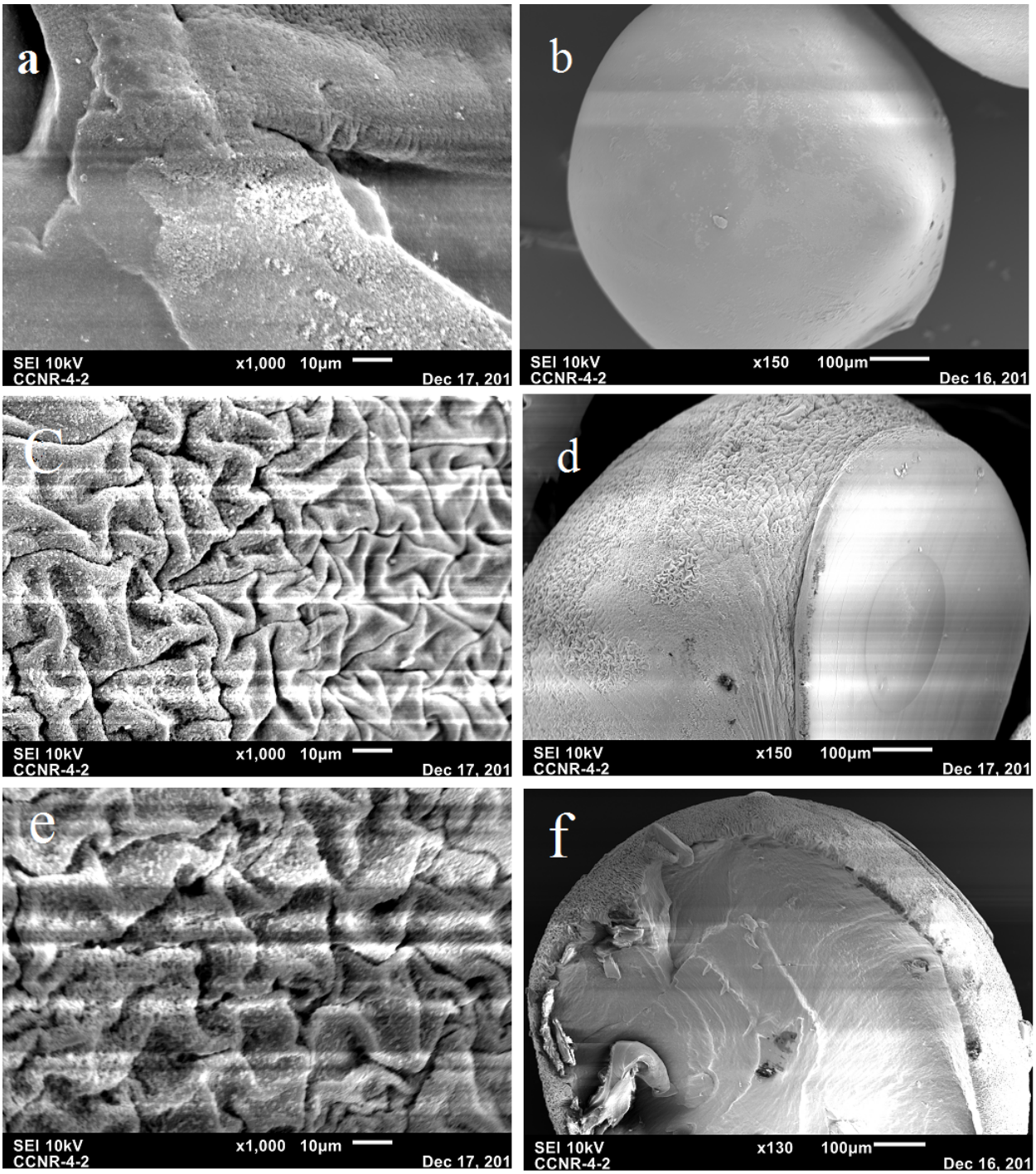

Figure 3.8 SEM images of (a, b) NCL beads; (c, d) EP cross-linked bead systems; and (e, f) GA cross-linked beads.

3.2.1.5 Powder X-Ray Diffraction (PXRD)

The structural properties of chitosan after cross-linking and doping with calcium was investigated by means of PXRD, which provides information on the degree of sample crystallinity. The XRD pattern of non-cross-linked chitosan bead (NCL) displayed two sharp diffraction peaks at 2θ = 10° and 20°, indicating the high crystallinity of chitosan. The occurrence of abundant hydroxyl and amino groups contribute to the crystalline nature of chitosan. Although bead materials cross-linked with EP do not display sharp XRD signatures but show a dissimilar spectral pattern as chitosan powder, indicating that the structure of NCL is not preserved. With reference to the materials cross-linked with GA, the characteristic peaks at 2θ at 10° disappeared, and a very weak and broad peak centered at 2θ = 15° appeared (*cf.* Fig. 3.9). This difference in XRD patterns was attributed to the cross-linking reaction that parallels the reduction in crystallinity upon crosslinking of chitosan. This is due to deformation of the hydrogen bonds in original chitosan after the substitution of hydroxyl and amino groups, which noticeably reduce the regular packing arrangement of the chitosan chains and result in the formation of an amorphous structure. Doping with calcium has significant effects on the XRD signature at 2θ = 10°, in accordance with a reduced crystallinity of bead materials due to calcium doping. The structural change of chitosan due to calcium doping shows suggests that calcium may introduce defects into the hydrogen bond network that parallels the effect of covalent cross-linking via EP or GA, described above.

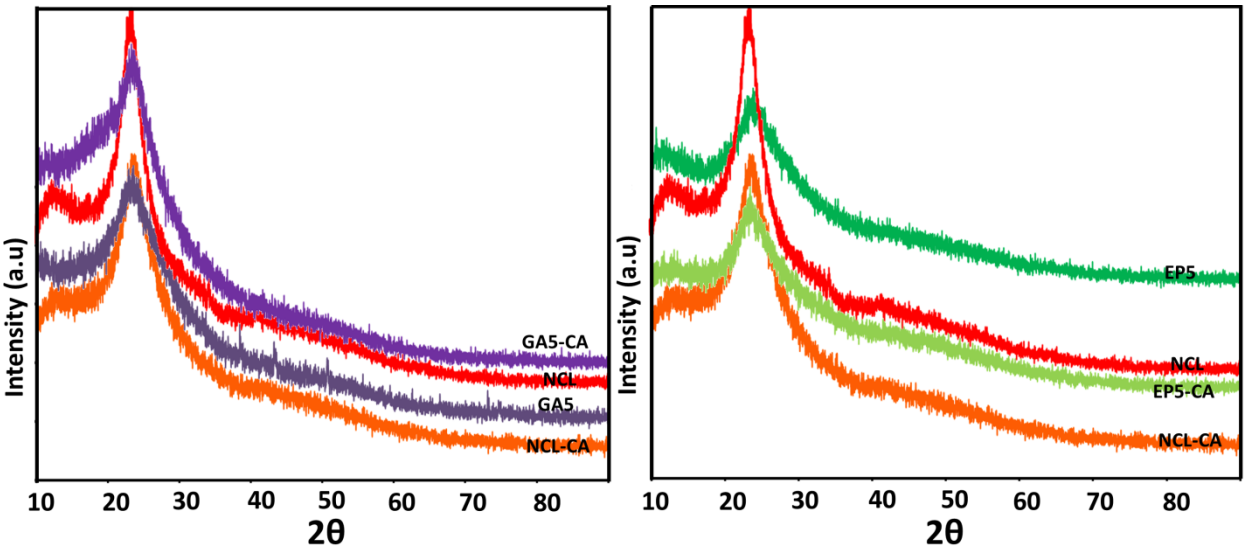

Figure 3.9 PXRD pattern of different chitosan bead materials.

3.2.1.6 Solid-state NMR studies

The characterization of the bead materials has limitations due to alteration of the structural properties after dissolution. The effect can be understood by desorption of calcium ions upon dissolution of chitosan. However, the greater issue is the limited solubility of chitosan materials in solvents. Limited choice exits such as urea/NaOH or ionic liquids. Therefore, solid- state NMR spectra were obtained for samples using CP-MAS NMR methods, as shown in Fig. 3.10 and 3.11. A comparison of the spectra for the cross-linked materials indicates greater line broadening occurs relative to chitosan powder and NCL. The broadening is due to the reduced chain dynamics (longer correlation times) of the polysaccharide upon cross-linking, as reported in a previous study for polymers cross-linked with EP and GA.[61,62] Generally, spectra observed for each chemical shift in the different polymers and calcium doped polymers all have similar patterns which indicates that level of incorporation of calcium is low. However by introducing calcium to the chitosan structure even greater line broadening occurred. Broadening can occur in solids due to strong spin-spin coupling and short T2 relaxation times so that the resonances are spread over a large spectral bandwidth resulting in a decrease in resolution and peak amplitude. Bonding the calcium with chitosan results in more rigidity in the structure so the stronger spin-spin coupling is required.

The C1 site of the chitosan units was assigned to 105.3 ppm, C4 to 83.6 ppm, C3-5 to 57.6, C6 to 60.8 ppm and C2 to 57.7 ppm. The carbonyl carbon (C7) at 173.0 ppm corresponding to the acetyl groups is not observable may due to high deacetylation degree of used chitosan or chosen pulse parameters and delay times was not optimized to observed the carbonyl signature. Nevertheless, appearance of CH_3 spectra to 23.9 ppm indicated the presence of acetyl groups of chitosan. Increasing in the intensity of chemical shift at 60.8 due to the C6 group can confirm successful cross-linking with EP. The formation of the C=N bond between chitosan and glutaraldehyde was verified by presence of C=N resonance at 149 ppm.

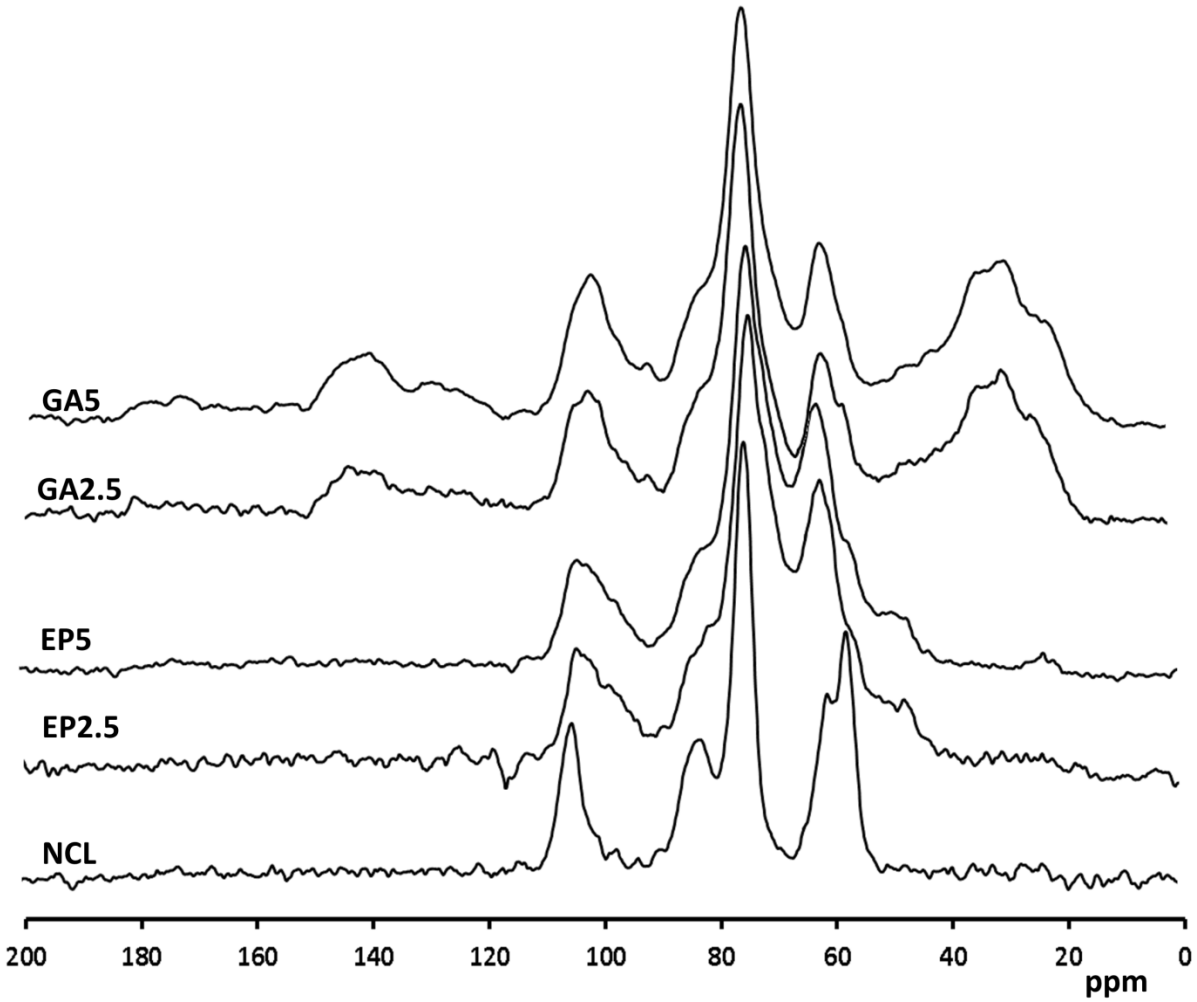

Figure 3.10 Solids ^{13}C NMR spectra of different chitosan bead materials. Spectral acquisition used MAS at a rotational speed of 5 kHz, 2-s recycle delay and 750 μs cross- polarization time.

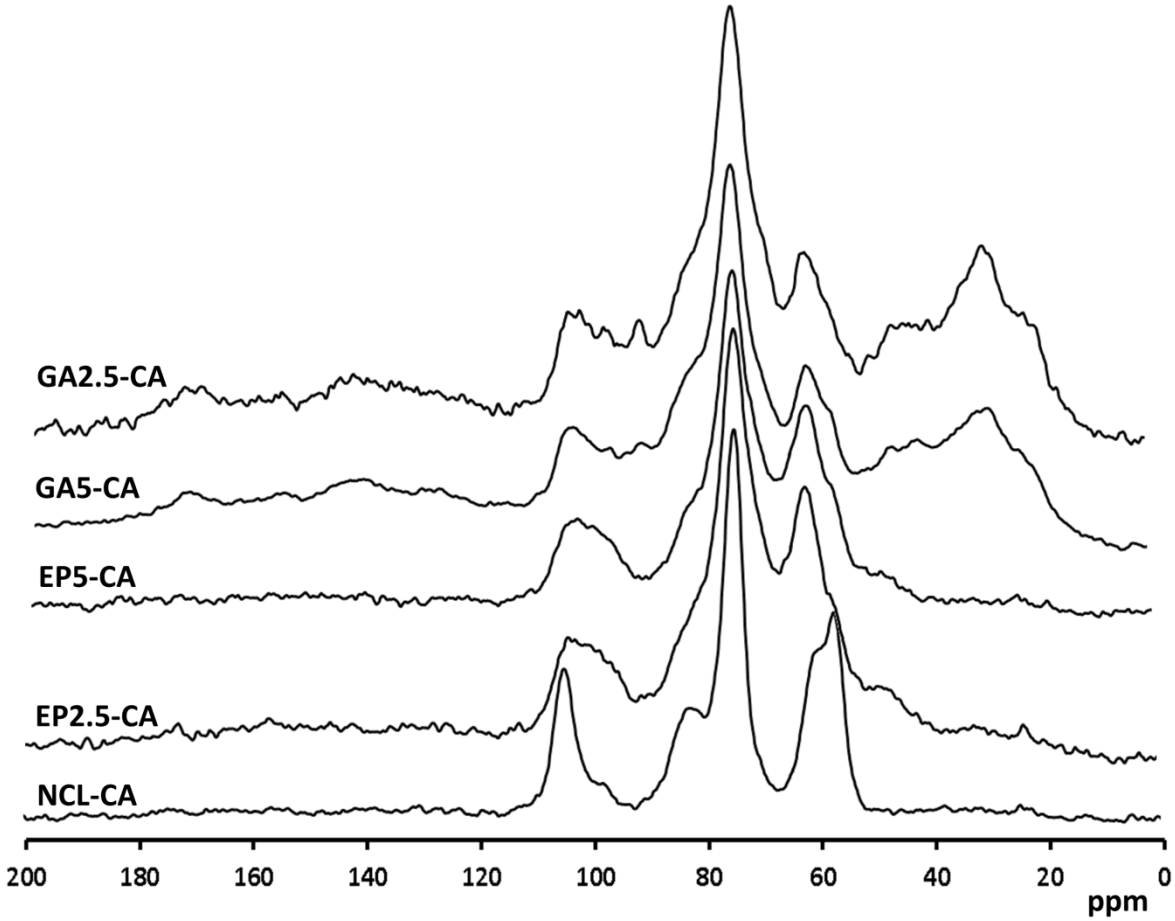

Figure 3.11 Solids ^{13}C NMR spectra of different chitosan bead materials after doping with calcium. Acquisition was carried out using MAS at a rotational speed of 5 kHz, 2-s recycle delay and 750 μs cross-polarization time.

3.2.2 Analytical characterization

3.2.2.1 Determination of chitosan pK_a

Chitosan is soluble in acidic solution due to the protonation of free amine groups (*cf.* eqn.3.3).

$$R\text{-}NH_3^+(aq) + H_2O(l) \rightleftharpoons R\text{-}NH_2(s) + H_3O^+(aq) \qquad (3.3)$$

$$k_a = \frac{[H_3O^+]}{[R - NH_3^+]} \qquad (3.4)$$

At the point where [R-NH_2] is equal to [R-NH_3^+], eqn (3.4) will reduce to K_a= [H_3O^+], so that pK_a= pH.[63] This allows a determination of the pK_a of the protonated amine groups in chitosan using a potentiometric titration as shown in Fig. 3.12. The potentiometric results for chitosan include two inflections, where the first point correspond to the equivalence points in the titration of the HCL with NaOH, and second point corresponds to the titration of protonated amine groups of chitosan amine groups (R-NH_2) with NaOH. The estimated pH by this method was 6.2, in agreement with an independent estimate for the pK_a value of commercial chitosan.[55]

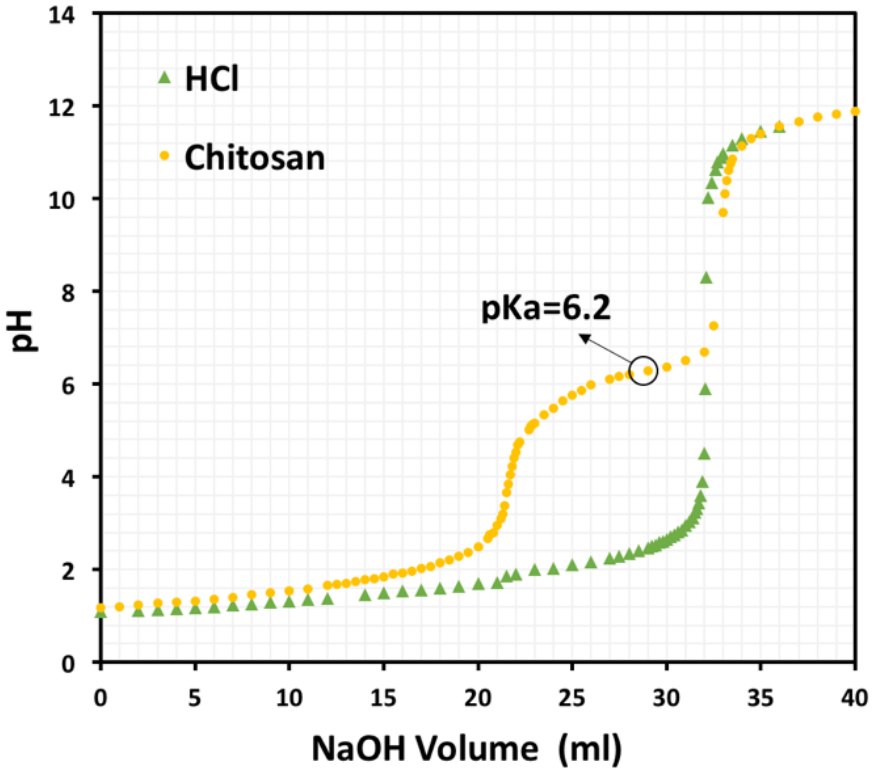

Figure 3.12 Potentiometric titration of chitosan and aqueous HCl solution at 295 K.

3.2.2.2 pH at point of zero charge (pH_{pzc})

The results of pH_{pzc} (*cf.* Fig. 3.13) yield the following calculated values for the chitosan bead materials listed in parentheses: NCL bead (6.3), GA 2.5 (6.9), and EP 2.5 (7.1). At pH values below the pH_{pzc}, the adsorption sites on the surface are protonated and the surface has a net positive charge. At pH values above the pH_{pzc}, the surface has a negative charge. Electrostatic interactions between positively charged surfaces at acidic conditions favor the adsorption of negatively charged

phosphate species ($H_2PO_4^-$). In basic solution, the adsorption of positively charged species is favoured for the interaction between $H_2PO_4^-$ and NH_3^+, especially near pH 6.5. A corresponding decrease in interaction occurs at elevated pH conditions above pH 7.

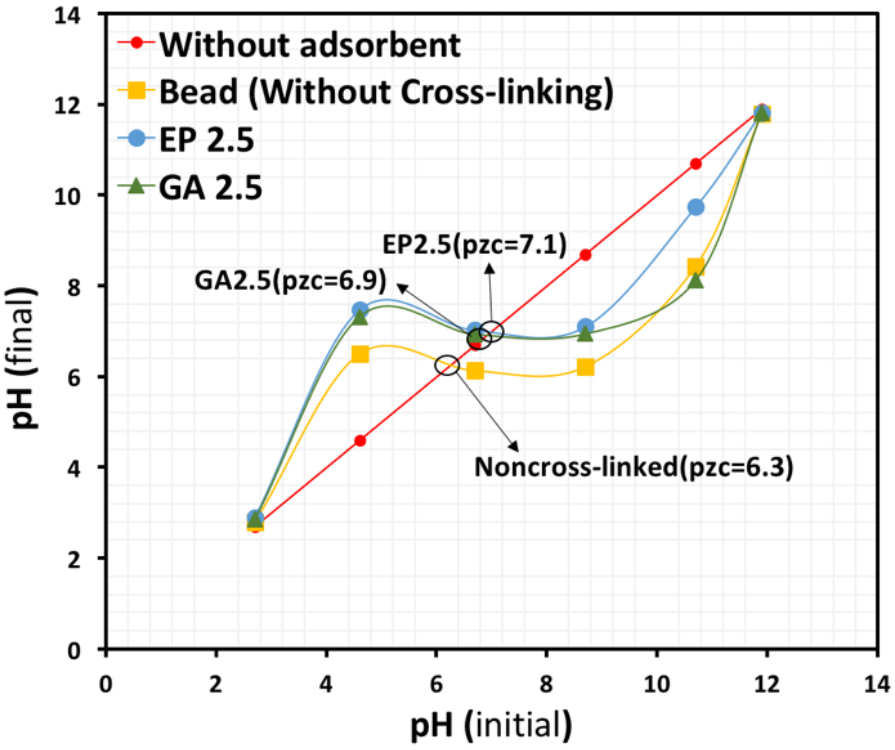

Figure 3.13 the determination of the pH_{pzc} of chitosan at 295 K.

CHAPTER 4

4 RESULTS AND DISCUSSION: Sorption of PNP and PHP

4.1 Introduction

For this section, the use of water for adsorption and swelling tests followed by PNP and PHP sorption results will be discussed. Swelling test results can provide important information on HLB (hydrophile-lipophile balance) character of the chitosan bead materials. The HLB character of an adsorbent/adsorbate system provides insight about the observed adsorptive behaviour of a system. In addition, comparison the swelling test results along with PNP and PHP sorption results will provide more details on the physicochemical properties of the chitosan bead materials.

In addition, the sorption trends for synthesized chitosan bead materials toward PNP and PHP will be interpreted based on the structure and chemistry of adsorbates and adsorbents to show how this information can provide better understanding over phosphate species (organic *vs.* inorganic phosphates) sorption in aqueous solution.

4.2 Water-based porosimetry and swelling test

The diameter (D), porosity (ε), and swelling properties of the different types of hydrated chitosan beads are shown in Table 4.1. A slight reduction in the diameter of the beads was found after cross-linking. This reduction in bead diameter can be related to change in the surface chemistry of the chitosan bead from the addition of the five carbon alkyl group of GA upon cross-linking of chitosan (*cf.* Fig. 3.3).[64] The cross-linking of chitosan with EP involves the net loss of one OH group for complete reaction of EP, a three-carbon alkyl cross-linker. The EP cross-linker unit is estimated to be more hydrophilic in nature due to its shorter alkyl chain length and the presence of a hydroxyl group at the C-2 position (*cf.* Fig 3.2) when compared against GA (*cf.* Fig. 3.3), as supported by the swelling results of the chitosan bead systems (*cf.* Table 4.1).

Table 4.1 Porosity, diameter, and swelling of different types of chitosan beads in water.

Sample ID*	Hydrated weight (W_W, g)	Dry weight (W_D, g)	Swelling (%)	Porosity of Wet bead (ε, %)	Diameter of hydrated bead (D, mm)
NCL	7.198	0.195	35.91	96.9±0.06	2.40
EP 2.5	6.691	0.182	35.76	96.9±0.06	2.34
GA 2.5	6.912	0.189	35.57	96.9±0.06	2.37
EP 5	6.580	0.179	35.75	96.9±0.06	2.33
GA 5	6.621	0.181	35.58	96.9±0.06	2.33

* The sample ID was defined in Chapter 2 in Table 2.1.

4.3 Sorption of *p*-nitrophenol (PNP)

4.3.1 Introduction

PNP is the conjugate base (anion form) in aqueous solution at pH 8.5 (Note: The pKa value for PNP is 7.1 and solubility in water is 11.6 g/L at 20 °C). This study aims to address the following question; can the PNP anion serve as a surrogate dye species at pH 8.5 to simulate the sorption properties for the orthophosphate in aqueous solution? At pH values above the pK_a the sorption properties of the PNP anion may serve as a probe for hydrogen phosphate ion to enable a deeper understanding over sorption properties of bead materials. The main factor of importance in this question is the pH of the solution. Alkaline pH (pH 8) conditions were considered elsewhere by Pratt et al.[64] for PNP sorption on chitosan-glutaraldehyde copolymer containing glutaraldehyde which provided results for the sorption capacity of Q_m = 0.2-0.8 mmol/g which provided a comparison for this study. Thus, a choice of pH 8.5 seems ideal since almost the pH condition of the most lakes and rivers is alkaline with a typical range of pH 6-8.5 for normal aquatic environments. Therefore, this study focused on pH 8.5 to address the uptake of the hydrogen phosphate ion in typical aquatic environment conditions (pH 8.5) and to avoid contributions to mixtures of other phosphate anion species and to evaluate the application of chitosan adsorbent

materials. Based on this assumption that the adsorbent has no electrostatic charge, the uptake capacity of charged species in a monolayer are inferred to be less than uncharged species based on grounds of electrostatic repulsions and packing efficiency according to a simple Langmuir isotherm model. However, it is reported that chitosan cross-linked materials containing glutaraldehyde have unusual affinity towards anion species.[46,65] Therefore, our goal was to focus on orthophosphate species in order to compare their adsorption properties with arsenate, as reported elsewhere.[46,64] Therefore, chosen pH for PNP was 8.5 to address all mentioned points above.

4.3.2 Sorption of PNP at pH 8.5

The adsorption properties of the chitosan beads was studied in aqueous solution using PNP at pH 8.5 and 20 °C. At these conditions, PNP exists mostly as a singly charged anion species (*p*-nitrophenolate ion) since the pH lies above the pK_a value (7.1) of the dye species (*cf.* Fig. 4.1).[64] PNP is a versatile dye probe for estimating the textural properties of sorbent materials using UV–Vis spectrophotometry.[50] The well-defined molecular structure and occurrence of proteolytic equilibria allows for the study of PNP as a surrogate anion to mimic the uptake behavior of inorganic oxyanions,[64] especially singly charged anion species such as phosphate.

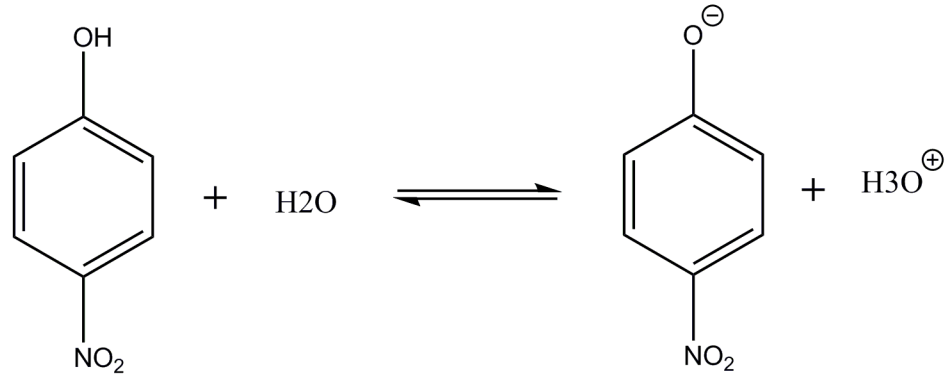

p-nitrophenol *p*-nitrophenolate

Figure 4.1 Illustration of the acid-base equilibria of PNP.

The uptake characteristics of the PNP anion can provide insight on the thermodynamics of adsorption processes to enable characterization of the textural (surface area and pore volume) properties of the synthetic chitosan beads. Figure 4.2 illustrates the adsorption isotherm results for

PNP at 20 °C with different types of bead materials. The adsorption of NCL beads toward PNP is relatively low and the GA 2.5 bead system has greater uptake of PNP relative to the other bead materials. The values for NCL beads are similar to an estimate obtained for cross-linked chitosan powders reported at pH 9 in aqueous solution.[66] Interestingly, the value of Q_e for GA 2.5 and EP 2.5 beads exceed those observed for the GA 5 and EP 5 beads.

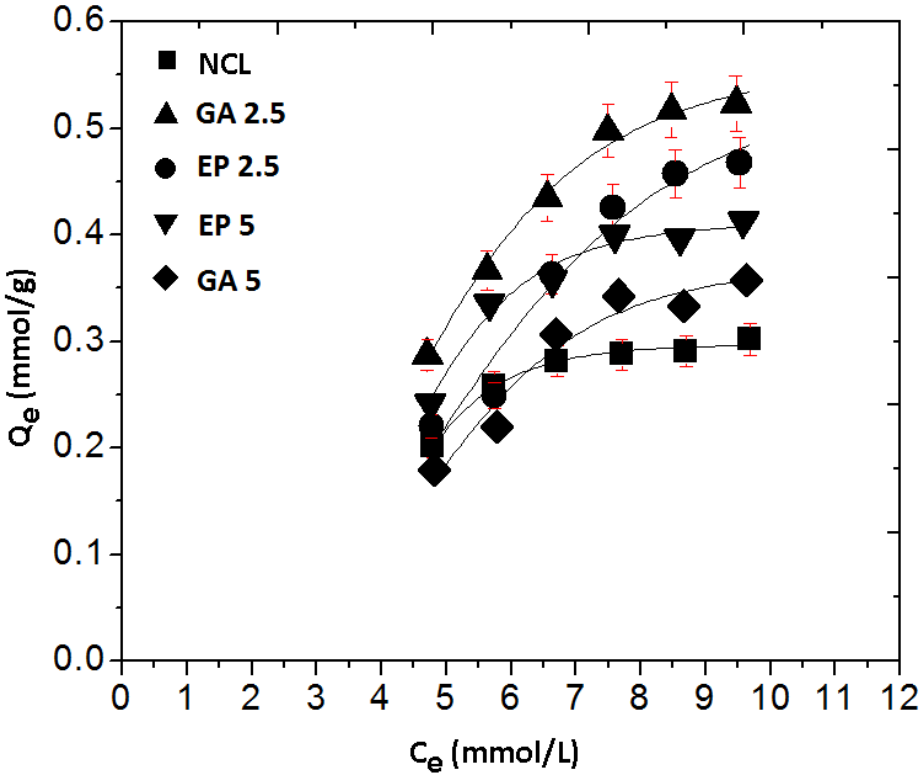

Figure 4.2 Sorption isotherms for PNP with different various bead materials at 20 °C and pH 8.5.

The concentration dependence for Q_e is well-described by the Sips model, as evidenced by the best-fit line through the experimental data. The corresponding adsorption parameters from the Sips model are listed in Table 4.2 for the various bead/PNP systems. A comparison of the cross-linked bead systems at variable cross-linker content (wt %) reveals that the Q_m values follow a reverse-ordering according to the relative cross-linker content. As the EP content (wt %) increases, the Q_m values decrease for this bead system. By contrast, the GA cross-linked bead systems have greater PNP uptake, according to the Q_m values listed in Table 4.2. A comparison of the NCL beads and the cross-linked systems reveal that the variable uptake properties are related to structural and

physicochemical properties of the cross-linkers (GA vs. EP). The variation in the uptake of PNP uptake can be related to variable textural and surface chemistry effects.[50] Surface effects are known to influence the hydration properties of cross-linked chitosan because of the HLB character for each cross-linker system varies according to the composition of the cross-linked bead system, as described above for differences between GA and EP.

Table 4.2 Sips isotherm adsorption parameters for the PNP anion in aqueous solution with different beads at 20 °C and pH 8.5 (Unbuffered in aqueous solution).

	Equilibrium sorption parameters for PNP*			
Bead ID	Q_m **(mmol·g^{-1})**	K_s **(L mmol^{-1})**	n_s	R^2
NCL	0.31	8.7×10^{-2}	0.24	0.98
EP2.5	0.54	4.6×10^{-2}	0.95	0.96
GA2.5	0.57	4.1×10^{-2}	1.2	0.99
EP 5	0.42	3.7×10^{-2}	1.1	0.98
GA 5	0.37	6.3×10^{-2}	1.1	0.97

*PNP is in its ionized state as the *p*-nitrophenolate anion since the solution pH exceeds pK_a value for PNP, where pK_a is 7.1.

4.4 Sorption of phenolphthalein (PHP)

In a previous study by Bertau and Jorg,[67] amylose-based polysaccharides caused decolourization of phenolphthalein (PHP) due to the formation of noncovalent complexes. The molecular structure of PHP is illustrated in Figure 4.3.

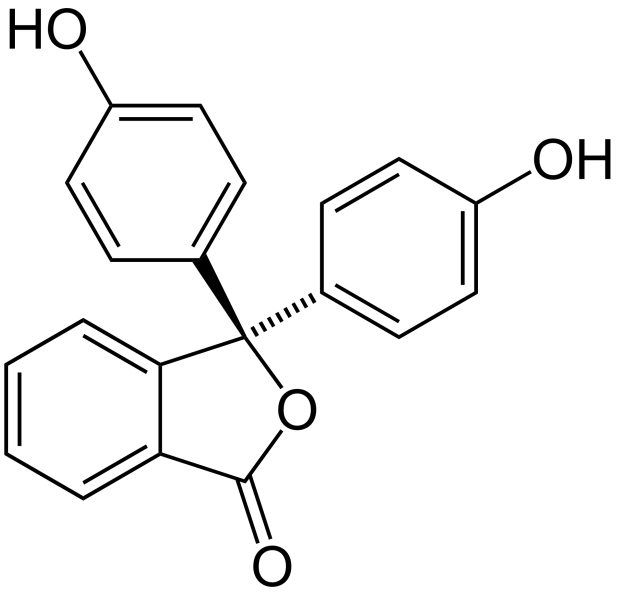

Figure 4.3 The molecular structure of phenolphthalein (PHP) in its protonated form.

The marked change in the molar absorptivity was shown by a drastic decolourization from pink to colorless in alkaline solution due to complex formation, especially for β-cyclodextrin and its polymer forms.[68] Similar decolorization effects were observed for the adsorption of PHP in the presence of cellulose[69] and chitosan,[51] including their cross-linked forms. This study was aimed at achieving a greater understanding of the nature of the active sites of chitosan that participate in the adsorption of phosphate species. PHP is a dianion species at pH 10.5 which may serve as a surrogate dye probe of hydrogen phosphate ion. Thus, a greater understanding of the role of steric and electronic effects of phosphate ions was anticipated by studying the adsorption of PHP with chitosan bead systems. Figure 4.4 shows the variable binding affinity of PHP toward different beads at pH 10.5 as follows: GA5> GA2.5> EP5> NCL > EP2.5, where the slopes of GA2.5 and GA5 do not level off for the mass range of materials examined. By comparison, the isotherms for EP2.5 and EP5 bead systems show saturation over this range of masses. The adsorptive affinity can be related to the relative water solubility of PHP is 400 mg/L at 20 °C.[70] The lipophilic character of adsorbates are a consideration in the sorption process due to the role of hydrophobic effect and the availability of suitable binding sites on the bead surface.[71] Despite the difference in hydrophilic character of orthophosphate and PHP (the water solubility of disodium phosphate is 77 g/L at 20 °C), the adsorption behaviour of each dianion species may be similar if ion-dipole interactions between the dye with the polar functional groups of chitosan are predominant. At pH

values above the pK_a of the adsorbate (pK_a=9.3 for PHP), ionization of the functional groups occur and the dye interconverts between the lactone and quinoid forms. [67] Neglecting potential steric effects at the adsorption site, an argument for the difference in polarity of adsorbate due to ionization of PHP can be made. In alkaline media (pH 8.2-12) PHP undergoes decolourization upon binding with chitosan due to the formation of the lactonoid-leuko forms [67]which possess reduced polarity and greater stability in a lipophilic environment. As glutaraldehyde can provide more lipophilic sites, GA2.5 (and GA5) reveals greater uptake capacity toward PHP, in agreement with the parallel results reported for *p*-nitrophenol in section 4.2. As well, cross-linking of chitosan contributes to *pillaring effects* and enhance the anion binding properties (*cf*. Scheme 1 in Ref. 48). [51,72,73]

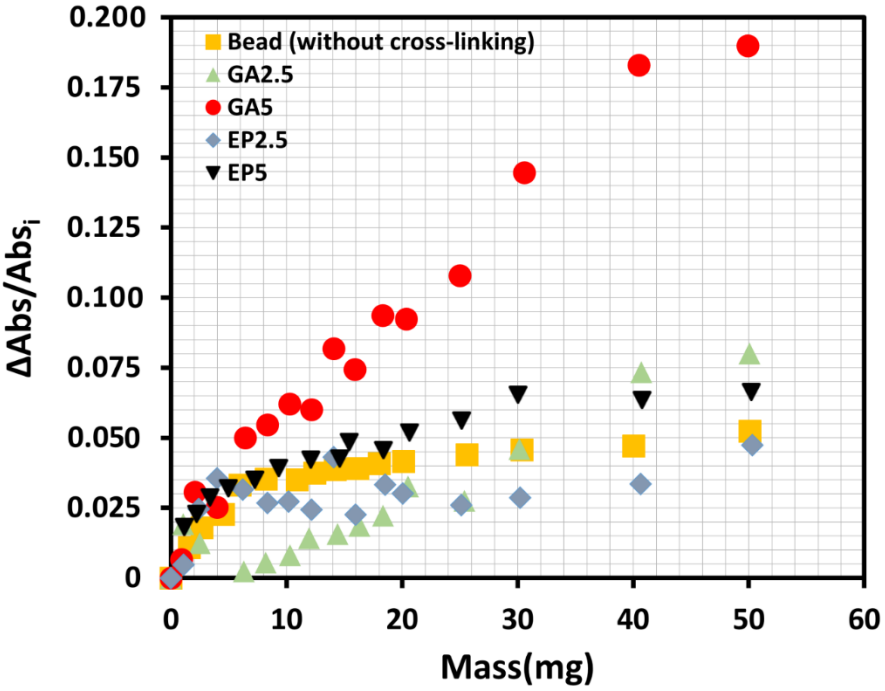

Figure 4.4 Trends for uptake of phenolphthalein (PHP) dianion versus mass of different sorbents at T=20 °C and pH=10.5.

4.5 Dye-based surface area calculations

The calculated surface area (S_A) and accessible surface volume (S_V) of the various types of chitosan beads are given in Table 4.3, according to the adsorption parameters derived from the PNP isotherm results. The relative uptake of PNP was reported to be dependent on the surface

area, the relative molecular weight, and polydispersity of the chitosan beads.[66] The textural properties and surface chemistry correlate with the cross-linker content, as described elsewhere.[50] According to the results in Table 4.3, a decrease in surface area (SA) and accessible surface volume (SV) occur as the level of cross-linking increases. Generally, the textural parameters are greater for chitosan cross-linked by GA since pristine chitosan has a lower surface area, attributed due to its hydrogen bonded network structure.[64] This trend is compatible with the average size of the pore surface area estimated from the SEM results in Figure 3.8,[74] along with the supporting results in Table 4.3.

Table 4.3 Dye-based surface area (SA) estimates of chitosan beads with PNP as the adsorptive probe in aqueous solution at 20 °C and pH 8.5.

Bead Systems	**SA** ($m^2.g^{-1}$)	**V_{ads}** ($m^3.g^{-1}$)	**Average pore SA** (m^2)*
NCL	129	24.2	3×10^{-14}
EP 2.5	149	25.7	8×10^{-11}
GA .5	165	28.5	3×10^{-10}
EP 5	123	21.3	-
GA 5	108	18.6	-

*Calculated using SEM images by "ImageJ 1.48" software.

CHAPTER 5

5 RESULTS AND DISCUSSION: Sorption of orthophosphate and organophosphate

5.1 Introduction

Physicochemical features related to adsorption properties of the chitosan bead materials was elucidated by use of suitable dye probes that share several traits such as the mode adsorption via hydrogen bonding and van der Waal's interactions. In the previous chapter, cross-linked chitosan was shown to display adsorption toward anions such as PNP and PHP possess high uptake capacity. Bead materials cross-linked with glutaraldehyde (GA2.5 and GA5) have relatively high sorption capacity. Therefore, the positive results from studies involving PNP indicate that binding of phosphate anions is expected with beads cross-linked with glutaraldehyde (GA2.5 and GA5). The predicted binding of hydrogen phosphate ion is likely lower with beads containing cross-linked with epichlorohydrin (EP2.5 and EP5). However, the bead materials cross-linked with GA display properties that show variable uptake toward PNP. This compares with relatively high capacity for beads cross-linked with EP and high uptake capacity toward phosphate. In this chapter, by combining and analyzing the obtained results from confocal microscopy, Raman, DSC, kinetic, and a thermodynamic study; the molecular details of the sorption process will be inferred.

The use of fluorescein dye (an anionic surrogate) as an adsorbate for evaluation of the sorptive behaviour of chitosan beads with confocal microscopy affords a method for monitoring the dye diffusion at variable time intervals. This method provided important information on sorption process into the bead. The analogous structure of fluorescein dye to PHP enables comparative study to understand the role of HLB and steric effect. The idea behind this experiment was using fluorescein as an anionic surrogate probe to determine how effectively it partitions into the microstructure of chitosan bead systems.

The adsorption of *p*-nitrophenyl phosphate (PNPP) may not parallel the uptake properties of PNP. In part, this may be due to the water structuring effects of each anion (RO- vs. R-O-PO_3^{2-}) in accordance with variable Lewis base character predicted by the Hofmeister series.[75] Based on this series, large singly charged ions, with low charge density (e.g., PNPP dianion) are chaotropes and exhibit weaker interactions with water than water with itself. By contrast, small or multi-

charged ions, with high charge density are referred to as kosmotropes (e.g., PNP monoanion, HPO_4^{-2}) which exhibit stronger interactions with water molecules than water with itself. Evaluation of phosphate and chitosan interaction with water (hydration) have examined using Raman spectroscopy and DSC which to develop an understanding of inorganic phosphate diffusion through inner and outer sphere interactions with the chitosan bead surface.

An investigation of the sorption behaviour of beads toward hydrogen phosphate ion was conducted to examine the bead adsorption properties. A comparison of the uptake properties of hydrogen phosphate ion *vs* organic dye anions such as PNP and PHP will provide insight on the role of steric hindrance and hydrophile–lipophile balance (HLB) according to the size and solubility properties of each dye. In addition, the pH dependent adsorption studies along with kinetic uptake studies at different temperature provide additional insight regarding the sorption of inorganic phosphate species. Lastly, the phosphate species were regenerated through a desorption process. Evidence for the reusability of the bead materials in this study was achieved according to the adsorption-desorption test for EP2.5 with hydrogen phosphate species.

5.2 Confocal microscopy

Fluorescein images of the GA5 bead at defined times (2, 10, and 30 min) were taken and the fluorescein penetration visualized by measurement of the fluorescence profile along the diameter of the bead in a 30 μm deep section below the midpoint. The molecular structure of fluorescein is illustrated by Figure 5.1. The relative similarity between molecular structure of the fluorescein and PHP, the fluorescein penetration into the bead can mimic the adsorptive behaviour of dianion species such as phosphate species.

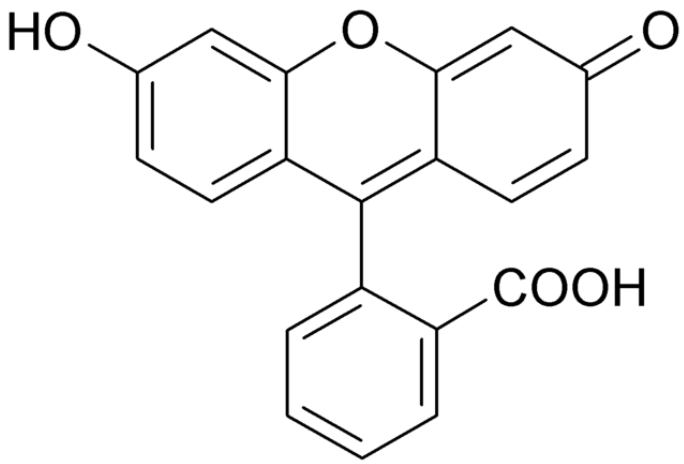

Figure 5.1 The molecular structure of Fluorescein in its protonated form.

By taking samples at three sampling time points and 0.001M concentrations (C_o), the progression of dye adsorption was observed. Figure 5.2 shows a series of scanning images for the fluorescein uptake in GA5. This indicates cross-linking has no apparent steric effect for penetration of adsorbates and the chitosan surface is permeable enough to allow fluorescein diffuse into the inner microporous adsorption sites of the chitosan bead network (mainly chitosan functionalities).

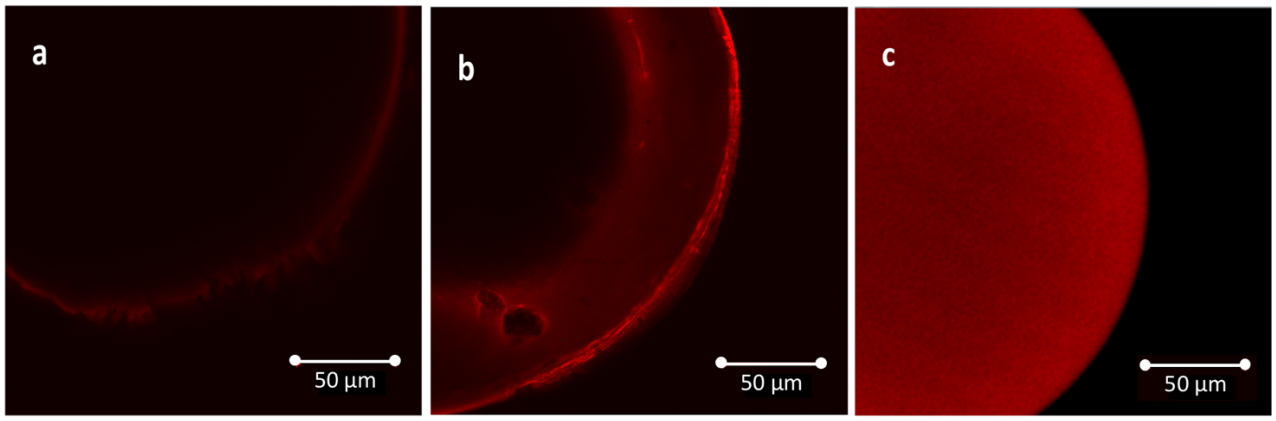

Figure 5.2 Confocal images of sample chitosan bead (GA5) from batch uptake of fluorescein (0.001 M) after, a) 2 min, b) 10 min, and c) 30 min.

5.3 Raman Spectroscopy

The Raman spectra of chitosan in powder and bead forms was shown in Figure 5.4 and 5.5. The occurrence of Raman vibrational bands relates to changes in polarizability and are especially relevant in the case of complex formation when dispersion interactions play a key role.[76] Hydrated samples cannot be readily studied by IR spectroscopy due to the strong IR absorption band of water. In this study of hydrated beads, the weak scattering cross-section of water enables an investigation of the hydration processes using Raman spectroscopy. [14] By investigation of the role of hydration during the hydrogen phosphate ion sorption, an understanding the sorption process is possible by considering the formation of outer or inner sphere complexes (*cf.* Fig. 5.3). The role of hydration effects on the adsorption process in aqueous solution was studied using hydrated chitosan beads in 5% D_2O w/w (H_2O/D_2O mixtures), in the presence and absence of HPO_4^{2-} at variable loadings (0, 100, 1000 ppm).

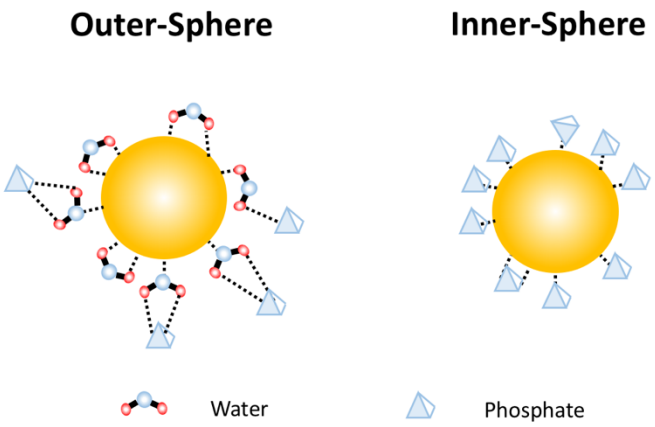

Figure 5.3 Schematic diagram illustrating the outer- and inner-sphere chitosan-phosphate complexes in water. [Note: one possible structure for each type are shown, where the ΔS of adsorption would differ according to their binding mode].

In Fig. 5.4 and 5.5, the appearance of Raman bands at 1375 and 1461 cm^{-1} are characteristic of chitosan that relate to the CH_2 deformation vibrations of and the C–H rocking band vibrational transitions. Phosphate has a prominent Raman signature assigned to a symmetric stretching mode of the various P-OH groups at 899 cm^{-1}, whereas; chitosan has a signature near 900 cm^{-1} that corresponds to the C–C bond vibrations of the pyranose ring units of chitosan. Adsorbed phosphate onto chitosan appears at *ca*. 895 cm^{-1} and another prominent band at 1070-1100 cm^{-1} occurs due

to the asymmetric P-O stretching mode for the HPO_4^{2-}. The hydrogen phosphate ion displays a spectral shift (*ca*. 10 cm^{-1}) in D_2O solution and the data in pure water are not shown. The band corresponding to the adsorbed phosphate species is close to the Raman band of unbound phosphate, where no significant changes in bonding occur upon complex formation between phosphate and chitosan. [77] The foregoing is consonant with the importance of hydrogen bonding and relative strength of hydration described by the Hofmeister series for such adsorptive processes. [75]

The Raman signature at 2900 cm^{-1} was assigned to the asymmetric C–H stretching vibration of the aliphatic groups of the beads (e.g., methine and methylene groups) for chitosan and or the cross-linker units. The peak at 1465 cm^{-1} relates to the C–H scissor vibration while the peak at 1384 cm^{-1} is expected from the CH_2 wagging. [78] Raman bands near 1200 and 1640 cm^{-1} were assigned to C–N stretching from the amine group. [79] The solvent (H_2O) was isotopically diluted with D_2O (5%) at pH 8.5 which results in two distinct vibrational bands observed at 557$cm^{-1}$and 1091cm^{-1}. Another notable feature is the appearance of uncoupled OD oscillator bands *ca*. 2500 cm^{-1} which provide an estimate of the degree of hydrogen bonding according to the bound *vs*. unbound water [14,79] The results for the OD oscillator bands (*cf*. Table 5.1 and Fig. 5.4, and 5.5) reveal the nature of hydration at the chitosan bead interface. The uncoupled OD oscillator band was measured at full-width-half-maximum (fwhm) for the various chitosan bead samples at different loadings of phosphate.

The spectral Raman shifts at fwhm for the chitosan samples are listed in Table 5.1, where the spectral signatures for phosphate are consistent with a physical adsorption process. The spectral intensity varies with the phosphate doping level (0, 100, 1000 ppm). An increase in the phosphate concentration by 100 ppm results in a change of the peak width at fwhm (68 to 86 cm^{-1}) for NCL beads, as compared with the peak width at fwhm (95 to 103 cm^{-1}) for chitosan powder. In contrast, the peak width at fwhm decreased for bead and powder forms of chitosan with increasing phosphate levels (100 to 1000 ppm). These changes in fwhm can show water molecule rearrangement around the chitosan is in agreement with change in entropy (ΔS) due to solvent rearrangement contributions.

Table 5.1 Calculated full-width-half-maximum (fwhm) peak with and related Raman shifts for chitosan powder and bead systems at different phosphate loading levels (ppm).

Phosphate level (ppm)	**NCL bead**		**Chitosan powder**		**Quartz cell****	
	fwhm*(cm^{-1})	λ(cm^{-1})	fwhm*(cm^{-1})	λ(cm^{-1})	fwhm*(cm^{-1})	λ(cm^{-1})
0	68	2485	95	2495	102	2499
100	86	2494	103	2502	-	-
1000	72	2482	92	2496	123	2507

*Calculation was obtained based on Gaussian fitting
** The values for quartz cell are given as blank sample

The Raman results indicate that the hydrogen bonded character of the solvent (H_2O) varies with the phosphate loading and may be understood in terms of competitive hydration processes at the bead surface due to adsorption of phosphate and the strong coordination of water with the hydrogen phosphate ion. [80,81]

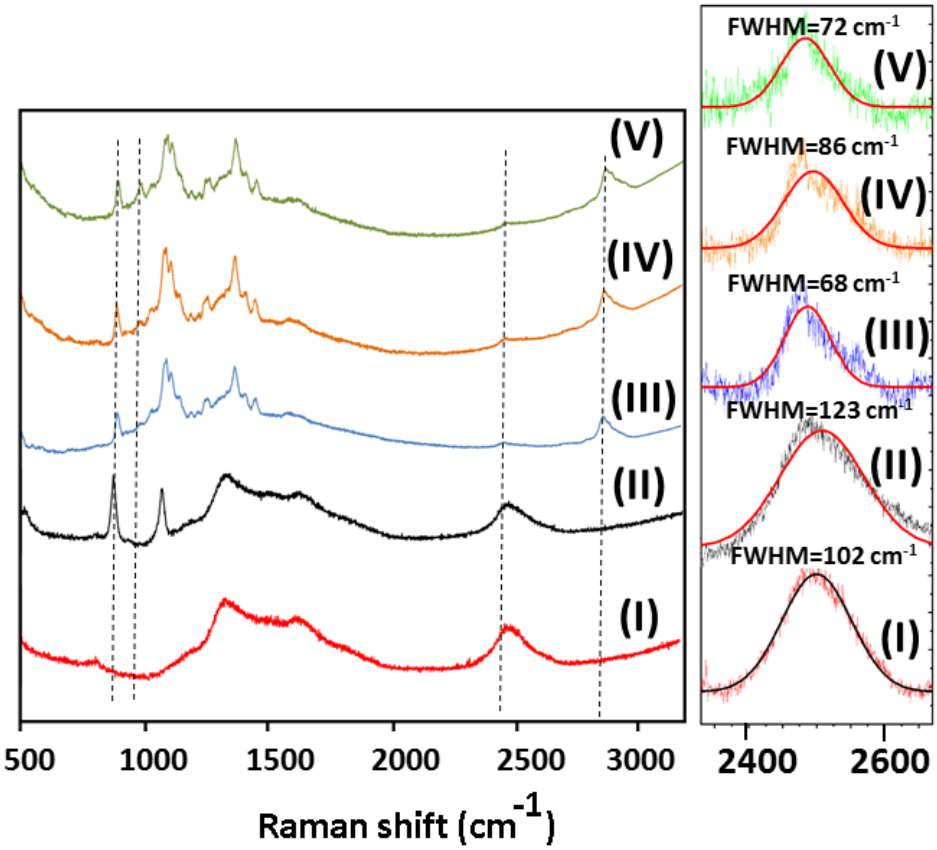

Figure 5.4 Raman spectra of bead systems: **a.** (I) H_2O/D_2O (5%), (II) H_2O/D_2O and phosphate (1000 ppm), (III) chitosan bead in H_2O/D_2O, (IV) chitosan bead after adsorption of phosphate (100 ppm) in H_2O/D_2O, (V) chitosan bead after adsorption of phosphate (1000 ppm) in a H_2O/D_2O solvent system.

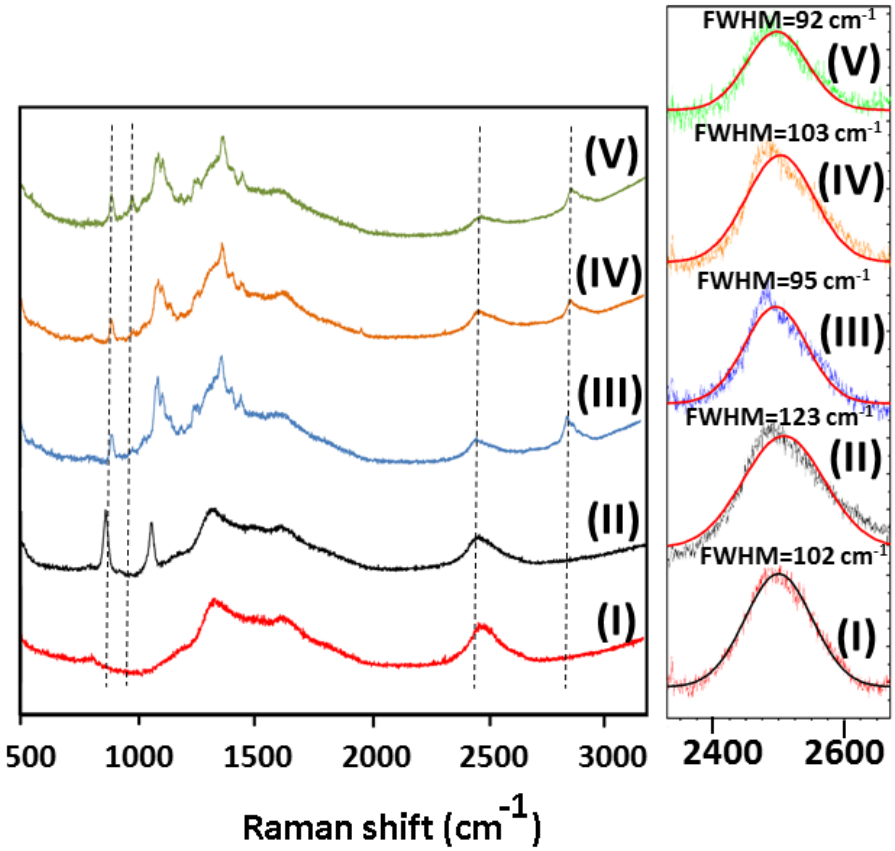

Figure 5.5 Raman spectra of chitosan powder: (I) H_2O/D_2O (5%), (II) H_2O/D_2O and phosphate (1000 ppm), (III) chitosan powder in H_2O/D_2O, (IV) chitosan powder after adsorption of phosphate (100 ppm) in H_2O/D_2O, (V) chitosan powder after adsorption of phosphate (1000 ppm) in a H_2O/D_2O solvent system.

5.4 Differential scanning calorimetry (DSC)

Similar types of samples were prepared by the same method for Raman spectroscopy were used to obtain the DSC results for the NCL beads and chitosan powder; the results can be seen at Fig. 5.6. At 100 °C, an increase in the phosphate concentration (up to 1000 ppm) revealed a dramatic decrease in the observed signature of water. The signal attenuation is understood in terms of competition for available adsorption sites on chitosan since more water is displaced by phosphate species when adsorbed at the bead surface and this can be due to the greater tendency of ion-dipole interactions over H-bonding. A relatively high amount of water uptake for chitosan powder relative to beads was shown by a decrease in the corresponding broader DSC signature for the decomposition of an amine group.

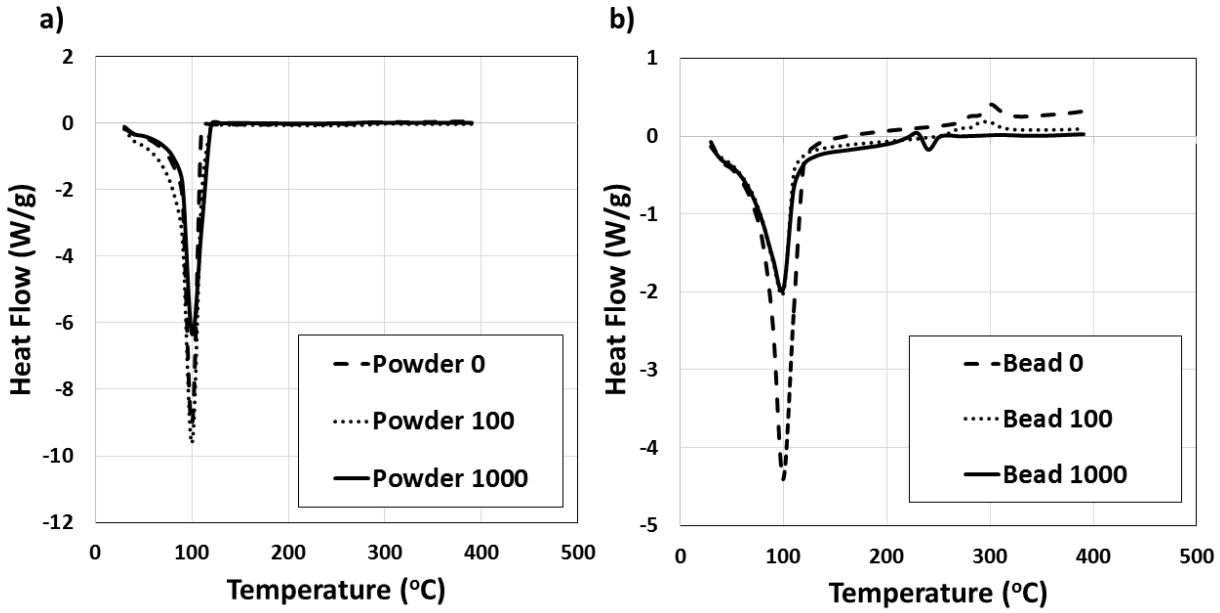

Figure 5.6 DSC curves for various chitosan systems: **a)** chitosan powder after sorption of phosphate ion with different concentration in H_20/D_2O (5%), **b)** NCL bead after sorption of phosphate ion at different concentration (100, 1000 ppm) in mixture of H_20/D_2O (5%) where the pH of the solution was 8.5.

5.5 Sorption isotherms and uptake capacity of chitosan beads

5.5.1 Sorption isotherms for hydrogen phosphate ion (HPO_4^{-2})

Figure 5.7 illustrates the adsorption isotherms of phosphate ion with different chitosan beads in aqueous solution. In general, the adsorption of hydrogen phosphate ion for each type of bead increases nonlinearly as C_e increases until the surface sites become saturated at elevated adsorbate levels. By comparison, the adsorption of NCL beads toward phosphate species is relatively low. At these alkaline conditions (pH 8.5 and 20°C), phosphate exists as a dianion (HPO_4^{-2}) species and the isotherm behavior is well described by the Sips model.[23] The adsorption capacity of the beads decrease as the level of cross-linking increases, as following: EP 2.5>GA2.5>EP 5>GA 5.

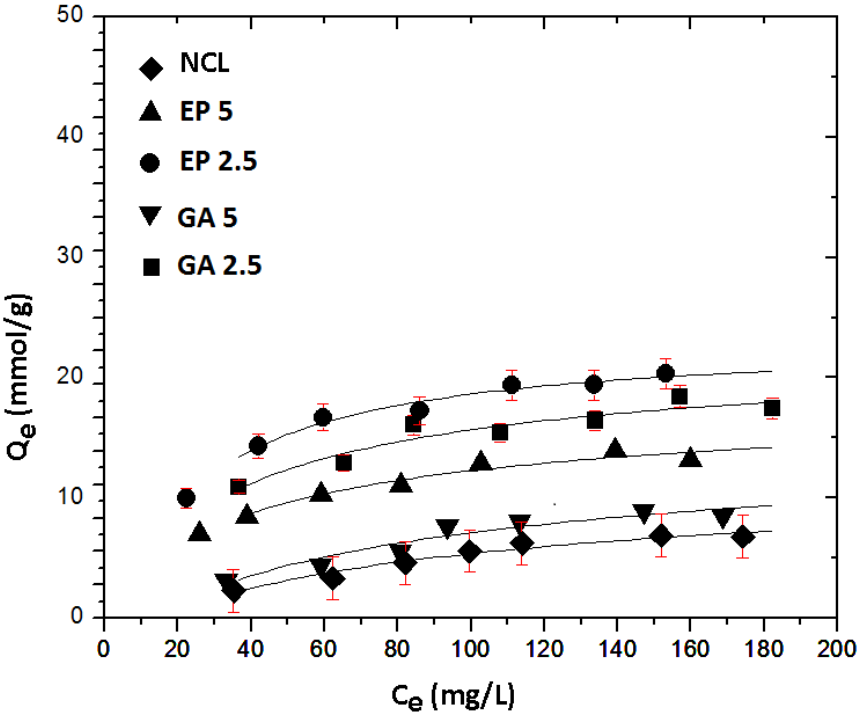

Figure 5.7 Sorption isotherms of phosphate ion for different bead systems at 20°C and pH 8.5 in aqueous solution. The error bars for the corresponding isotherm results denote the standard error determination.

Table 5.2 shows the best-fit parameters for each sorbent material. Overall, the isotherm results for the bead/ HPO_4^{-2} systems is well-described by the Sips model, according to the goodness-of-fit results in Table 5.2. In Figure 5.7, the Q_e values for various beads show an incremental uptake of phosphate as C_e increases, in agreement with the variable adsorption affinity for each chitosan bead/HPO_4^{-2} system. The value of Q_m for the bead system without cross-linking is lower than the cross-linked beads, in accordance with the nature and composition of the cross-linker employed. The Q_m values for both GA and EP beads adopt a reverse ordering (decreasing uptake) as the cross-linker content increases. An understanding of this trend is based on the polar nature of the OH group at the C-2 skeletal carbon position on the propyl moiety of EP at the cross-linked bead surface, along with the potential for ion-dipole interactions between phosphate and the linker unit. Greater cross-linking does not significantly alter the availability of active adsorption active sites (mainly OH groups for cross-linking via EP or NH_2 groups for cross-linking via GA). However, steric hindrance effects may reduce the diffusion rate of phosphate ions through the outer layer of the chitosan bead (*cf.* Fig.5.8) at moderate vs. high levels of cross-linking.

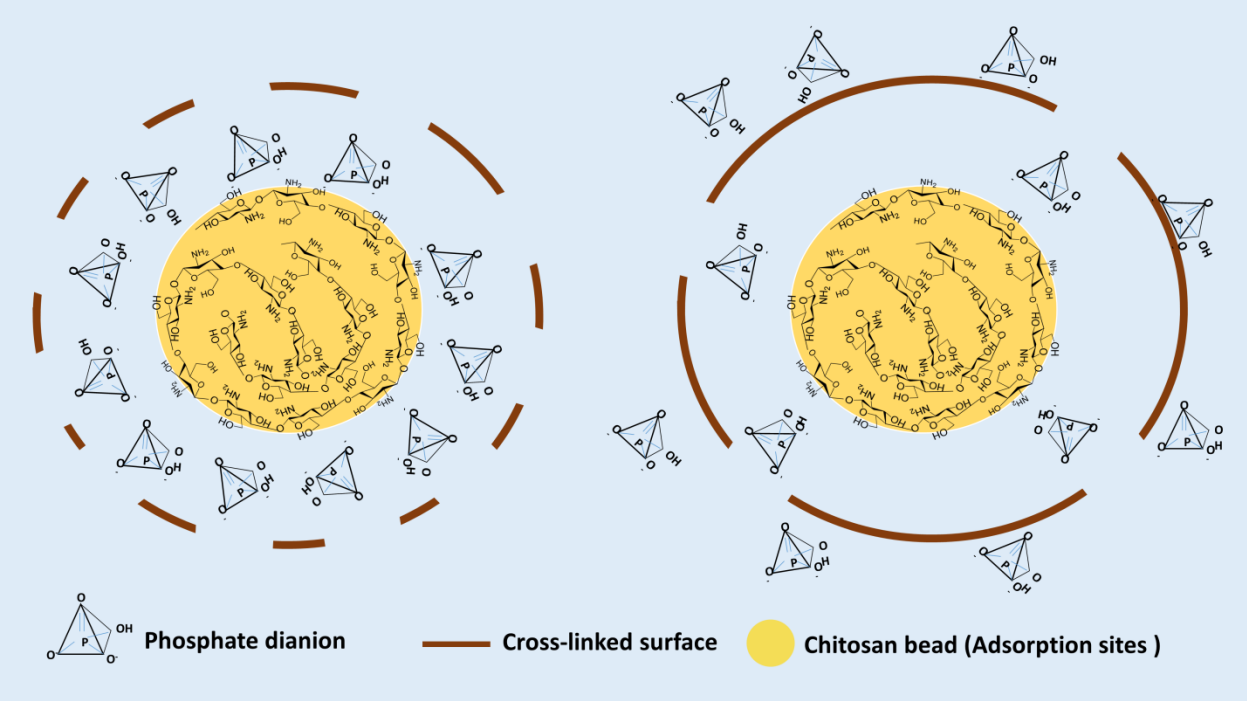

Figure 5.8 Variable steric effects for the adsorption of hydrogen phosphate ion (HPO_4^{2-}) for chitosan beads with variable cross-linking. Left hand side (moderate cross-linking) *vs.* right hand side (high cross-linking) where the orientation of the hydrogen phosphate ion is arbitrary.

The Sips isotherm provides a good description of the uptake behavior for the various bead systems, as evidenced by the best-fit results. The heterogeneity parameter (n_s) is near unity and approximates a type of Langmuir adsorption behavior anticipated for these systems. Thus, the bead surface is relatively homogeneous in accordance with the monolayer surface coverage anticipated for the adsorption of such divalent phosphate anions.

Table 5.2 Sips isotherm sorption parameters for the PNP anion and hydrogen phosphate ion in aqueous solution with different beads at 20 °C and pH=8.5 (non-buffered) in aqueous solution.

	Equilibrium sorption parameters for hydrogen phosphate ion*			
Bead ID	Q_m ($mg \cdot g^{-1}$)	K_s ($L \cdot g^{-1}$)	n_s	R^2
NCL	22.4	0.03	0.92	0.91
EP2.5	52.1	0.05	0.98	0.98
GA2.5	46.1	0.11	0.65	0.97
EP 5	41.1	0.05	0.69	0.92
GA 5	36.9	0.06	0.63	0.95

*Uptake of the Na^+ counterion was neglected. Phosphate exists as a dianion at this condition (i.e. HPO_4^{2-}).

As indicated above, the adsorption properties of beads cross-linked with EP or GA cross-linkers tend to show variable uptake toward singly charged PNP and hydrogen phosphate ion, respectively. This effect is consistent with two facts: *i*) PNP possesses a lipophilic phenyl ring moiety that differs relative to the more hydrophilic hydrogen phosphate ion (HPO_4^{-2}). The charge delocalization over the phenyl ring of PNP contributes further to its lipophilic character; *ii*) PNP is a weaker kosmotrope over HPO_4^{-2} which displays weaker interactions with water molecules.

The greater uptake of PNP with cross-linked beads containing GA present binding sites that are more organophilic in nature relative to EP due to its shorter alkyl chain and polar hydroxyl groups at C2, and such factors contribute to more favorable apolar binding in the case of GA-based cross-linked beads with PNP. The isotherm parameters (Q_m, β and E values) obtained from the D-R model at 20 °C for phosphate adsorption are listed in Table 5.3 for various bead systems. The E

values are below 8 kJ/mol which provide further support that adsorption between the hydrogen phosphate ions and chitosan bead surface are stabilized by physical interactions.[41]

Table 5.3 Parameters obtained by Dubinin-Radushkevich (D-R) isotherm model for hydrogen phosphate ion with different beads at 20°C and pH=8.5 (Unbuffered) in aqueous solution.

Bead ID	Q_m ($mg \cdot g^{-1}$)	β ($mol^2 \cdot KJ^{-2}$)	E ($KJ \cdot mol^{-1}$)	χ^2 (DOF)	R^2
NCL	18.3	6.4	0.28	1.8	0.77
EP 2.5	44.8	5.5	0.30	8.6	0.83
GA 2.5	33.7	5.5	0.30	6.5	0.74
EP 5	25.4	6.7	0.27	6.3	0.67
GA 5	22.3	6.5	0.28	3.3	0.72

* Uptake of the Na^+ counterion was neglected. Phosphate exists as a dianion at this condition (i.e. HPO_4^{2-}).

5.5.2 Regeneration study

The concentration of bound HPO_4^{-2} for the EP 2.5 bead system is shown in Figure 5.9 for several adsorption–desorption cycles. The adsorption of phosphate approaches equilibrium within approximately 1 h; whereas 95% of the bound phosphate species are desorbed within the first 15 min of the desorption process. The EP 2.5 beads were regenerated by washing with water and subjected to additional cycles of adsorption–desorption of phosphate. In Figure 5.9, the process was repeated for four cycles where the uptake capacity of phosphate was relatively constant (12.6±0.1%) illustrating the efficacy of the beads for recycling and re-use as adsorbents for phosphate uptake. The elution process using NaCl (*aq*) with moderate ionic strength is efficient for the removal of adsorbed phosphate for each cycle, and offers a versatile method for the

regeneration of chitosan beads without intermediate drying steps between the adsorption-desorption cycles.

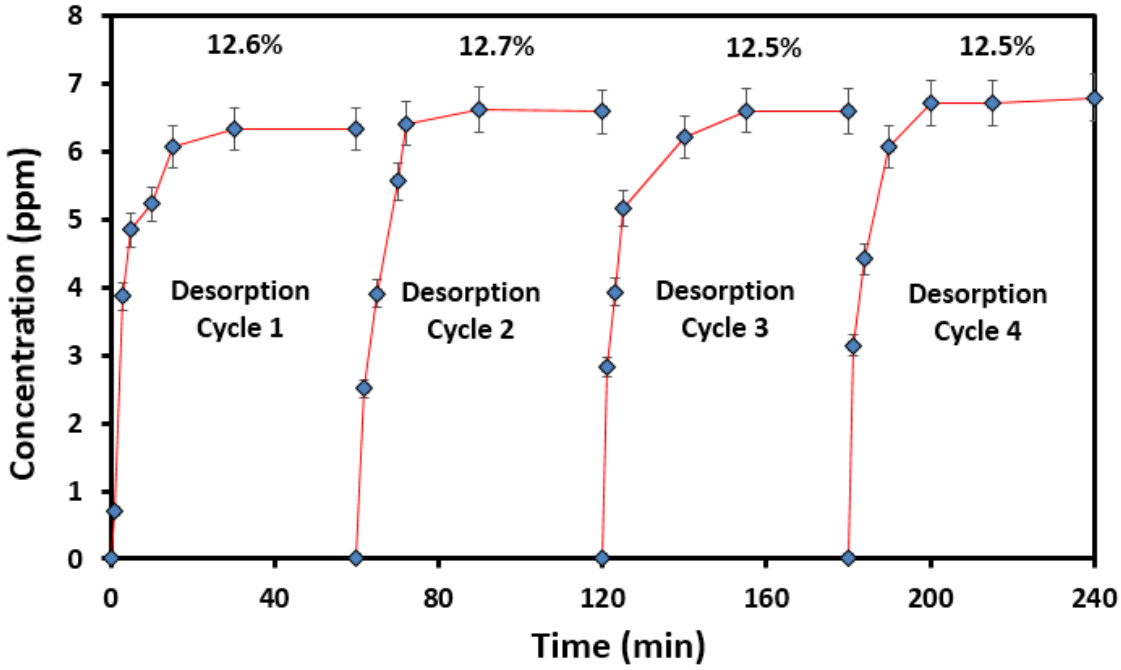

Figure 5.9 Adsorption–desorption cycle of a phosphate bead (EP2.5)/ hydrogen phosphate ion system at 20 °C. The error bars for the corresponding isotherm results denote the standard error.

5.5.3 Sorption isotherms for *p*-nitrophenyl phosphate (PNPP)

In order to provide a detailed understanding for sorption capacity and affinity for PNPP with the various chitosan bead materials, an isotherm study was carried out at pH 8.5 and 20 °C. The monolayer adsorption capacity (Q_m) represents the maximum amount of PNPP adsorbed on these adsorbents.

Table 5.4 Sips and Langmuir isotherm parameters for uptake of PNPP using various bead materials.

Bead materials (Sample ID)	Sips isotherm model				Langmuir isotherm model		
	Q_m (mmol/g)	K_s (L/mmol)	n_s	R^2	Q_m (mmol/g)	K_L (L/mmol)	R^2
NCL	0.18	0.21	1.8	0.98	0.23	0.14	0.98
EP 2.5	0.35	0.11	1.5	0.99	0.53	0.09	0.98
GA 2.5	0.49	0.13	1.4	0.98	0.57	0.12	0.99
EP 5	0.40	0.10	1.3	0.99	0.54	0.07	0.99
GA 5	0.51	0.14	1.2	0.99	0.62	0.08	0.98
NCL-CA	0.29	0.21	1.5	0.99	0.40	0.12	0.98
EP2.5-CA	0.75	0.06	0.90	0.99	0.67	0.07	0.99
GA2.5-CA	0.77	0.11	1.08	0.99	0.78	0.12	0.98
EP5-CA	0.81	0.06	1.08	0.98	0.90	0.05	0.98
GA5-CA	0.85	0.09	1.16	0.99	0.97	0.07	0.99

The isotherm results were evaluated by the Sips and Langmuir models, where the best-fit parameters are listed in Table 5.4. A comparison of the adsorption capacity of bead materials indicates that the Q_m value for GA5 is highest among all other bead systems. According to the CHN analysis, GA5 consists of higher glutaraldehyde. The relationship between cross-linker content and the adsorption capacity can be reverse or proportional.[39] As reported elsewhere, the greater adsorption capacity of hydrogen phosphate ion (HPO_4^{-2}) was higher for the EP2.5 when

compared with EP5 bead system. The difference relates to the many factors such as accessibility of the adsorption sites and HLB properties of the adsorbent, along with the presence of micropore domains. As stated before, the surface nature of the adsorbate such as its HLB will significantly contribute to the observed adsorptive relationship due to difference in the hydrophobic effect and relative contribution of dipolar interactions for the adsorption process.

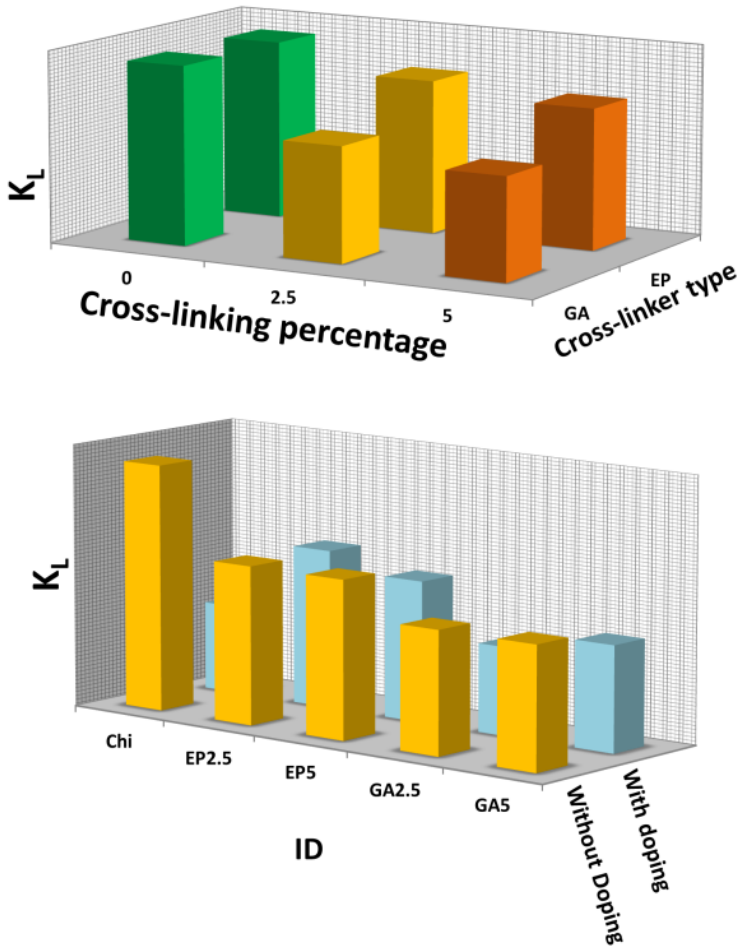

Figure 5.10 Effects of cross-linking and doping on K_L values (Langmuir adsorption constant for the uptake of PNPP).

Figure 5.10 demonstrates the cross-linking and doping effect on K_L values. The magnitude of K_L represents the relative affinity of PNPP for binding with the adsorbent. Therefore, the trend in K_L values may provide a useful tool for assessing the role of modification on the adsorption properties of the materials. The attenuation in K_L appears to be between 10 to 20% due to cross-

linking which again shows a drop after doping with calcium ions. The largest effect is evident for NCL and NCL-CA and may indicate the importance of amine and hydroxyl groups as the active sites for adsorption. However, the NH_2 groups may be the key adsorption sites for calcium ions as evidenced by dramatic drop-off in K_L value. Although cross-linking reduces the abundance of -OH or -NH_2 groups on the surface of the chitosan bead but it increases the surface area due to *pillaring effects*.[69] Consequently, cross-linked bead materials show higher Q_m value with lower K_L values, as compared with NCL.

As Figure 5.11 and 5.12 shows, the calcium doping has no significant effect on the adsorption capacity of beads with greater content of cross-linker like GA5 and EP5 compare to the GA2.5 and EP2.5. This observation can be justified by this fact that chitosan beads that are highly cross-linked cannot accommodate enough binding sites for calcium ions. It is concluded that calcium doping enhanced the adsorption capacity of NCL, GA2.5, and EP2.5 significantly. Bead materials cross-linked with GA (GA2.5 and GA5) were affected significantly.

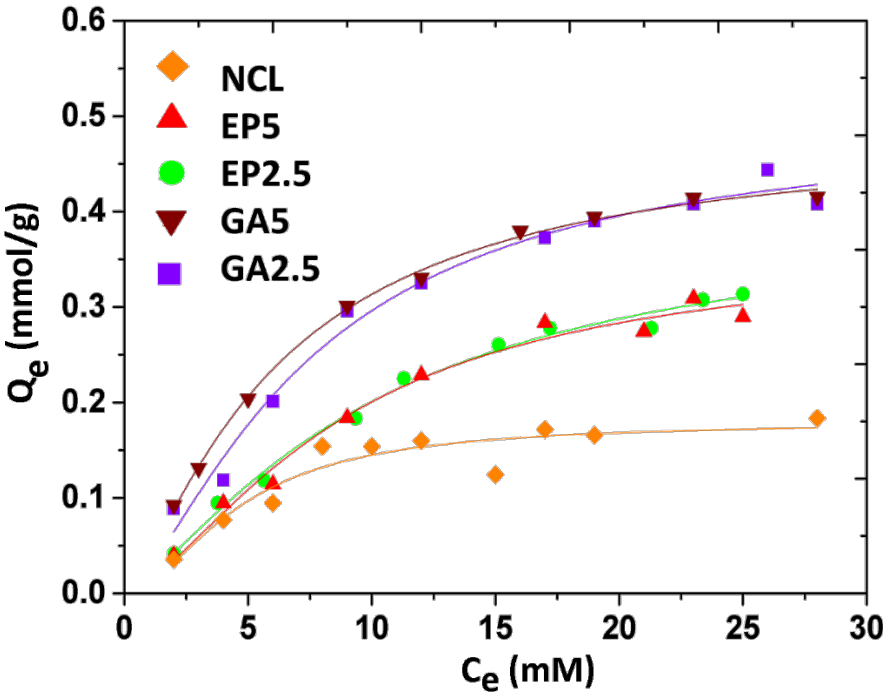

Figure 5.11 PNPP adsorption isotherms for different bead materials at 20°C and pH 8.5 in aqueous solution. The best-fit line through the data represent the Sips model.

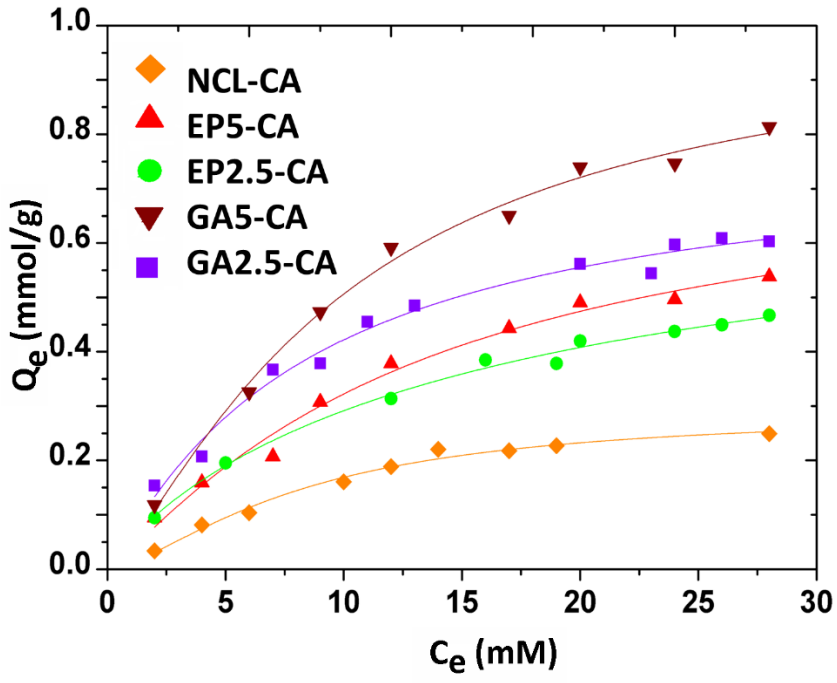

Figure 5.12 PNPP adsorption isotherms of different bead materials at 20°C and pH 8.5 in aqueous solution. The best-fit line through the data represent the Sips model.

The judgment for the best-fit criteria between the experimental and calculated data was judged according to the favorable value of R^2 (R^2 close to unity) of the Sips and Langmuir models. Both isotherm models showed good agreement for the sorption of PNPP. As the cross-linker ratio increases, Q_m values increase which suggest that cross-linking will provides adsorption sites for PNPP binding to the surface mainly because of an increase in surface area due to pillaring effects.[69] Beads with glutaraldehyde may offer secondary binding sites,[13] and surface bound glutaraldehyde species may exist as open-chain and cyclic forms depending on the preferred chemical structure (*cf.* Fig. 5.13). The presence of open chain cross-linker can serve as secondary sorption sites for phenolic compounds. The presence of unreacted functional groups such as hydroxyl or amine groups may also contribute to the heterogeneity of the adsorption sites due to their variable adsorption energy. As cross-linkers undergo reaction with chitosan or undergo self-polymerization, the resulting materials may contain different surface functional groups such as pyridine, hydroxyl. These surface groups would favor binding of PNPP through potential hydrogen bonding or π– π interactions.

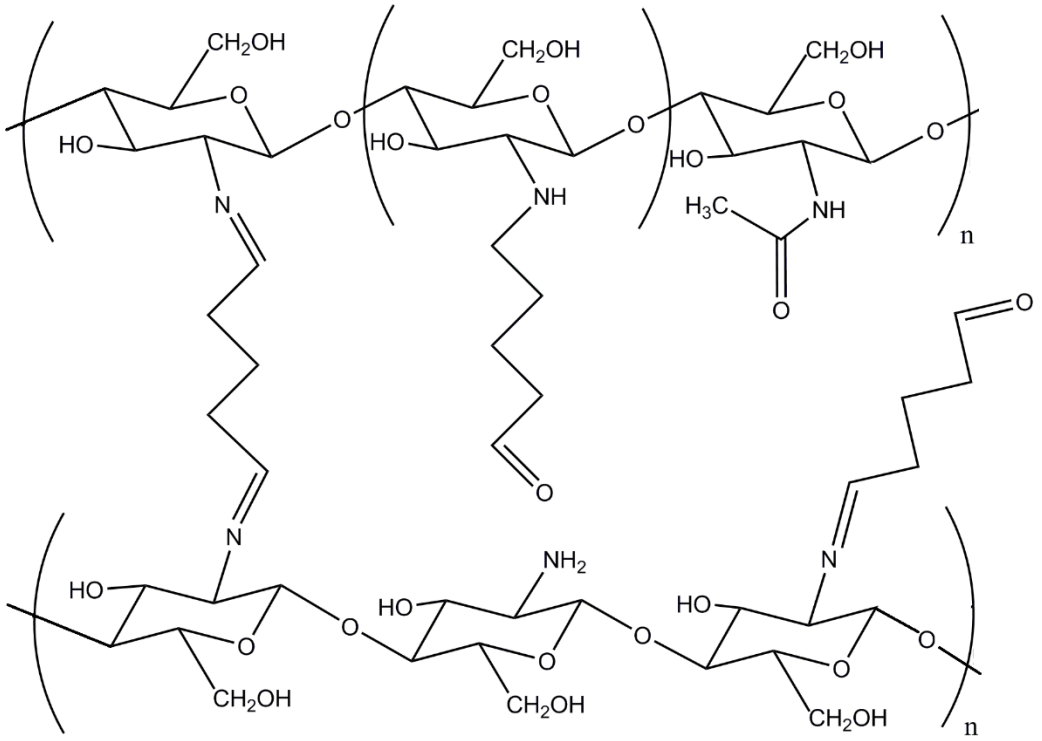

Figure 5.13 Pendant chain motif in chitosan partially cross-linked with GA.

A conclusion from the model parameters suggests that the beads with greater cross-linker content (5% *vs.* 2.5%) have highly heterogeneous surfaces with greater adsorptive properties. Furthermore, calcium doping has significant effect on bead materials with lower cross-linking ratio.

Fig. 5.11 illustrates the PNPP adsorption results for calcium-doped beads at pH 8.5 in aqueous solution. The adsorption results are comparable to those in Fig. 5.11; however, as mentioned above, the uptake of PNPP for the NCL, GA2.5, and EP2.5 complexes boosted significantly, which can reveal some important differences about precursors. Chitosan bead with lower cross-linker content carrying higher free functionalities likes hydroxyl and amine groups for binding with calcium cations.

Complexation between calcium and chitosan can provide favorable coordination sites for PNPP due to the presence of Ca^{2+}. In addition to the hydroxyl and amine groups within the chitosan structure, the incorporation of Ca^{2+} introduces favorable Lewis acid coordination sites for PNPP, as illustrated in Figure 2.3. The synthetic procedure for the bead materials here illustrates a rational

approach for tuning the sorption capacity. By comparison with chitosan as an adsorbent, the sorption properties improved through cross-linking with glutaraldehyde and epichlorohydrin, along with the formation of chitosan bead/Ca^{2+} complexes.

5.1 Kinetic and thermodynamic studies

5.1.1 Kinetic study

Kinetic uptake studies provide estimates of uptake rate constants but may also provide further insight about the molecular level details of the adsorption process, along with complementary thermodynamic parameters. Saturation of the active adsorption sites of the beads with hydrogen phosphate ions occur within *ca*. 30 min. To analyze the kinetic uptake results, two models were investigated; the pseudo-first-order (PFO) and pseudo-second-order (PSO) kinetic models which are described in the section 2.6. The value of q_e and k_2 can be determined using eqns (1.11 and 1.12) by plotting Q_t against time (*cf*. Fig. 5.14-5.18).

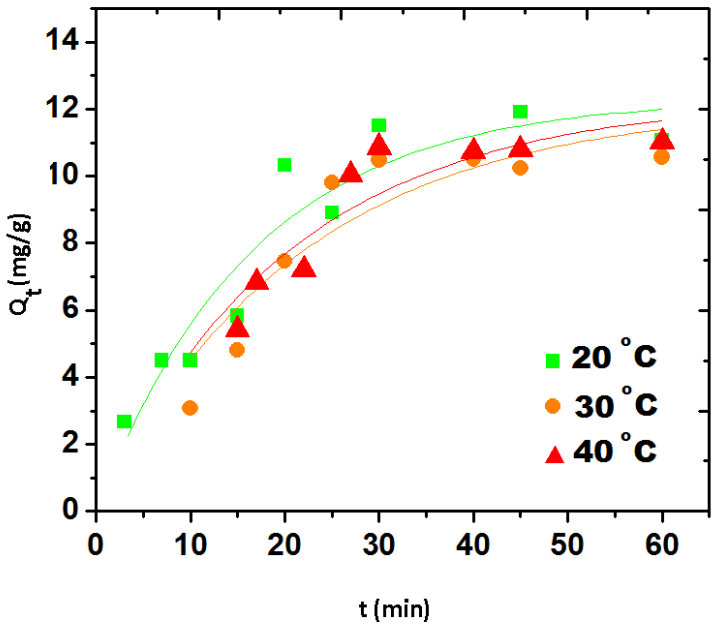

Figure 5.14 The kinetic uptake profile of hydrogen phosphate ion *vs*. time for chitosan bead (NCL) at different temperatures (20, 30, 40 °C) and pH 8.5.

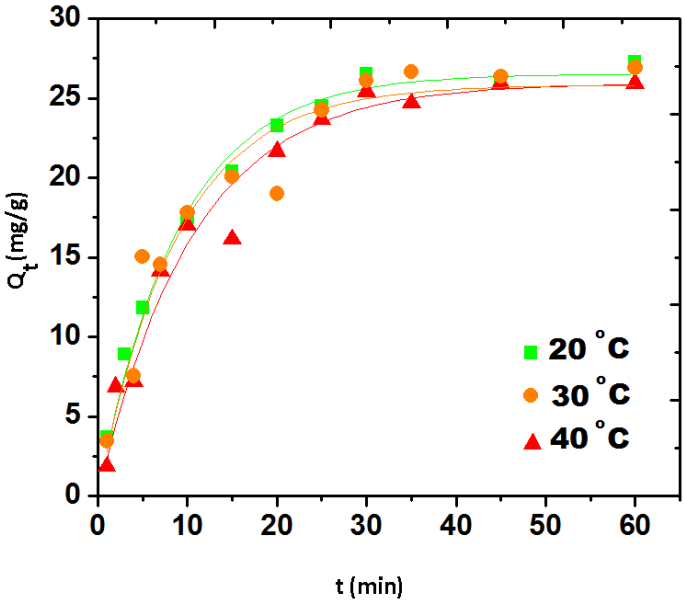

Figure 5.15 The EP2.5 kinetic uptake profile of hydrogen phosphate ion vs. time for EP2.5 at different temperatures (20, 30, 40 °C) and pH 8.5.

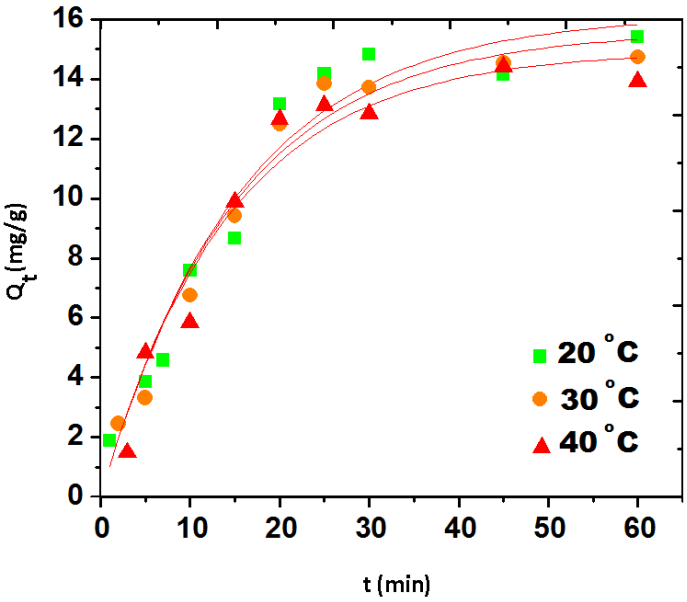

Figure 5.16 The kinetic uptake profile of hydrogen phosphate ion vs. time for EP5 at different temperatures (20, 30, 40 °C) and pH 8.5.

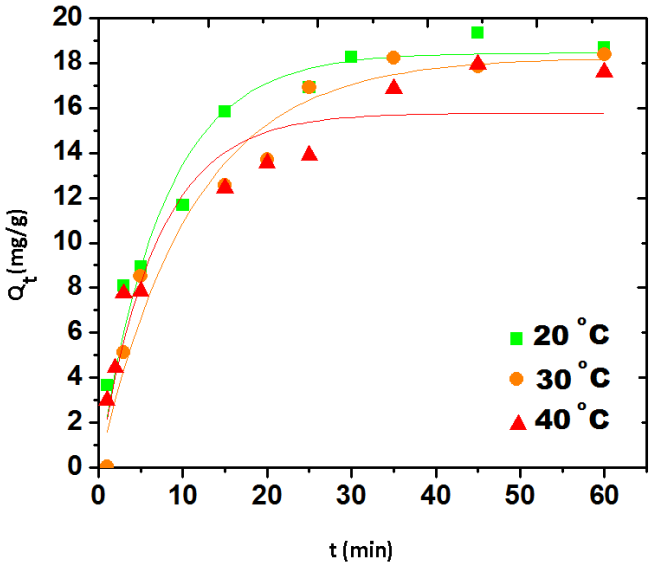

Figure 5.17 The kinetic uptake profile of hydrogen phosphate ion vs. time for GA2.5 at different temperatures (20, 30, 40 °C) and pH 8.5.

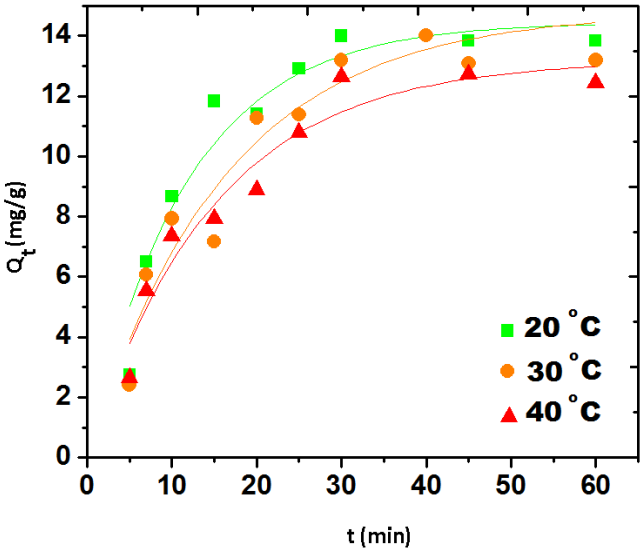

Figure 5.18 The kinetic uptake profile of hydrogen phosphate ion vs. time for GA5 at different temperatures (20, 30, 40 °C) and pH 8.5.

The kinetic parameters derived from the PFO and PSO models in Table 5.5 show good agreement for the uptake of hydrogen phosphate ions at variable temperature. However, the R^2 and χ^2 values obtained by the PSO model are lower when compared with the PFO model, where the kinetic uptake process is well-described by eqn (1.11). The PFO model describes a reversible

exchange between the solid phase of the adsorbent and the aqueous phase with two stages[82]; *i*) a rapid rate of adsorption occurs at the initial stage, and *ii*) a slower rate of uptake is maintained at longer time intervals as equilibrium is approached. The two stages can be explained by the presence of two different adsorption sites (chemisorption at two active sites is rate determining step), or alternatively by two rates of diffusion at readily accessible external and macropores and for less accessible mesopore and micropore sites.[82] The uptake behavior of phosphate at variable temperature (20, 30, and 40°C) was well-described by the PFO model for the chitosan systems since χ^2 was minimized to yield reliable best-fit values. It is worthwhile to note that the sorptive uptake (Q_e; mg/g) of phosphate estimated from the *one-pot* setup (*cf*. Fig. 2.4) agrees with the uptake parameters from batch studies at equilibrium (*cf*. Table 5.2 and 5.3).

The monolayer sorption capacity (Q_m) of chitosan beads from isotherm study adopted the following order: EP 2.5 > GA 2.5> EP 5> GA 5, where the foregoing results parallel the kinetic uptake values (*cf.* Table 5.5).

Table 5.5 Kinetic parameters of phosphate uptake onto different bead systems at variable temperature as described by the PFO and PSO kinetic models.

Bead System	Pseudo-first-order (PFO)					Pseudo-second-order (PSO)			
	T (°C)	Q_e (mg·g^{-1})	k_1 (min^{-1})	R^2	$\chi^2_{/DoF}$	Q_e (mg·g^{-1})	k_2 (g.mg^{-1}.min^{-1})	R^2	$\chi^2_{/DoF}$
NCL	20	12.3	0.060	0.94	1.2	16.1	0.0027	0.93	1.4
	30	12.3	0.048	0.86	0.8	16.5	0.0026	0.82	1.1
	40	12.1	0.042	0.86	1.4	16.9	0.0021	0.83	1.7
EP 2.5	20	26.1	0.113	0.99	0.5	32.1	0.0039	0.99	0.5
	30	26.1	0.101	0.95	2.1	31.3	0.0039	0.97	2.9
	40	25.9	0.097	0.97	2.1	31.6	0.0032	0.97	2.3
GA 2.5	20	18.4	0.111	0.97	1.4	21.2	0.0038	0.98	0.7
	30	18.2	0.090	0.97	1.5	22.1	0.0045	0.97	1.3
	40	16.3	0.084	0.93	1.1	19.2	0.0035	0.97	1.1
EP 5	20	16.6	0.069	0.96	1.3	23.3	0.0029	0.95	1.6
	30	15.7	0.066	0.97	0.8	20.5	0.0028	0.95	1.4
	40	14.9	0.064	0.96	1.1	19.3	0.0033	0.93	1.7
GA 5	20	14.5	0.068	0.96	1.0	18.0	0.0028	0.94	1.7
	30	14.8	0.067	0.93	1.3	17.3	0.0025	0.92	1.5
	40	13.2	0.061	0.95	0.7	16.9	0.0027	0.93	0.9

5.1.2 Thermodynamic study

The kinetics of the phosphate uptake at variable temperature will yield different rate constants (k_1 and k_2). Based on the temperature dependence of the rate, the activation energy (E_a) of the adsorption process was estimated by the Arrhenius equation.[22,47] The thermodynamic parameters ($\Delta H^{\ddagger}$ and $\Delta S^{\ddagger}$) assume that transition-state theory describes the energetics of the activated complex described by the Eyring equation eqn (5.1).[83]

$$\ln\left(\frac{k_i h}{K_B T}\right) = -\frac{\Delta H^{\ddagger}}{R}\frac{1}{T} + \frac{\Delta S^{\ddagger}}{R} \qquad (5.1)$$

k_i is rate constant according to the PFO and PSO models, k_B is the Boltzmann constant (1.381×10^{-23} J/K), T is the temperature (K) and h is the Planck constant (6.626×10^{-34}Js).

In Table 5.5, the rate constants (k_i) for the various bead systems decreased with increasing temperature. The derived thermodynamic results are given in Table 5.6 according to the Eyring plots (*cf.* Fig. 5.19).

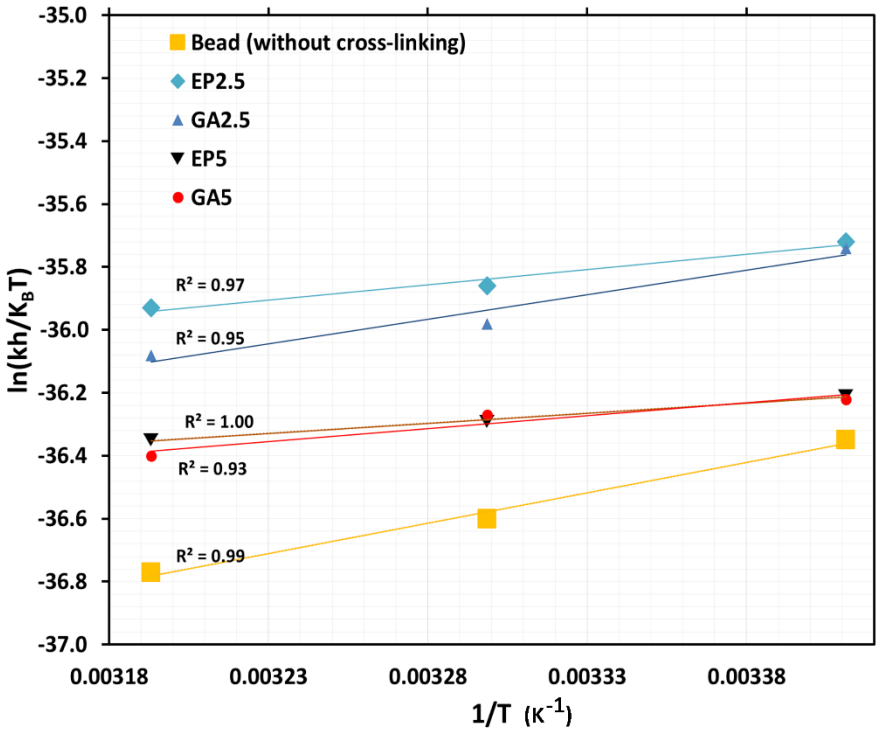

Figure 5.19 Eyring plots for hydrogen phosphate ion uptake at variable temperature at pH 8.5. The parameters as defined by eqn (5.1).

A decrease in the rate constant result coincides with an "apparent" negative value of E_a. A negative value for $\Delta H^{\ddagger}$ coincides with the increased activation barrier for the sorption process.[47] The relationship between the values of $\Delta H^{\ddagger}$ and E_a are in good agreement with the magnitude of the measured rate constant. The results follow the general rule that lower values of $\Delta H^{\ddagger}$ reflect processes with faster rates of adsorption and vice versa. Examples of negative E_a for adsorption processes were reported[47] for the uptake of selenium with magnetite and its supported materials onto activated carbon. The hydrophilic nature of phosphate and the presence of polar surface sites on the adsorbent can account for changes in hydration of the activated complex. The negative $\Delta S^{\ddagger}$ value may coincide with the formation of an outer-sphere complex because of entropic contributions during formation of the activated complex due to exchange of phosphate and contributions due to hydration. A possible two-step uptake mechanism of the hydrogen phosphate ions (HPO_4^{2-}) onto the chitosan surface at pH 8.5 is shown in Figure 5.20. The first step of the formation of an outer-sphere complex involves hydration and the second step involves ligand exchange where water is replaced by hydrogen phosphate ion (*cf.* Fig. 5.20).[44,47,84]

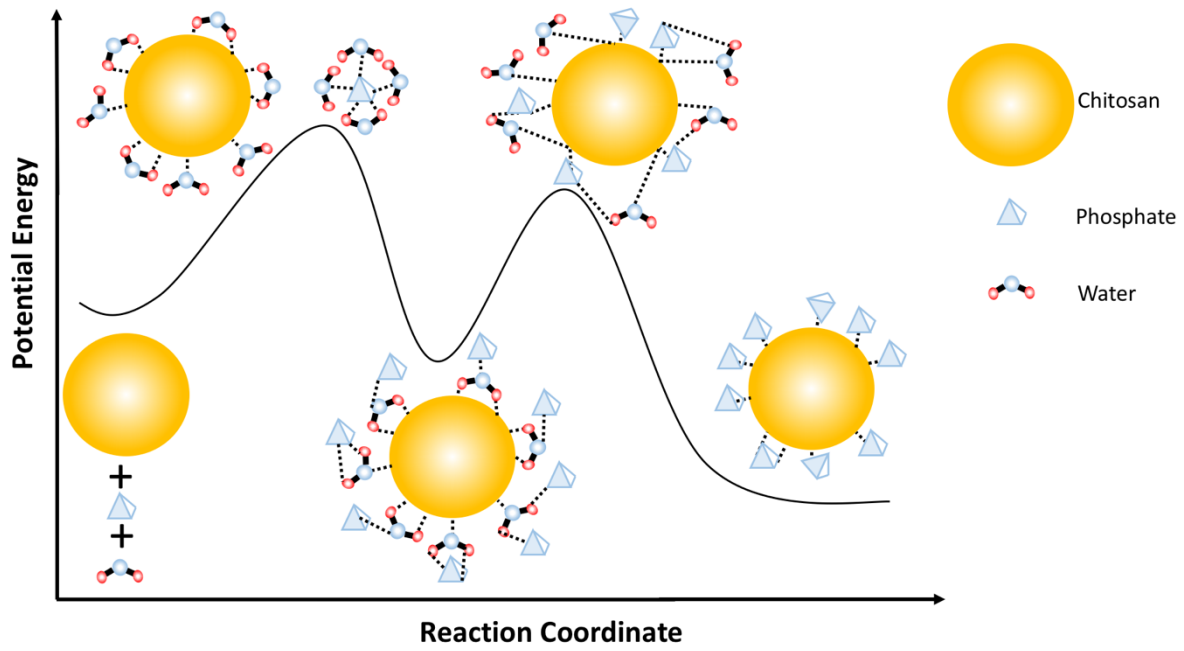

Figure 5.20 Proposed reaction coordinate diagram for the adsorption process of hydrogen phosphate ion (HPO_4^{2-}) inner sphere adsorption on the surface of chitosan beads at pH 8.5 in aqueous solution.

Table 5.6 Thermodynamic parameters for phosphate adsorption using different bead systems based on an obtained rate constant in PFO model (C_o ~200 ppm, adsorbent dose = 50 mg, V = 0.20 L) at various temperatures and pH 8.5 without added buffer.

Bead System	$\Delta H^{\ddagger}$ (kJ/mol)	$\Delta S^{\ddagger}$ (J/mol K)	T (K)	$\Delta G^{\ddagger}$ (kJ/mol)	E_a* (kJ/mol)
NCL	-16.05	-357	293.16	88.6	-1470
			303.16	92.2	
			313.16	95.8	
EP2.5	-8.04	-324	293.16	86.9	-5900
			303.16	90.2	
			313.16	93.4	
GA2.5	-13.02	-341	293.16	87.0	-6360
			303.16	90.4	
			313.16	93.8	
EP5	-5.34	-320	293.16	88.5	-9327
			303.16	91.7	
			313.16	94.9	
GA5	-6.83	-324	293.16	88.2	-9660
			303.16	91.4	
			313.16	94.6	

*Calculated using the Arrhenius equation.

Raman spectroscopy has been used for structural characterization along with studies related to changes in hydration.[14] Isotopic dilution of normal water with D_2O is suitable for investigating the hydration effect for sorption processes. According to previous studies[14] for clathrates and hydrogen bonded complexes, OD oscillator bands band ~2500 cm^{-1} provides an indication of the degree of hydrogen bonding. This can provide insight about the solid hydration characteristics and/or the adsorbate/adsorbent system.

The Raman signature at 2500 cm^{-1} provides support that chitosan with adsorbed phosphate at higher loadings results in reduced hydration of chitosan. The results suggest that adsorption of phosphate on the surface of chitosan occurs *via* competitive hydrogen bonding with available hydration sites. The hydrophilic nature of phosphate species and the presence of different surface sites due to variable surface functionality of the adsorbents may account for the observed uptake parameters. Phosphate uptake closely resembles changes in hydration properties of the surface sites due to the important role of hydrogen bonding for each phosphate species. The 3D structured bonding network of water can be perturbed by competitive binding interactions with hydrogen phosphate ions at the chitosan surface. Cross-linking of beads alters the HLB of chitosan as evidenced by the variation in uptake with the type of cross-linker and its relative composition. Cross-linking of the chitosan at the bead surface contributes to a *pillaring effect* of the polymer network alters the relative accessibility of the active binding sites on the bead surface, as compared to the more crystalline form of unmodified chitosan (*cf.* Scheme 1 in Ref. 48). Therefore, phosphate anions may diffuse through the boundary layer of cross-linked beads more rapidly, in agreement with its observed rate constant for cross-linked beads. The observed rate of phosphate uptake parallels the increase in the polarity of chitosan bead surface (*cf.* Scheme 1 in Ref.48).

5.2 pH effect on orthophosphate (P_i) sorption

5.2.1 Models for the pK_a and fraction of total species

The potentiometric results for chitosan include two inflections, where the first and second points correspond to the equivalence points in the titration of the amine groups ($R\text{-}NH_2$) of chitosan by eqn (3.4) with HCl and the titration of protonated amine groups of chitosan, respectively (*cf.* Fig. 3.12). The estimated pK_a of the protonated amine groups in chitosan by this method was pH 6.2, in agreement with an independent pK_a value.[40] According to the speciation curve for chitosan (*cf*. Fig. 5.21), the protonated species ($R\text{-}NH_3^+$) on the surface of chitosan decrease in abundance

with increasing pH. Over the pH range of 6 to 8.5, two anions ($H_2PO_4^-$ and HPO_4^{2-}) species are present in solution. According to the speciation curves of phosphoric acid (*cf.* Fig. 1.2) and chitosan (*cf.* Fig. 5.21), the interaction of phosphate species with chitosan has four possible outcomes at variable pH including the interaction of non-ionized chitosan (R-NH_2) with $H_2PO_4^-$ and HPO_4^{2-}. By contrast, protonated chitosan (R-NH_3^+) likely forms a complex with phosphate monoanion ($H_2PO_4^-$) on its surface. These adsorptive interactions are consistent with the variable speciation of phosphate at variable pH conditions. In Figure 5.22, of the likely interaction between R-NH_2 and HPO_4^{2-} at pH 8.5 represents an optimal condition for adsorption for the chitosan/phosphate system. By contrast, other electrostatic interactions involving R-NH_2 with $H_2PO_4^-$ and the interaction of R-NH_3^+ with $H_2PO_4^-$ or HPO_4^{2-} are attenuated at alkaline pH conditions. Cross-linked bead materials will show slight differences relative to chitosan powder, according to the observed variable protolytic behaviour at higher pH_{pzc} values.

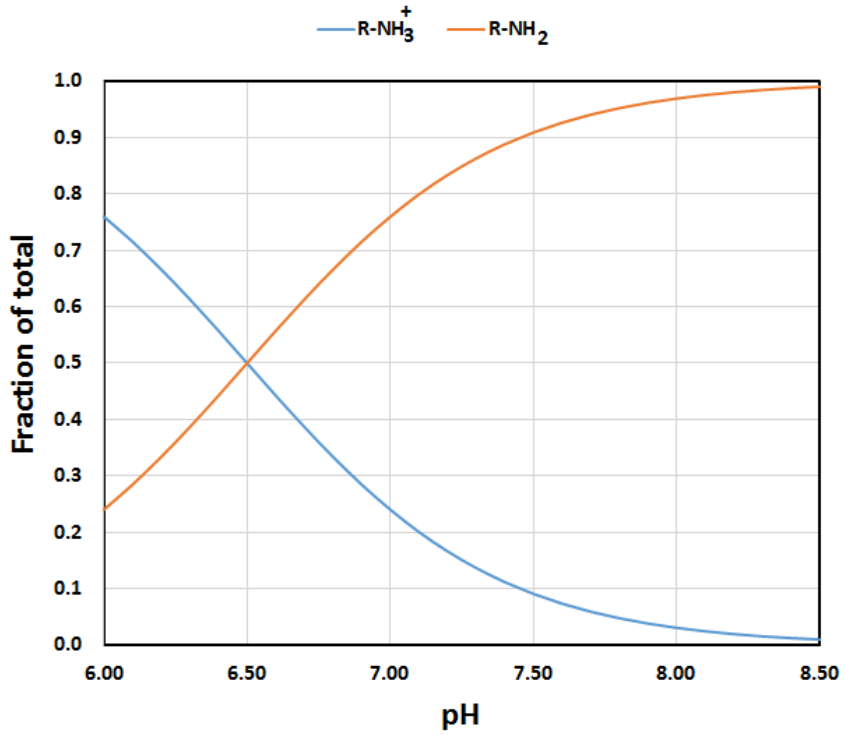

Figure 5.21 Acid-base speciation of chitosan vs. pH at 298 K in aqueous solution.

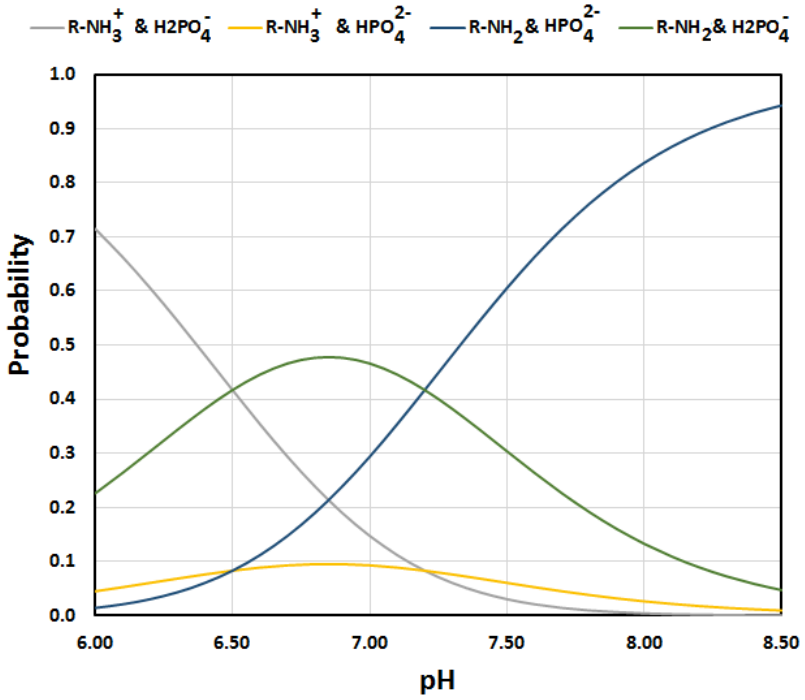

Figure 5.22 Probability of scenarios (interaction of ions and functional groups) *vs.* pH.

The effect of pH on the phosphate adsorption profile is shown in Fig. 5.23. At conditions near pH 5, the sorption capacity of the chitosan materials is systematically higher. It is noted that NCL beads dissolve at that pH values near the pK_a of the protonated amine groups in chitosan. The dependence of the phosphate uptake capacity at pH values above pH 7 is not well defined. The uptake properties of EP2.5 show a sudden drop-off as evidenced by decreased sorption capacity at pH values above the pH_{pzc}. Interestingly, the pH dependent adsorption properties of GA2.5 toward phosphate are lower than EP2.5 due to the phosphate speciation at these conditions. GA2.5 adsorbed phosphate ions *via* the hydroxyl groups and possibly with the amine groups for EP2.5. Amine groups are inferred as the active site for phosphate adsorption, therefore, an increase in the pH results in charge neutralization of the amine groups of chitosan and accounts for the attenuated phosphate adsorption observed in accordance with a change in the zeta-potential due of the adsorbent surface. A decrease in the adsorption capacity of chitosan materials occurs above pH 7, however; favourable interactions likely occur between the chitosan surface and phosphate anion species at these conditions. The foregoing is in agreement with the results of the speciation curve for phosphate and chitosan (*cf.* Fig. 5.22) and the role of hydration effects.

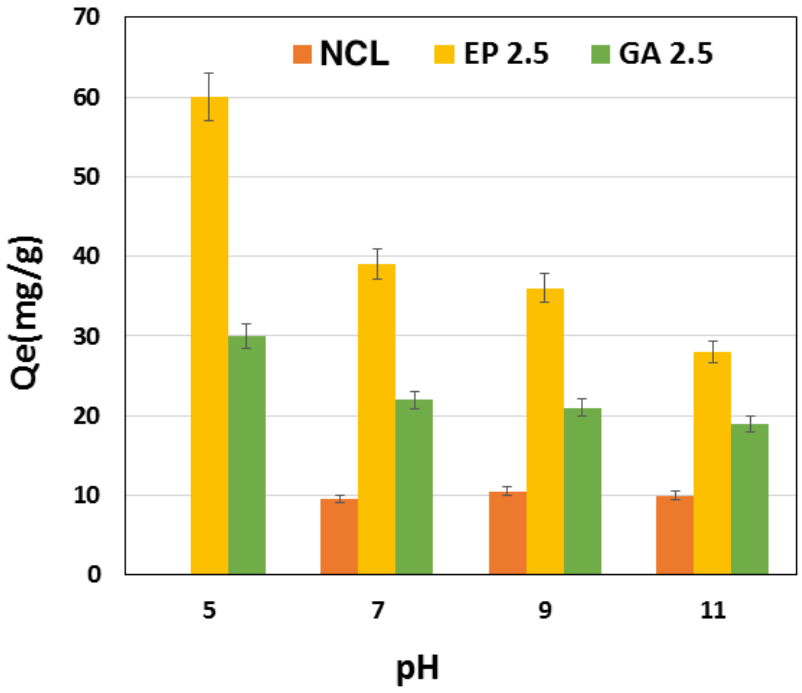

Figure 5.23 Effect of pH on the removal of phosphate with different chitosan bead systems.

5.2.2 Interactions of phosphate (P_i) with chitosan beads

Chitosan and chitin differ due to the presence of primary amine groups versus acetyl groups (*cf.* Fig. 1.9), where the amine groups of chitosan serve as active adsorption sites for species with hydrogen bond donor or acceptor sites. The amine group of chitosan have variable states of protonation, neutral ($pH > pK_a$) or positively charged ($pH < pK_a$). For example, the amounts of -NH_2 (99%) and -NH_3^+ (1%) species at pH 8.5 can be calculated according to eqn (3.4). The abundant NH_2 groups of chitosan favor the binding of non-ionized adsorbates or species with Lewis acid character. The binding of phosphate species such as HPO_4^{2-} implicate the role of electrostatic and van der Waals interactions that occur with complementary Lewis acid sites of chitosan (NH and OH groups). Directional interactions such as hydrogen bonding between HPO_4^{2-} and the polar functional groups (-OH, -NHR; where R = acetyl or H) of chitosan are anticipated to play an important role, especially if one considers the role of hydration for outer-sphere complexes. The hydrogen phosphate ion may preferentially form hydrogen bonds with the amine groups of chitosan (*cf.* Fig. 5.24a). In the case of EP2.5 (and EP5), the NH_2 group is an active site for binding of phosphate species (*cf.* Fig. 5.24b) while fewer amino groups are available in GA2.5 (and GA5) due to the formation of imine linkages with glutaraldehyde *via* the Schiff base reaction (*cf.* Fig.

5.24c). Alternately, cross-linked chitosan beads such as GA 2.5 (and 5) have available imine groups that interact favourably depending on the protonation state of the polymer. A comparison between the pK_a value of amine (piperidine, 11.2) and imine (1-piperideine, ≈9) compounds illustrate the range of pK_a values.[85] Imine groups represent a soft base ligand relative to amino or hydroxyl groups, where this functional group interacts favourably with soft base species such as $H_2PO_4^-$. This fact can explain the lower adsorption capacity of GA 2.5 (or 5) for the dominant phosphate species at pH 8.5 (HPO_4^{2-}), in agreement with the "*law of matching water affinities*".[86,87] Raman spectral results, adsorption energy parameters from the D-R isotherm, and the pH adsorption study illustrate how reversible electrostatic interactions play an important role for the binding of phosphate onto chitosan materials. However, electrostatic interactions such as ion-dipole and hydrogen bonding are key interactions for the phosphate/chitosan/water system at alkaline pH (8.5).

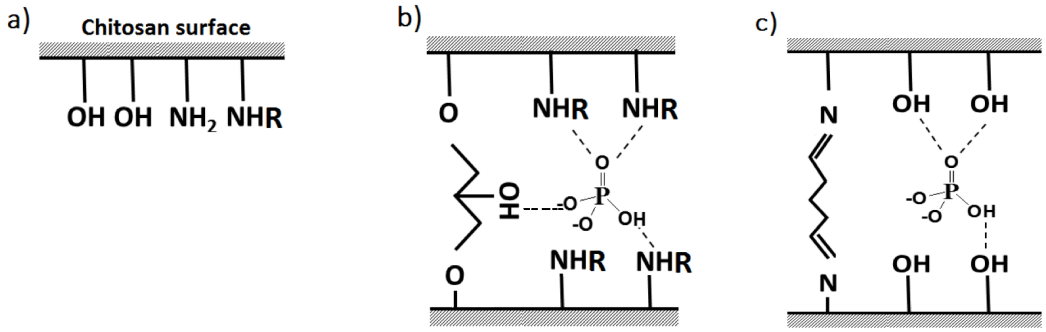

Figure 5.24 A model of interaction between hydrogen phosphate ion (HPO_4^{2-}) and, a) chitosan, b) cross-linked chitosan with epichlorohydrin, c) cross-linked chitosan with glutaraldehyde. (Note: the solvent (water) and counterions are not shown for the sake of clarity).

CHAPTER 6

6 CONCLUSION AND FUTURE WORK

6.1 Introduction

To remove inorganic and organic phosphate species in aqueous solution, several questions were raised at the beginning of the project: *i*) Does the nature of the cross-linker (GA vs. EP) and its composition have an effect on the chitosan bead physicochemical properties (*e.g.* structure, hydration, accessibility of functional groups (OH *vs.* NH_2), HLB, porosity, surface area and sorption capacity)? *ii*) Does doping the beads with calcium affect the bead adsorptive properties toward *p*-nitrophenyl phosphate (PNPP)?; and *iii*) Can the sorption capacity of chitosan beads toward inorganic/organic phosphate species be understood through the adsorption of surrogate dye probes such as *p*-nitrophenol (PNP) and phenolphthalein (PHP)?

6.1.1 Does the type of cross-linker and its relative mole ratio have an effect on adsorption properties of the chitosan bead materials?

The answer to this question is yes. All test results for sorption isotherm including the phosphate species and dye sorption have shown the effect of cross-linker's composition in different ways according to the variable nature of adsorbate species (HPO_4^{-2}, PNP, PHP, and PNPP). SEM images demonstrated the "*pillaring effect*" of cross-linking on chitosan where the outer surface layer of beads are amorphous and cross-linked. The core of the bead has a layered textural porosity similar to surface of the bead system without cross-linking and is visually recognizable.[69] Characterization including TGA, FTIR, SSNMR, elemental analysis, PXRD proved that cross-linking and calcium ion doping the NCL resulted in variable HLB chitosan bead materials.

Monolayer adsorption capacity (Q_m) for PNP ranged from 0.30 to 0.52 mmol g^{-1} and (ii) Q_m values for the bead systems with HPO_4^{2-} ranged from 0.22–0.53 mmol g^{-1}(iii) Q_m values for the bead systems with PNPP ranged from 0.18–1.07 mmol g^{-1}. The increase in mole ratio of the cross-linker did not necessarily result in greater uptake in all cases, as evidenced by a decrease in the sorption capacity or small variation in some cases. The apparent surface area increased with cross-linking (for EP and GA) according to the dye adsorption results for surface coverage with PNP, where greater uptake of PNP and PNPP was observed relative to NCL chitosan beads.

EP and GA cross-linked beads have variable properties (*e.g.* HLB, surface area, pore size, and functional groups due to the physicochemical properties of each cross-linker (alkyl chain length and variable heteroatom functional groups). Based on the HLB properties, the driving force for sorption of adsorbates on the adsorbents can be understood from the variable polarity of materials. Thus, adsorbents with greater hydrophilic nature will have greater uptake of inorganic *vs.* organic phosphate in accordance with the role of dipolar interactions. Swelling results showed increasing HLB properties for cross-linked chitosan bead material as supported by the swelling results of the chitosan bead systems (35.76% for EP2.5 and 35.57% for GA2.5). The factors like low molecular weight and low polar surface area along with availability of functionalities (*e.g.* OH) governs hydrophile-lipophile properties of adsorbates.[88] Based on these factors, the lipophilicity of the adsorbates used herein have the following trend: PHP > PNPP>PNP. EP imparts hydrophilic properties to the chitosan and this in a more hydrophilic bead when chitosan is cross-linked with EP. Chitosan beads are less hydrophilic when cross-linked with GA. The higher sorption capacity of chitosan bead materials cross-linked with epichlorohydrin (EP2.5 and EP 5) toward HPO_4^{2-} despite their lower surface area (*e.g.* 149 m^2/g for EP2.5 and 165 m^2/g for GA2.5) can be justified by this difference in hydrophilicity.

Beads with variable pore size result depending on the type of cross-linker used and is understood according to the variable number of definite number of carbon atoms and surface chemical groups for cross-linked chitosan beads. Definitely, the pore size is an effective factor for sorption of different adsorbates. Since the pore size of EP and GA bead materials are different (*e.g.* 25.7 m^2/g for EP2.5 *vs.* 28.5 m^2/g GA2.5), this can affect sorption affinity toward each adsorbate regarding their molecular size.

An increase in the degree of cross-linking up to 5% in this study do not cause significant steric hindrance based on the size of the adsorbate relative to the pore volume of the cross-linked chitosan, there is some variation between each type of cross-linked bead. The variable sorptive behaviour of different bead materials are shown for GA5 and EP5 by their different sorption capacity (compare to GA2.5 and EP2.5) is reduced for PNP and the PNPP.

Adsorption kinetics of chitosan bead/ hydrogen phosphate ion systems reveal relatively fast adsorptive uptake with an “apparent” negative activation energy, in agreement with a composite kinetic adsorption process that involves the formation of an outer-sphere complex with

significant rearrangement in hydration.[46] The formation of an outer-sphere complex also approved by Raman and DSC results. Adsorption results for phenolphthalein reveal that the uptake depends on the type of cross-linker and the cross-linker content, in accordance with accessibility of the polar surface adsorption sites of such bead systems.[89] As well, the isotherm adsorption results at variable pH reveal a strong dependence on the ionization state of the adsorbate and the chitosan bead surface (e.g., Q_e for EP2.5 is 28 mg/g at pH 5 and 60 mg/g at pH 11).

Favourable interactions are concluded between PNPP and HPO_4^{2-} with chitosan via hydrogen bonding, ion-dipole, and van der Waals interactions, along with stabilizing hydration effects.

6.1.2 Are the chitosan bead materials capable of variable phosphate species removal?

This question addresses the first and second proposed hypotheses in chapter 1. The answer to this question is yes. Non-cross-linked chitosan (NCL) beads have low uptake toward all phosphate species either HPO_4^{-2} or PNPP. Contrary, all of cross-linked chitosan beads show good performance for phosphate uptake species in aqueous solution. The existence of functionalities (hydroxyl and amine groups) along with extended surface area and available pores make the cross-linked chitosan bead systems possess unique adsorption properties for phosphate species. Also, stability and insolubility of cross-linked beads enables regeneration of the adsorbents using simple washing procedure with saline solution at pH 7. The comparison of two types of cross-linkers reported herein for the chitosan bead/phosphate species systems is highly relevant to remediation of alkaline aquatic environments.

Modified chitosan beads described herein are anticipated to have considerable application in fields of agriculture and environmental science due to their tunable and recyclable properties, especially for the controlled uptake of phosphate species (*e.g.* organic and inorganic) in aquatic environments.

6.1.3 Does doping the beads (cross-linked and NCL) with calcium affect the adsorptive properties of the bead system?

This question addresses the third proposed hypothesis in chapter 1. The answer to this question is yes. As indicated from a pH study and interaction of different ions with chitosan in aqueous solution, the electrostatic forces have lesser role for interaction of phosphate species and

chitosan bead materials where hydration competes for potential adsorption sites at pH 8.5. The law of "matching water affinities" can describe interaction of ions (ion-pairing) qualitatively. Based on this law, small ions of high charge density (e.g., phosphate) are strongly hydrated (kosmotropes) whereas large monovalent ions of low charge density (e.g., PNP, PNPP, PHP) are weakly hydrated (chaotropes) and will be bound at hydrophilic and lipophilic domains of the adsorbent surface, respectively.[86,87]

Doping the chitosan with calcium cations alters the Lewis acid-base character of the bead surface accessible site. The doping (or coordinate cross-linking) with calcium cation enhanced the organophosphate sorption capacity of the chitosan bead material surface by increasing the Lewis acid character of the bead, but also by increasing the number of functionalities (hydroxyl and amine groups) thorough the "*pillaring effect"* related to cross-linking between chitosan polymer units.[69]

Calcium doping of chitosan bead materials enhanced the effect of cross-linking degree. This means that sorption capacity of the chitosan beads cross-linked with 2.5% of cross-linkers (EP2.5 and GA2.5) has reached to the sorption capacity of EP5 and GA5 after doping with calcium ions. The result is explained by compensation effect of doping. Materials with low level of cross-linking (EP2.5 and GA2.5) still have sufficient surface accessible sites for chelation of calcium; whereas highly cross-linked materials (EP5 GA5) have fewer available groups for chelation to calcium ions. However, surface accessible functional groups and hydrophilic-hydrophobic nature of cross-linked chitosan beads still can be used to interpretation the different sorption trend among the bead materials.

6.1.4 Can sorption properties of chitosan beads be explained through the adsorption of *p*-nitrophenol (PNP) and phenolphthalein (PHP)?

This question partly addresses the fourth proposed hypotheses in chapter 1. Due to the structural and chemical differences among adsorbates (*e.g.* relative hydrophile-lipophile balance, size, and charge state), the sorptive behaviour of each dye is variable in nature. Hydrophile-lipophile (HLB) properties of each dye are dependent on factors like size, molecular weight, and presence of intermolecular and intramolecular hydrogen bonding. Adsorption of dyes occurs by matching the size of dye molecule and pore size or by HLB properties of adsorbent-adsorbate. Using electrostatic interactions and law of *"matching water affinities",* the effect of charge state on dye molecules adsorption can be understood. Thus, analyzing the obtained data for adsorption

of each dye on each adsorbent enables an improved understanding of the structure and surface chemistry of chitosan bead materials.

PHP is a dianion species at pH 10.5 and is a suitable surrogate dye probe for hydrogen phosphate ions because it can be monitored directly using UV-Vis spectrophotometry. Hence, an understanding of the role of steric and electronic effects of phosphate species can be understood by studying the adsorption of PHP with chitosan bead systems. PNP is a singly charged ionic dye at pH 8.5 where the phenolic moiety may serve as a surrogate dye probe of the aromatic moiety of the PNPP species. Analyzing the physicochemical properties of the various adsorbate species (*e.g.* phosphate vs. PHP, PNP vs. PNPP vs. phosphate) allow a detailed understanding of the physicochemical structure of the chitosan beads.

6.2 Future research involving phosphate species

Several knowledge gaps were addressed by studying the chitosan bead materials described herein. Some potential experiments and methods are proposed that will extend beyond the boundaries of the present study.

An interpretation of the sorptive behaviour of variable adsorbates on the chitosan beads with variable hydrophile-lipophile balance (HLB) was employed in this study. Calculation of the HLB of adsorbates and adsorbents can be achieved by simulation using Spartan software. If so, this calculation will provide important data to understand the sorptive behaviour of variable chitosan beads toward different adsorbates.

PNPP adsorption measurement cannot be carried out at variable pH since it is very sensitive dye probe and tends to decompose in highly acidic or alkaline conditions. Devising a plan to solve this problem could lead to understand the sorption mechanism of PNPP adsorption into the synthesized materials in this project. Maybe using another compound with analogous structure (*e.g.* roxarsone) to PNPP but has improved stability at variable pH range may serve as an alternative surrogate dye probe. Roxarsone (ROX) is an organic arsenical feed additive for the poultry industry to control intestinal parasites.[46] Thus, employing the synthesized chitosan beads herein to roxarsone uptake would be worthwhile.

There are experiments that may be useful to perform to gain more insight on the sorption process of phosphate species by the chitosan beads. Raman and DSC results provided with useful results that may provide a greater understanding the sorption mechanism of hydrogen phosphate

ion with the chitosan beads. This thesis reports that the interaction of phosphate species with chitosan is driven by physical adsorption, in accordance with the parameters from the D–R isotherm model. However, contribution of other techniques enables greater experimental support concerning this proposed mechanism. For example, ^{31}P NMR can be used to monitor interaction involving phosphorus compounds and chitosan functionalities due to the sensitivity of local interactions of ^{31}P NMR spectroscopy. This technique can be employed for determination of phosphate bonding during adsorption on both organic and inorganic phosphates. Also, the investigation of sorption mechanism for phosphate species from kinetic and thermodynamic point of views contributed to understand the physicochemical properties of the chitosan beads. However, detailed study on fluorescence diffusion into the beads using confocal microscopy could be a strong tool to obtain a comprehensive information for understanding the sorption process.

PNPP was chosen for investigation of the synthesized bead sorption capability as a modeling compound for organophosphate (OPs) sorption. Although this study provides insight on the sorption properties of chitosan bead systems, employing another OP (such as paraxon and parathion; *cf.* Table 1.1) which are still used by the agriculture industry may be more useful.

The effect of cross-linking used in this study can be extended to include higher levels of cross-linking to provide more accurate results on its effect with the sorption capacity. Therefore, greater range of cross-linking (*e.g.* 0.5 to 10%) can be studied for sorption of different phosphate species.

Furthermore, field studies can be used for comparison of experimental results in order to demonstrate *proof-of-concept* to establish the utility of the chitosan bead materials for practical applications in real water samples to determine the contribution of other known competitive ions (*e.g.,* SO_4^{2-}, NO_3^-, Cl^-) in sorption properties of chitosan bead systems. A possible field study may involve collecting data outside of lab setting. For instance, water samples can be obtained by *Buffalo Pound Lake which* is a eutrophic lake in Saskatchewan, Canada.[90]

References

(1) Foley, R. N. *Clin. J. Am. Soc. Nephrol.* **2009**, *4* (6), 1136–1139.

(2) Bricker, S. B.; Longstaff, B.; Dennison, W.; Jones, A.; Boicourt, K.; Wicks, C.; Woerner, J. *Harmful Algae* **2008**, *8* (1), 21–32.

(3) Johnston, A. M.; Roberts, T. L. In *Proceedings of the 2001 Manitoba Agronomists Conference*; **2001**; pp 74–82.

(4) Freed, A. V. H.; Haque, R.; Schmedding, D.; Kohnert, R. **2016**, *13*, 77–81.

(5) Ghafari, S.; Hasan, M.; Aroua, M. K. *Bioresour. Technol.* **2008**, *99* (10), 3965–3974.

(6) Shrimali, M.; Singh, K. . *Environ. Pollut.* **2001**, *112* (3), 351–359.

(7) Bernardes, A. M.; Rodrigues, M. a S. In *Electrodialysis and Water Reuse: Novel Approaches*; Andrea Bernardes, Marco Antônio Siqueira Rodrigues, J. Z. F., Ed.; **2014**; pp 63–75.

(8) Akpor, O. B.; Muchie, M. *Sci. Res. essays* **2010**, *5* (21), 3222–3230.

(9) Nassef, E. *Int. J.* **2012**, *2* (3), 409–413.

(10) Zuo, G. M.; Cheng, Z. X.; Li, G. W.; Shi, W. P.; Miao, T. *Chem. Eng. J.* **2007**, *128* (2-3), 135–140.

(11) Vlyssides, A.; Barampouti, E. M.; Mai, S.; Arapoglou, D.; Kotronarou, A. *Environ. Sci. Technol.* **2004**, *38* (22), 6125–6131.

(12) Fei, X.; Sun, G. *Ind. Eng. Chem. Res.* **2009**, *48* (12), 5604–5609.

(13) Kim, D. B.; Gweon, B.; Moon, S. Y.; Choe, W. *Curr. Appl. Phys.* **2009**, *9* (5), 1093–1096.

(14) Dhake, K. P.; Karoyo, A. H.; Mohamed, M. H.; Wilson, L. D.; Bhanage, B. M. *J. Mol. Catal. B Enzym.* **2013**, *87*, 105–112.

(15) Seger, M. R.; Maciel, G. E. *Environ. Sci. Technol.* **2006**, *40* (3), 797–802.

(16) Wagner, G. W.; Procell, L. R.; O'Connor, R. J.; Munavalli, S.; Carnes, C. L.; Kapoor, P. N.; Klabunde, K. J. *J. Am. Chem. Soc.* **2001**, *123* (8), 1636–1644.

(17) Seger, M. R.; Maciel, G. E. *Environ. Sci. Technol.* **2006**, *40* (2), 552–558.

(18) Meng, Q.; Doetschman, D. C.; Rizos, A. K.; Lee, M.-H.; Schulte, J. T.; Spyros, A.; Kanyi, C. W. *Environ. Sci. Technol.* **2011**, *45* (7), 3000–3005.

(19) Atkins, P.; Paula, J. De. *Atkins' physical chemistry*, 9th ed.; Paula, J. de, Ed.; Oxford University Press: Oxford, **2009**.

(20) Sing, K. S. W.; Everett, D. H.; Haul, R. a. W.; Moscou, L.; Pierotti, R. a.; Rouquérol, J.; Siemieniewska, T. *Pure Appl. Chem.* **1982**, *54* (11), 2201–2218.

(21) Langmuir, I. *J. Am. Chem. Soc.* **1918**, *40* (9), 1361–1403.

(22) Azizian, S. *J. Colloid Interface Sci.* **2004**, *276* (1), 47–52.

(23) Sips, R. *J. Chem. Phys.* **1950**, *18* (1948), 1024.

(24) Dubinin, M. M.; Radushkevich, L. V. *Dokl. Akad. Nauk SSSR* **1947**, *55*, 327–329.

(25) Adamson, a W.; Gast, a P. *SubStance* **1997**, *124*, 192C.

(26) Kargari, A.; Takht Ravanchi, M. *Greenh. Gases - Capturing, Util. Reduct.* **2012**, *1*, 3–30.

(27) College, B.; Pharmacy, O.; Nagara, B. *Int. J. Biol. Pharm. Technol.* **2011**, No. 2, 249–258.

(28) Usman, A.; Zia, K. M.; Zuber, M.; Tabasum, S.; Rehman, S.; Zia, F. *Int. J. Biol. Macromol.* **2016**, *86*, 630–645.

(29) Casey, L. S.; Wilson, L. D. *J. Geosci. Environ. Prot.* **2015**, No. April, 78–84.

(30) Filion, D.; Lavertu, M.; Buschmann, M. D. *Biomacromolecules* **2007**, 3224–3234.

(31) Zhao, Y.; Park, R. D.; Muzzarelli, R. A. A. *Mar. Drugs* **2010**, *8* (1), 24–46.

(32) Yuan, Y.; Chesnutt, B. M.; Haggard, W. O.; Bumgardner, J. D. *Materials (Basel).* **2011**, *4* (8), 1399–1416.

(33) Wang, Q. Z.; Chen, X. G.; Liu, N.; Wang, S. X.; Liu, C. S.; Meng, X. H.; Liu, C. G. *Carbohydr. Polym.* **2006**, *65* (2), 194–201.

(34) Muzzarelli, R. A. A. In *Polymer Science: A Comprehensive Reference, 10 Volume Set*; **2012**; Vol. 10, pp 153–164.

(35) Wu, F.-C.; Tseng, R.-L.; Juang, R.-S. *J. Hazard. Mater.* **2001**, *81* (1-2), 167–177.

(36) Filipkowska, U.; Jóźwiak, T.; Szymczyk, P. *Prog. Chem. Appl. Chitin its Deriv.* **2014**, *19*,

5–14.

(37) Chatterjee, S.; Lee, D. S.; Lee, M. W.; Woo, S. H. *J. Hazard. Mater.* **2009**, *166* (1), 508–513.

(38) Alhwaige, A. A.; Agag, T.; Ishida, H.; Qutubuddin, S. *RSC Adv.* **2013**, *3* (36), 16011.

(39) Crini, G.; Badot, P.-M. *Prog. Polym. Sci.* **2008**, *33* (4), 399–447.

(40) Wan Ngah, W. S.; Teong, L. C.; Hanafiah, M. A. K. M. *Carbohydr. Polym.* **2011**, *83* (4), 1446–1456.

(41) Sowmya, A.; Meenakshi, S. *Int. J. Biol. Macromol.* **2014**, *64*, 224–232.

(42) Sowmya, A.; Meenakshi, S. *J. Environ. Chem. Eng.* **2013**, *1* (4), 906–915.

(43) Liu, X.; Zhang, L. *Powder Technol.* **2015**, *277*, 112–119.

(44) Sowmya, A.; Meenakshi, S. *Desalin. Water Treat.* **2014**, *52* (13-15), 2583–2593.

(45) Sowmya, A.; Meenakshi, S. *Int. J. Biol. Macromol.* **2014**, *69*, 336–343.

(46) Poon, L.; Younus, S.; Wilson, L. D. *J. Colloid Interface Sci.* **2014**, *420*, 136–144.

(47) Kwon, J. H.; Wilson, L. D.; Sammynaiken, R. S. *J. Colloid Interface Sci.* **2015**, *457*, 388–397.

(48) APHA. *Standard Methods for the Examination of Water and Wastewater Standard Methods for the Examination of Water and Wastewater*; Rice, E. W.; Baird, R. B.; Eaton, A., D.; Clesceri, L. S., Eds.; American Public Health Association: Washington, DC, **2005**.

(49) Zhao, F.; Yu, B.; Yue, Z.; Wang, T.; Wen, X.; Liu, Z.; Zhao, C. *J. Hazard. Mater.* **2007**, *147* (1-2), 67–73.

(50) Wilson, L. D.; Mohamed, M. H.; Headley, J. V. *J. Colloid Interface Sci.* **2011**, *357* (1), 215–222.

(51) Mohamed, M. H.; Udoetok, I. A.; Wilson, L. D.; Headley, J. V. *RSC Adv.* **2015**, *5* (100), 82065–82077.

(52) Mohamed, M.; Wilson, L. *Nanomaterials* **2015**, *5* (2), 969–980.

(53) Noh, J. S.; Schwarz, J. A. *J. Colloid Interface Sci.* **1989**, *130* (1), 157–164.

(54) Xu, L.; Huang, Y.-A.; Zhu, Q.-J.; Ye, C. *Int. J. Mol. Sci.* **2015**, *16* (8), 18328–18347.

(55) Wan Ngah, W. .; Endud, C.; Mayanar, R. *React. Funct. Polym.* **2002**, *50* (2), 181–190.

(56) Vikhoreva, G. A.; Shablyukova, E. A. **2001**, *33* (3), 38–42.

(57) Jiang, H.; Chen, P.; Luo, S.; Tu, X.; Cao, Q.; Shu, M. *Appl. Surf. Sci.* **2013**, *284*, 942–949.

(58) Li, S.-D.; Zhang, C.-H.; Dong, J.-J.; Ou, C.-Y.; Quan, W.-Y.; Yang, L.; She, X.-D. *Carbohydr. Polym.* **2010**, *81* (2), 182–187.

(59) Ng, J. C. .; Cheung, W. .; McKay, G. *J. Colloid Interface Sci.* **2002**, *255* (1), 64–74.

(60) Cestari, A. R.; Vieira, E. F. S.; Matos, J. D. S.; dos Anjos, D. S. C. *J. Colloid Interface Sci.* **2005**, *285* (1), 288–295.

(61) Dehabadi, L.; Wilson, L. D. *Carbohydr. Polym.* **2014**, *113*, 471–479.

(62) Webster, A.; Halling, M. D.; Grant, D. M. *Carbohydr. Res.* **2007**, *342* (9), 1189–1201.

(63) Pillai, C. K. S.; Paul, W.; Sharma, C. P. *Progress in Polymer Science (Oxford)*. **2009**, pp 641–678.

(64) Pratt, D. Y.; Wilson, L. D.; Kozinski, J. A. *J. Colloid Interface Sci.* **2013**, *395*, 205–211.

(65) Wilson, L. D.; Pratt, D. Y.; Kozinski, J. A. *J. Colloid Interface Sci.* **2013**, *393*, 271–277.

(66) Poon, L.; Wilson, L. D.; Headley, J. V. *Carbohydr. Polym.* **2014**, *109*, 92–101.

(67) Bertau, M.; Jörg, G. *Bioorg. Med. Chem.* **2004**, *12* (11), 2973–2983.

(68) Taguchi, K. *J. Am. Chem. Soc.* **1986**, *108* (10), 2705–2709.

(69) Udoetok, I. A.; Dimmick, R. M.; Wilson, L. D.; Headley, J. V. *Carbohydr. Polym.* **2016**, *136*, 329–340.

(70) Yalkowsky, S. H.; He, Y.; Jain, P. CRC Press: New York, **2010**; p 1608.

(71) Mohamed, M. H.; Wilson, L. D.; Headley, J. V; Peru, K. M. *Energy & Fuels* **2015**, *29* (6), 3591–3600.

(72) Kusrini, E.; Sofyan, N.; Suwartha, N.; Yesya, G.; Priadi, C. R. *J. Rare Earths* **2015**, *33* (10), 1104–1113.

(73) Jadhav, S. V; Bringas, E.; Yadav, G. D.; Rathod, V. K.; Ortiz, I.; Marathe, K. V. *J. Environ.*

Manage. **2015**, *162*, 306–325.

(74) Ziel, R.; Haus, A.; Tulke, A. *J. Memb. Sci.* **2008**, *323* (2), 241–246.

(75) Vlachy, N.; Jagoda-Cwiklik, B.; Vácha, R.; Touraud, D.; Jungwirth, P.; Kunz, W. *Adv. Colloid Interface Sci.* **2009**, *146* (1-2), 42–47.

(76) Nakamoto, K. *Infrared and Raman Spectra of Inorganic and Coordination Compounds: Part B: Applications in Coordination, Organometallic, and Bioinorganic Chemistry*; **2008**.

(77) Xu, X.; Gao, B.; Yue, Q.; Zhong, Q. *Bioresour. Technol.* **2011**, *102* (9), 5278–5282.

(78) Jha, P.; Halada, G.; McLennan, S. *Coatings* **2013**, *3* (3), 140–152.

(79) Mundy, W. C. *J. Chem. Phys.* **1973**, *59* (5), 2173.

(80) Niaura, G.; Gaigalas, A. K.; Vilker, V. L. *J. Phys. Chem. B* **1997**, *101* (45), 9250–9262.

(81) Avila, G.; Fernández, J.; Maté, B.; Tejeda, G.; Montero, S. *J. Mol. Spectrosc.* **1999**, *196* (1), 77–92.

(82) Ibanez, J. G.; Mena-Brito, R.; Fregoso-Infante, a. *J. Chem. Educ.* **2005**, *82* (10), 1549–1551.

(83) Rooney, J. J. *J. Mol. Catal. A Chem.* **1995**, *96* (1), L1–L3.

(84) Leduc, J.; Leduc, R.; Cabana, H.; Engineering, E. *Adsorpt. Sci. Technol.* **2014**, *32* (7), 557–570.

(85) Clayden, J.; Greeves, N.; Warren, S.; Wothers, P. *Am. Nat.* **2001**, *40* (d), 1990–1992.

(86) Collins, K. D.; Neilson, G. W.; Enderby, J. E. *Biophys. Chem.* **2007**, *128* (2-3), 95–104.

(87) Collins, K. D. *Methods* **2004**, *34* (3), 300–311.

(88) Mannhold, R.; Poda, G. I.; Ostermann, C.; Tetko, I. V. *J. Pharm. Sci.* **2009**, *98* (3), 861–893.

(89) Wilson, L. D.; Guo, R. *J. Colloid Interface Sci.* **2012**, *387* (1), 250–261.

(90) Lo, F. A. *Buffalo pound water treatment plant annual report*; Regina, **2015**.